Crystallographic Studies of Some Tetracyanoquinodimethane Complexes

Deirdre A. Kennedy

A Thesis submitted to the Council for National Academic Awards in partial fulfilment for the Degree of Master of Philosophy

Sponsoring establishment: Sheffield City Polytechnic

Date: January 1982

Acknowledgements

I would like to thank my Director of Studies Dr.I.W.Nowell, for all his time, advice and guidance, during the course of this study, and without whom it would not have been made possible. My thanks to my supervisor, Dr.M.Goldstein, for the interest shown in this work.

I would also like to thank the members of the Chemistry Department at Sheffield City Polytechnic, especially Dr.M.P.MacDonald, for all their help and advice throughout my time here; the computing staff, for their patience; the staff of Educational Services at Sheffield City Polytechnic, for reproduction of the diagrams in this work; Miss Sue Hall (Eric Mensforth Library, Sheffield City Polytechnic) and Miss Ann Hughes (Physics Department, Sheffield City Polytechnic), for typing this thesis.

Finally, thanks to my Mother and my sisters for the support given especially when I needed it most.

<u>CONTENTS</u>

Crystallographic Studies of Some Tetracyanoquinodimethane Complexes

Abstract

The solid state structures of charge-transfer complexes of 7,7,8,8-tetracyanoquinodimethane, TCNQ, have been reviewed and classified into three main structural types viz homosoric (pseudosoric), heterosoric, and nonsoric. In an attempt to more fully understand the factors influencing the type of structure adopted in the solid state and to relate the structural features to the electrical conductivities, the crystal structures of five TCNQ complexes have been determined by X-ray analysis:

(i) Dimethyldibenzophospholium Bis-7,7,8,8-tetracyanoquinodimethanide, is a semi-conductor and belongs to the pseudosoric class of TCNQ complexes, with the cations and the TCNQ moieties forming segregated stacks. The TCNQ molecules are arranged in a diadic fashion with the diads being held together by an array of short intermolecular contacts to give two-dimensional sheets.

(ii) Dimethyldiphenylphosphonium Bis-7,7,8,8-tetracyanoquinodimethanide is a good semi-conductor which adopts a monadic/diadic stacking of the TCNQ moieties into columns. The resulting one-dimensionality of the structure is attributed to the presence of statistically disordered cations. The influence of such cation disorder upon the electrical conductivities has been examined for related phosphonium complexes.

(iii) N,N′-Dicyanophenyl-4,4′-bipyridylium Tetrakis-7,7,8,8-tetracyanoquinodimethanide, is found to be a pseudosoric complex with the TCNQ moieties contained within sheets in a tetradic manner. The poor semi-conducting properties are attributed to the presence of the cyanophenyl groupings which facilitate significant interactions between anion and cation stacks.

(iv) 1,2-Diethyl-4,4′-bipyridiniumethane Tetrakis-7,7,8,8-tetracyanoquinodimethanide is a poor semi-conductor containing tetradic stacks of TCNQ molecules within which there is poor overlap. The

tetrads are arranged in sheets containing extensive intermolecular electrostatic interactions.

(v) 4,4′-Bipyridylethylene 7,7,8,8-tetracyanoquinodimethane, (DPE)-(TCNQ), is a heterosoric complex and contains stacks of alternating donor (DPE) and acceptor (TCNQ) molecules. The large distances between donor and acceptor molecules within each stack and the geometry of the TCNQ molecule indicate little or no charge-transfer to be present.

Abbreviations

Abbreviation	Name
An	Anthracene

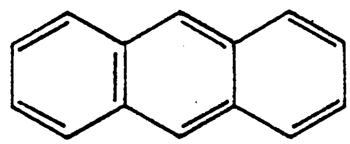

BD	Benzidine

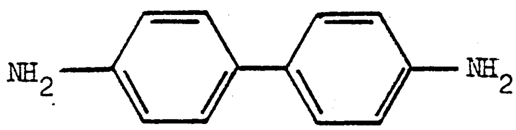

DBzBP	N,N′-Dibenzyl-4,4′-bipyridylium

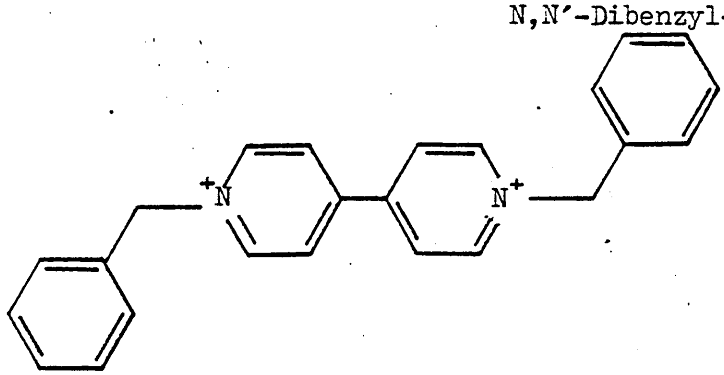

DBzPA	1,2-Di(N-benzyl-4-pyridinium)ethane

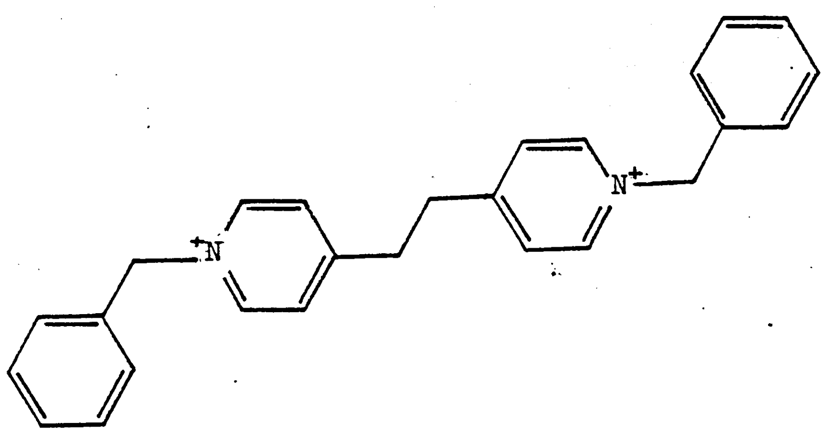

DBzPE 1,2-Di(N-benzyl-4-pyridinium)ethylene

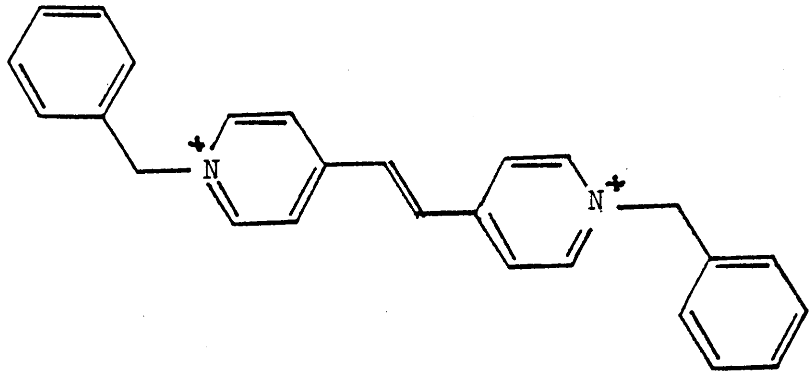

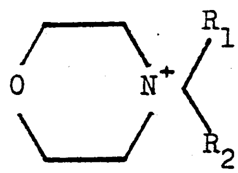

M	Morpholinium	$R_1,R_2 = H$
DEM	4,4-Diethylmorpholinium	$R_1,R_2 = CH_2CH_3$
DMM	4,4 -Dimethylmorpholinium	$R_1,R_2 = CH_3$
HEM	4-Ethylmorpholinium	$R_1 = CH_2CH_3$ $R_2 = H$
MEM	4 -Methyl-4-ethylmorpholinium	$R_1 = CH_2CH_3$ $R_2 = CH_3$

DEPE 1,2-Di(N-ethyl-4-pyridinium)ethylene

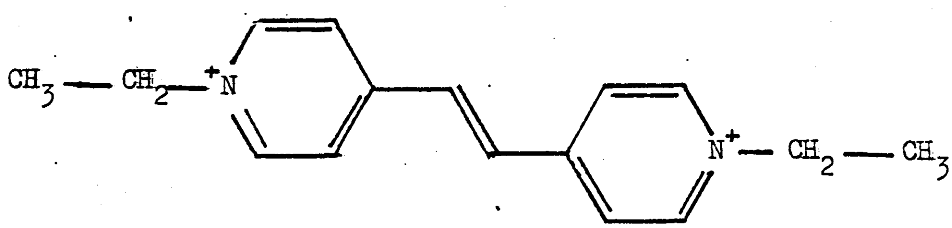

Dipy 2,2′-Dipyridyl

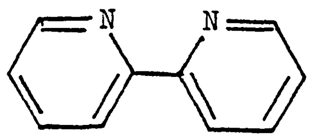

DMBP 1,1′-Dimethyl-4,4′-bipyridylium

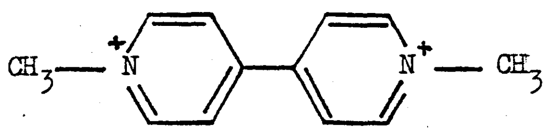

DMPA 1,2-Di(N-methyl-4-pyridinium)ethane

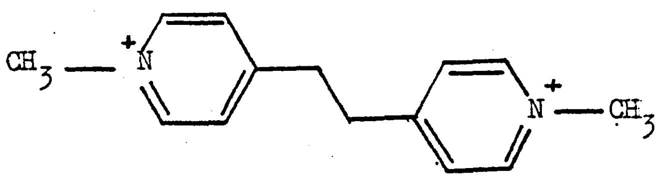

DPMBz 1,4-Di(N-pyridinium methyl)-benzene

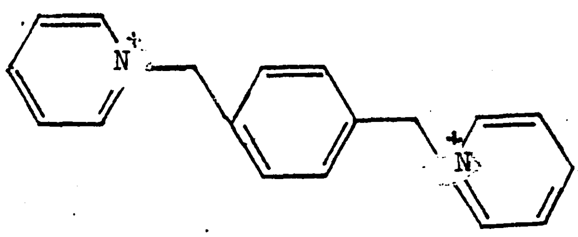

NEMTh N-ethyl-2-methylthiazolinium

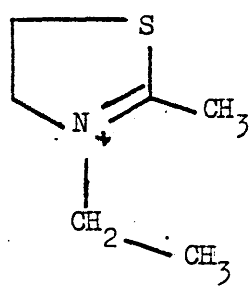

NEP N-ethylphenazinium

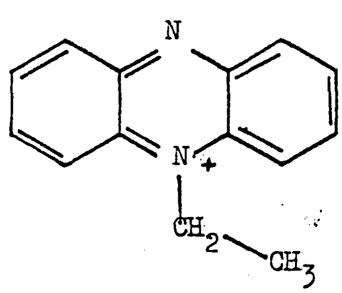

NMETh

N-methyl-2-ethylthiazoline

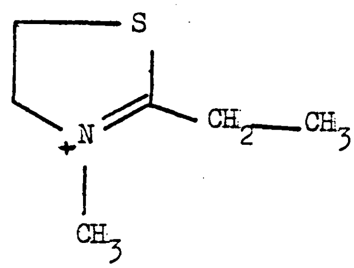

NMP

N-methyl phenazinium

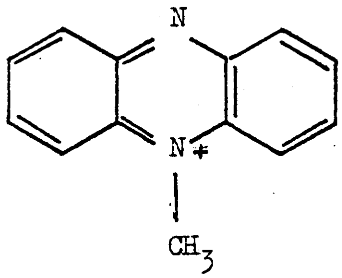

Perylene

Perylene

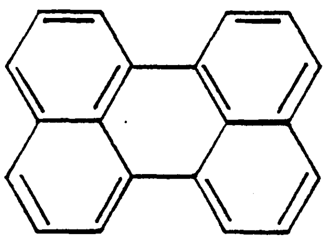

Pyrene

Pyrene

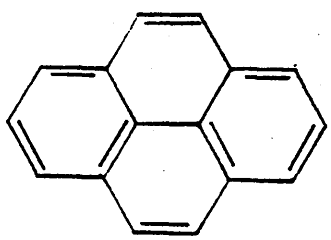

Q

Quinolinium

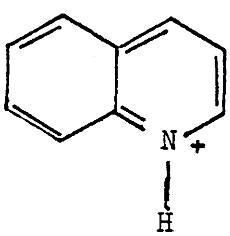

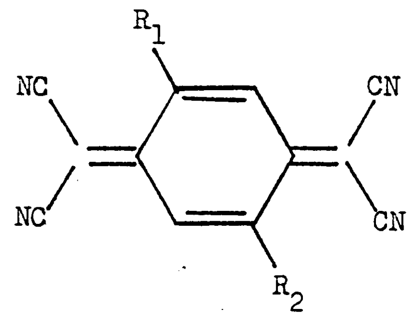

TCNQ	7,7,8,8-Tetracyanoquinodimethane	$R_1,R_2 = H$
DMTCNQ	Dimethyl-2,5-TCNQ	$R_1,R_2 = CH_3$
DIMEOTCNQ	Dimethoxy-2,5-TCNQ	$R_1,R_2 = OCH_3$

TEA	Triethylammonium
TMA	Trimethylamine
TMPD	N,N,N′,N′-tetramethyl-p-phenylenediamine

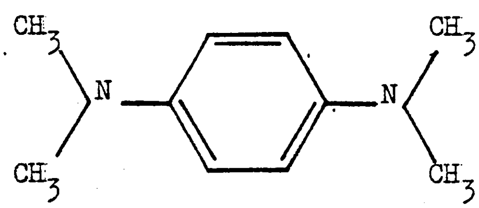

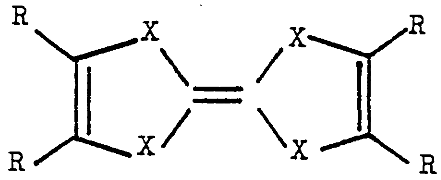

(a)

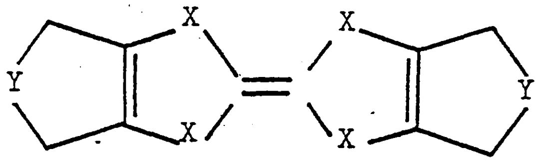

(b)

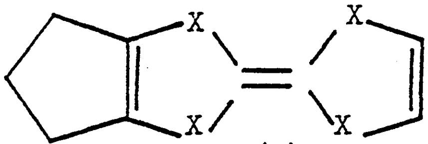

(c)

TTF	Tetrathia-2,2′,5,5′-fulvalene or 1,1′-bis-2,5-dithiole	(a), X = S, R = H
DMTTF	Dimethyl-TTF	(a), X = S, R = H or CH_3
TMTTF	Tetramethyl-TTF	(a), X = S, R = CH_3
TSeF	Tetraselenafulvalene	(a), X = Se, R = H
TMTSeF	Tetramethyl-TSeF	(a), X = Se, R = CH_3
DEDMTSeF	Diethyl-dimethyl-TSeF	(a), X = Se, R = CH_3, CH_2CH_3
t-DSeDTF	trans-Diselenadithiafulvalene	(a), X = Se or S, R = H
c-DSeDTF	cis-Diselenadithiafulvalene	(a), X = Se or S, R = H
TTTF	Trimethylene-3,4-TTF	(c), X = S
HMTTF	Hexamethylene-TTF or bis-(trimethylene) 3,4;3′,4′-TTF	(b), X = S, Y = CH_2
HMTSeF	Hexamethylene-TSeF	(b), X = Se, Y = CH_2
DTTSeF	Di-(3,4-dihydrothieno)-TSeF	(b), X = Se, Y = S
BTTF	Dimethyldibenzyotetrathiofulvalene	(b), X = S, Y = $CH{=}CCH_3$
OMTTF	Octamethylene-3,4;3′,4′-TTF	(b), X = S, Y = $CH{=}CH$

TTT Tetrathiotetracene or Tetrathionaphtacene

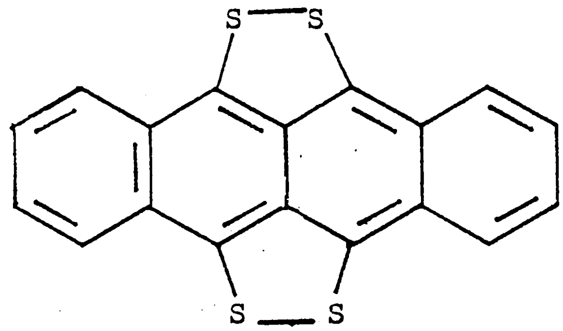

CHAPTER ONE

Structural characteristics of complexes formed by 7,7,8,8-tetracyanoquinodimethane, TCNQ, and their associated electrical conductivities.

Contents

1.1 Introduction

Over the past two decades considerable interest has been shown in the complexes formed by the strong π-acid, 7,7,8,8-tetracyanoquinodimethane, TCNQ, (I).

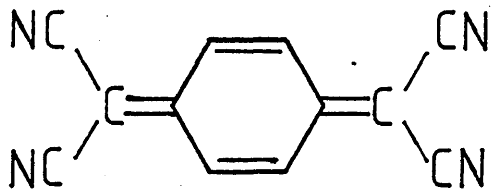

(I)

The TCNQ molecule is a closed-shell planar quinoid molecule and this, together with the presence of four highly electron-withdrawing cyanide groups, enables it to function as an acceptor molecule.

TCNQ, although only first synthesized[1-5] (Scheme 1.1) in 1960 has given rise to an extensive range of complexes which have been studied in the solid state. Crystallographic studies have often been used to aid an understanding of their solid state properties, in particular their conductivities. The latter are anisotropic and range from insulating to metallic, (Figure 1.1).

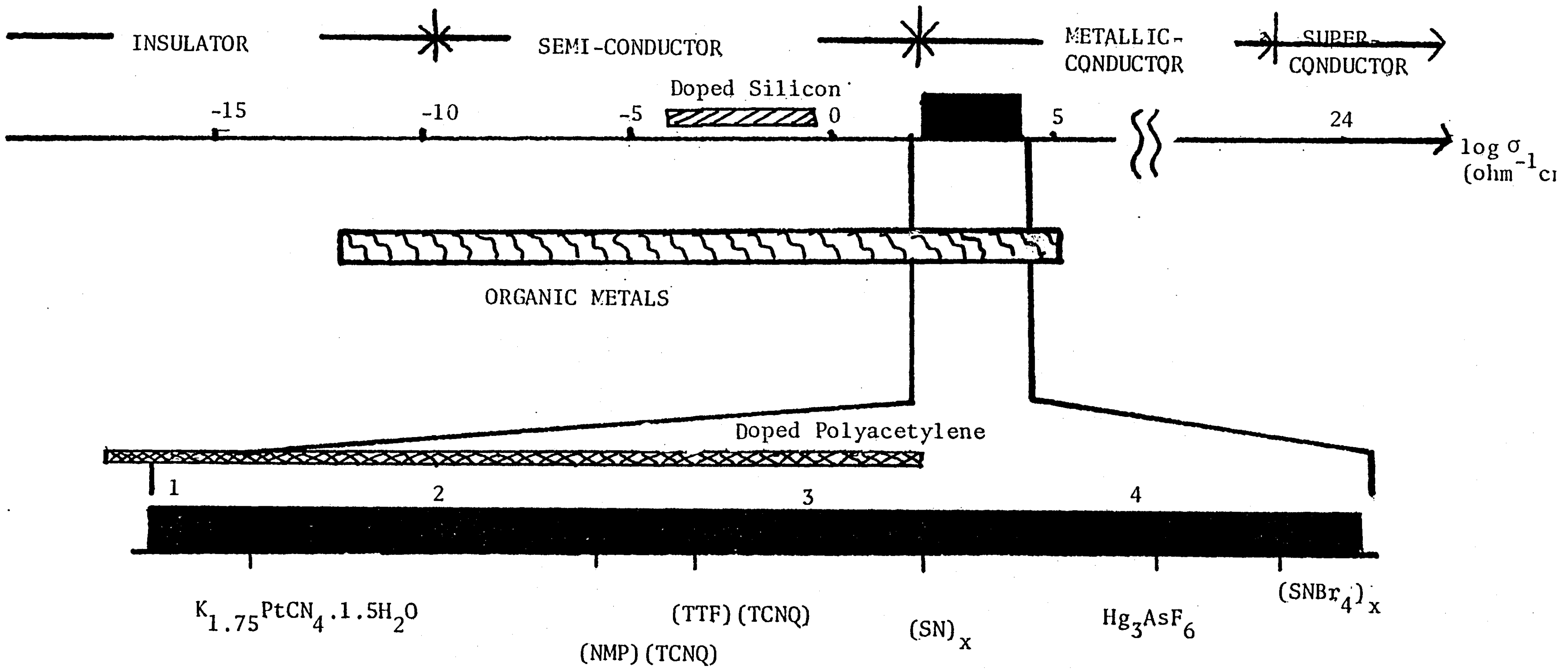

Figure 1.1 Classification of materials according to their room temperature conductivities

Scheme 1.1 Preparation of 7,7,8,8-tetracyanoquinodimethanide, (TCNQ)

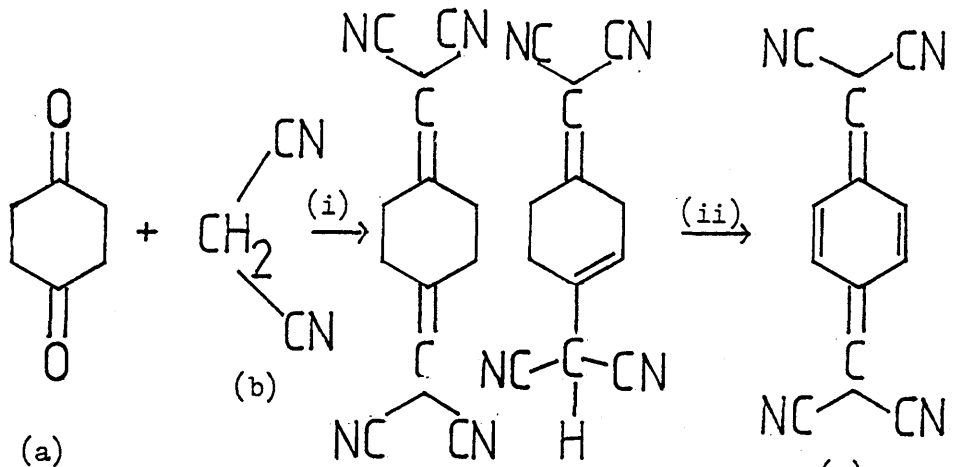

(a) (b) (c) (d) (e)

Step (i):- 100g of 1,4-cyclohexanedione, (a), and 119g of malononitrile, (b), are melted on a steam-bath. To the melt is added an aqueous solution of β-alanine (1g/200ml). The mixture is warmed on a steam-bath, with swirling, until crystals appear, and is then allowed to cool to room temperature. The product (c) is collected and washed with water and ether. Expected yield 97% of 1,4-bis-(dicyanomethylene)-cyclohexane, m.p. 216-217°C.

Step (ii):- (c)[0.037 mole], N-bromosuccinimide [0.09 mole], and CH_3CN (150ml) are stirred at -20°C, under N_2, while 7.2g pyridine in 100ml ether is added. The mixture is stirred for an additional 15 minutes and then allowed to warm to room temperature. Cold water is added to precipitate (e), which may be recrystallized from ethyl acetate. Expected yield 84%, m.p. 289-291°C.

1.2 Classification of TCNQ Complexes

The complexes of TCNQ may be classified in terms of their solid state structures[6] and in terms of their room temperature electrical conductivities. A further classification may be made in terms of the behaviour of the conductivity as a function of temperature.

1.2.1 Classification in Terms of Conductivity

Just as elements and compounds may be classified according to the magnitude of their room temperature conductivities, so the same classification may be applied to the complexes of TCNQ:

(i) very low conductivity (10^{-10} ohm^{-1}cm^{-1} and lower), characteristic of an insulator,

(ii) medium conductivity (10^{-10} – 10 ohm^{-1}cm^{-1}), characteristic of a semiconductor,

(iii) high conductivity (10 ohm^{-1}cm^{-1} and higher), characteristic of a metal.

Two distinct transport mechanisms for electrical conduction are often applied to these systems:

(a) Band Conduction, and (b) Hopping Conduction.[7]

1.2.2 The Band Model of Conduction

In order to explain the mechanism of electrical conduction it is necessary to discuss the state of the electrons in a solid. In the Band Model the electrons in a solid are considered to be located in energy bands. The formation of such energy bands results from the overlap of suitable atomic orbitals. In the case of two isolated atoms, when they are brought close enough together for their atomic orbitals to overlap, bonding and anti-bonding molecular orbitals are formed. In the case of a large number of atoms, as in a crystal, the number of energy levels (bonding and anti-bonding) formed are so numerous and so close in energy, that continuous bands of energy are formed. The width of such energy bands is determined by the extent of orbital overlap. The electrons are able to occupy the energy levels within a band, according to the Pauli Exclusion Principle.[8] The extent of occupation and the magnitude of the gaps between successive bands determine most of the electrical properties of a solid. The highest occupied band is often referred to as the valence band and the lowest unoccupied band as the conduction band.

Within a given band, the electrons are said to be delocalized i.e. free to move throughout the solid thereby giving rise to an electrical current. For such an electric current to be sustained, the movement of the electrons must be unidirectional. Insulating, semi-conducting and metallic behaviour may be interpreted in terms of the Band Model:

(i) Insulating behaviour

In an insulator the energy bands are either completely filled i.e. all energy levels are doubly occupied, or completely empty [Figure 1.2(i)]. Conduction cannot take place in an empty band because it contains no charge carriers. Likewise, conduction is not possible in a completely filled band as the total population of electrons in such a band can have no net motion. In addition, the energy gap (E_g) between the valence and conduction bands is so large that almost no charge carriers can be created by thermal excitation of electrons across the energy gap. The very low conductivity associated with insulators results mainly from defects and impurities in the system.

(ii) Semi-conducting behaviour

Semi-conducting properties in a solid may be attributed to a variety of features. The presence of a small energy gap between the valence and conduction bands for example facilitates the thermal excitation of charge carriers from the valence to the conduction band [Figure 1.2 (ii)]. The presence of impurities leads to the formation of energy levels between the valence and conduction bands, thereby creating an energetically favourable conduction pathway [Figure 1.2 (iii)].

The conductivity of a semi-conductor is given by the expression,

$$\sigma = n_o e \mu \exp(-E_a/kT)$$

where:

σ = conductivity ($ohm^{-1}cm^{-1}$)

e = charge on an electron

n_o = concentration of charge carriers

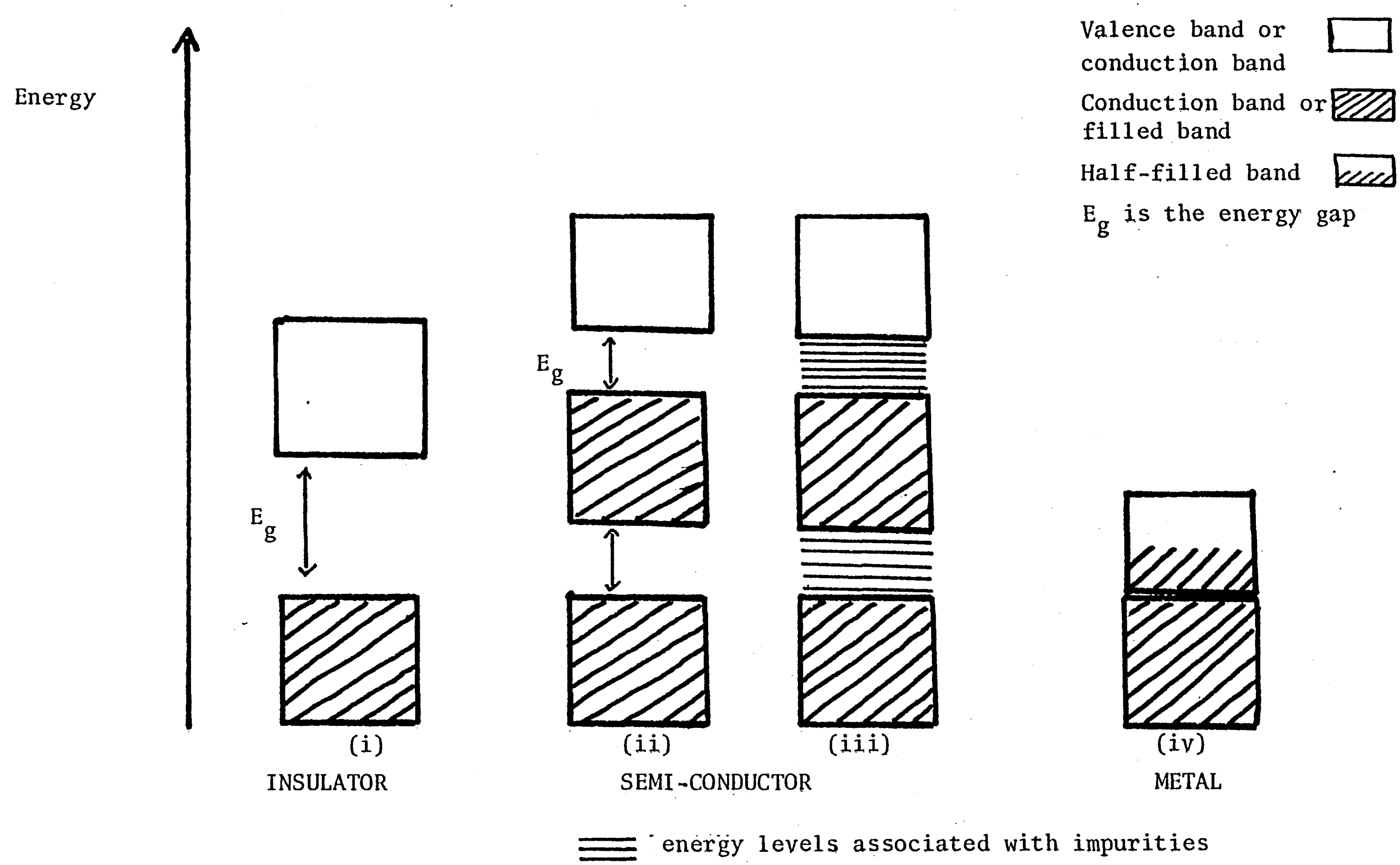

Figure 1.2 Schematic representation of energy bands in (i) insulators,(ii) semi-conductors, (iii) semi-conductors with impurities present,(iv) metals.

μ = mobility of charge carriers

E_a/kT = Boltzmann distribution

The concentration of charge carriers increases with temperature, due to thermal excitation, enabling passage across the energy gap. The movement of an electron effectively creates two charge carriers, (i) the electron and (ii) the positive hole left in the previously filled valence band. However, the lattice vibrations in a crystal also increase with temperature which causes an increase in the degree of scattering and thus a reduction in the mobility of the charge carriers. Thus, while the conductivity of a semi-conductor increases with temperature, the magnitude never reaches a very high value but lies between that of a metal and an insulator, (Figure 1.3).

(iii) Metallic behaviour

Metallic behaviour is associated with a high value of conductivity at room temperature and a characteristic increase in conductivity as the temperature is decreased (Figure 1.3). A metallic conductor has its uppermost energy band only partially occupied by electrons [Figure 1.2(iv)]. The electrons within this band can be readily promoted to unoccupied levels within this same band, these levels being only slightly greater in energy. This movement gives a net drift of electrons through the lattice.

The conductivity of a metal is limited by the scattering of electrons by lattice vibrations. This scattering increases as the temperature is increased and tends to change the direction and restore a state of zero momentum to all electrons. Thus, the conductivity decreases as the temperature is increased.

1.2.3 The Hopping Model of Conduction

A hopping mechanism can also be applied to the conduction processes in both simple and in complex TCNQ salts. In this approach the conduction process within the TCNQ stacks may be represented by a series of

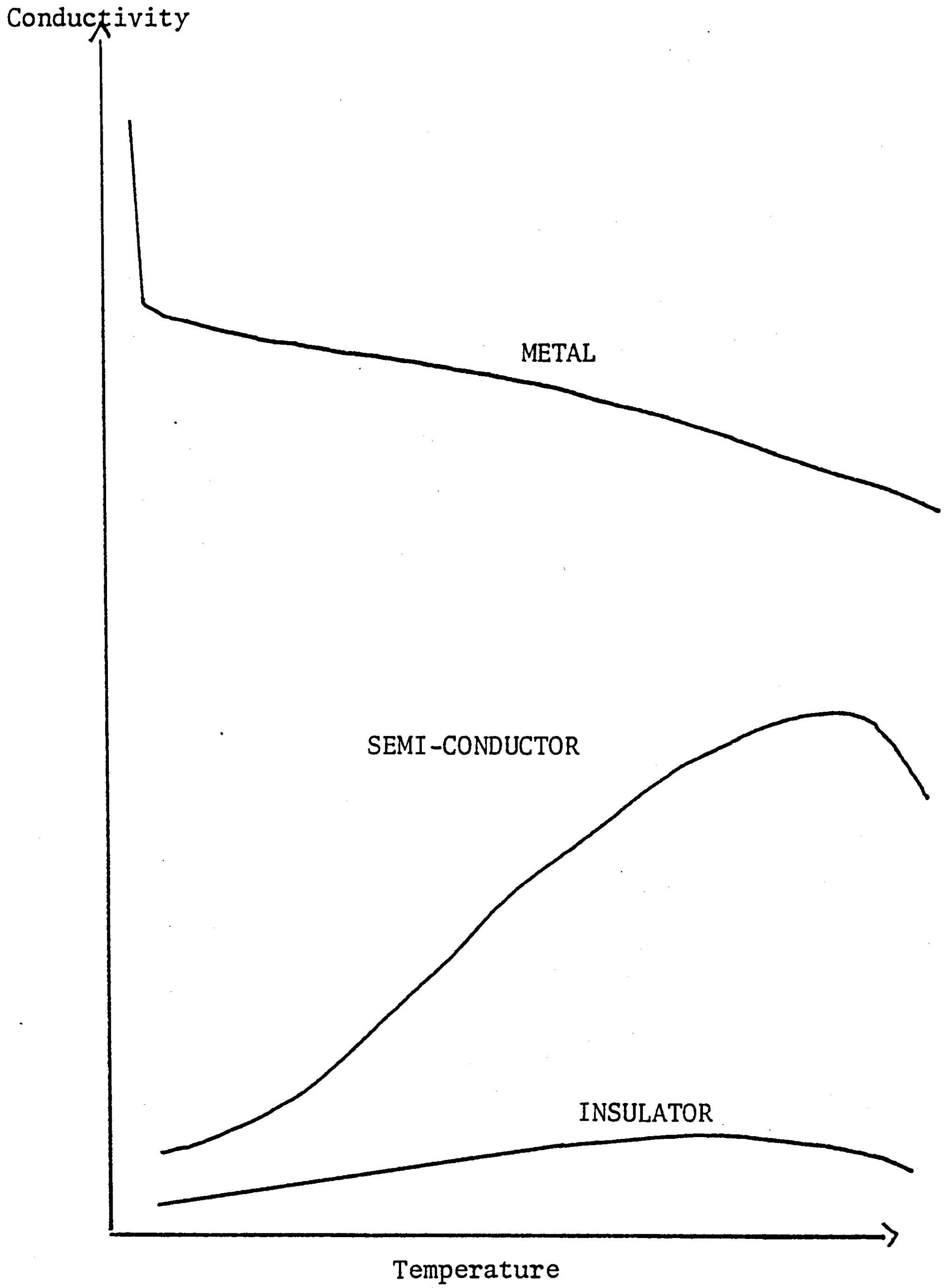

Figure 1.3 The electrical behaviour of metals, semi-conductors, and insulators as a function of temperature.

(i) Simple TCNQ salts

A simple TCNQ salt is one in which all the TCNQ moieties bear a negative charge as for example in (Rb)(TCNQ).[9,10] When a voltage is applied an electron hops from one TCNQ moiety onto another with the consequent formation of $TCNQ^{o}$ and the dianion $TCNQ^{2-}$. The formation of the dianion causes an energy barrier and the mobility of electrons is reduced, thus such simple TCNQ salts exhibit insulating to semi-conducting behaviour.

(ii) Complex TCNQ salts

A complex TCNQ salt is one which comprises charged and neutral TCNQ species. When a voltage is applied an electron from a charged TCNQ moiety hops onto a neutral TCNQ moiety. The movement results in the formation of $TCNQ^{o}$ and a charged TCNQ moiety with no resultant energy barrier. Thus, this type of salt exhibits good semi-conducting to metallic properties.

1.2.4 Classification of the Solid State Structures of TCNQ Complexes

The complexes of TCNQ have been classified into three major classes according to the nature of the stacking of the TCNQ moieties (Figure 1.5).

(i) The nonsoric class of TCNQ complexes

The nonsoric complexes of TCNQ are those in which the cation and TCNQ moieties are randomly arranged. The structures of few, if any, truly nonsoric complexes of TCNQ, have been reported. This is probably due to the crystallographic difficulties involved in solving such highly unsymmetrical structures. Some complexes, however, have been reported which do show limited randomness in the stacking of the TCNQ molecules.[11,12] In $(TCNQ)(perylene)_3$[12] for example the donor molecules (D; perylene) and the acceptor molecules (A; TCNQ) are stacked in a non-uniform manner; DDADDA . . . . Each stack is sandwiched between sheets of perylene molecules.

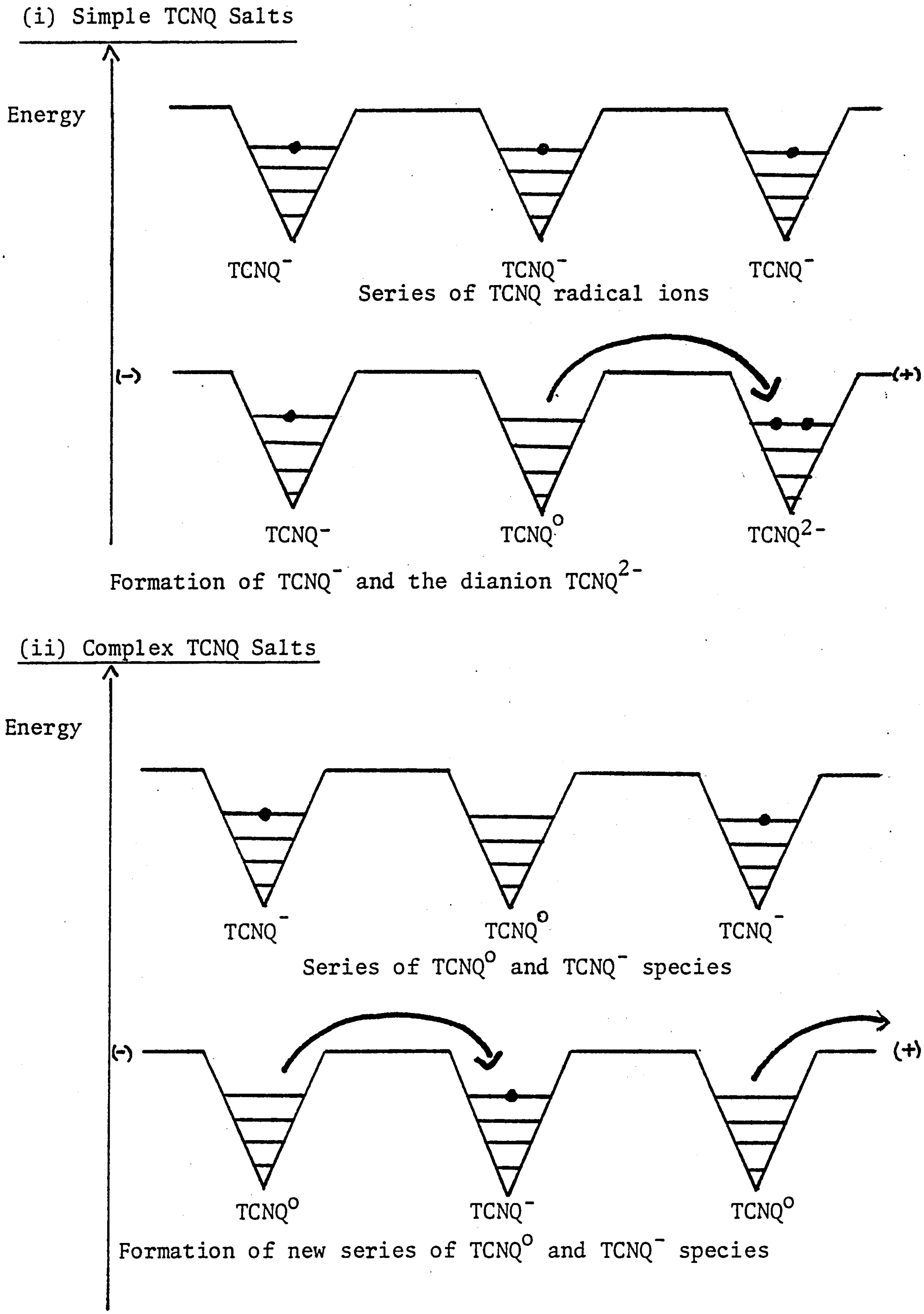

Figure 1.4 Hopping mechanism for conduction processes in TCNQ salts.

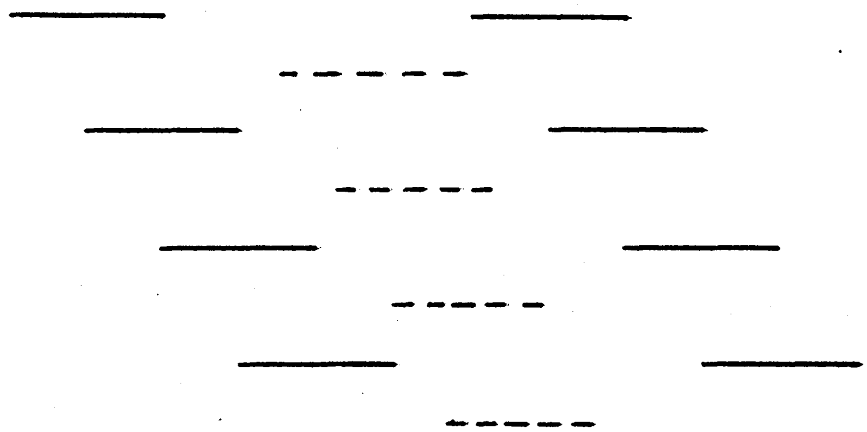

HOMOSORIC

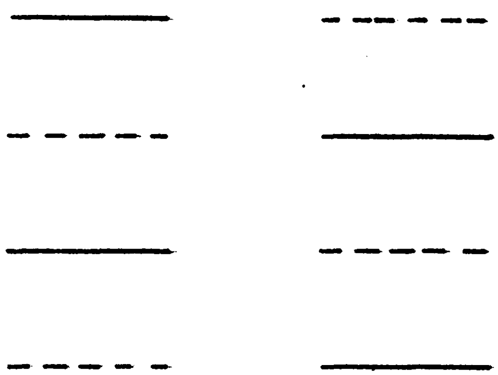

HETEROSORIC

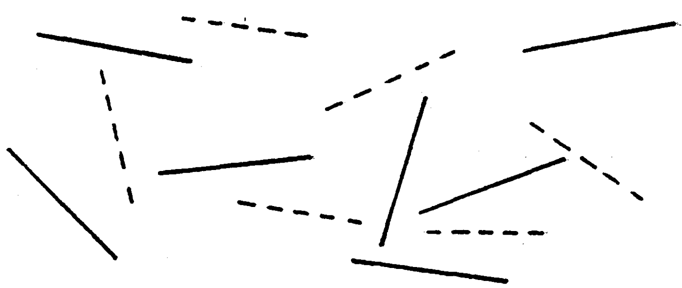

NONSORIC

represents a side-on view of a TCNQ molecule

represents a cation or donor molecule

Figure 1.5 Stacking characteristics in the homosoric, heterosoric, and nonsoric TCNQ complexes.

The heterosoric complexes of TCNQ are those in which the cation and TCNQ molecules are stacked alternately in columns. They exhibit the characteristic face-to-face stacking mode, DADA . . . . (D,A; donor, acceptor molecules), consistent with 1:1 π -molecular complexes. Structurally these complexes differ in the repeating distance along the stack and the associated molecular overlaps.

The first structure of this type to be reported was the anthracene-TCNQ complex, (An)(TCNQ)[13]. It exhibits the characteristic DADA . . . , stacking mode and adopts rather a loose packing arrangement in which the interplanar separation between adjacent molecules is relatively large (3.50Å) (Figure 1.6). There is little charge-transfer between donor and acceptor molecules and no short inter- or intrastack electrostatic contacts.

A complementary complex to (An)(TCNQ) is the benzidine complex, (BD)(TCNQ)[27]. In the latter, the TCNQ molecules are formally neutral and there is no evidence of hydrogen-bonding between the donor and acceptor molecules. The molecular columns are closely packed leaving no space to accommodate solvent molecules [Figure 1.7(i)]. In the solvent containing (BD)(TCNQ) complexes e.g. (BD)(TCNQ)(C_6H_6)[28] and (BD)-(TCNQ)(CH_2Cl_2)$_{1.7}$[18] two kinds of specific interaction exist: (i) the charge-transfer interaction and (ii) the hydrogen bonding. The latter gives infinite hydrogen-bonded sheets, (Figure 1.8). The overlaps between the benzidine (BD) and TCNQ molecules in both solvent-free and solvent containing complexes are similar, [Figure 1.7(ii)].

Several members of the TTF-family form mixed-stack complexes with TCNQ and substituted TCNQ moieties, e.g. (BTTF)(TCNQ),[29] (OMTTF)(DMTCNQ)[35] and (OMTTF)(DIMEOTCNQ).[34] These three complexes like all heterosoric salts, are characterized by large interplanar spacings between donor and acceptor molecules; 3.55, 3.56 and 3.53Å respectively.

The heterosoric TCNQ complexes have conductivities in the insulating

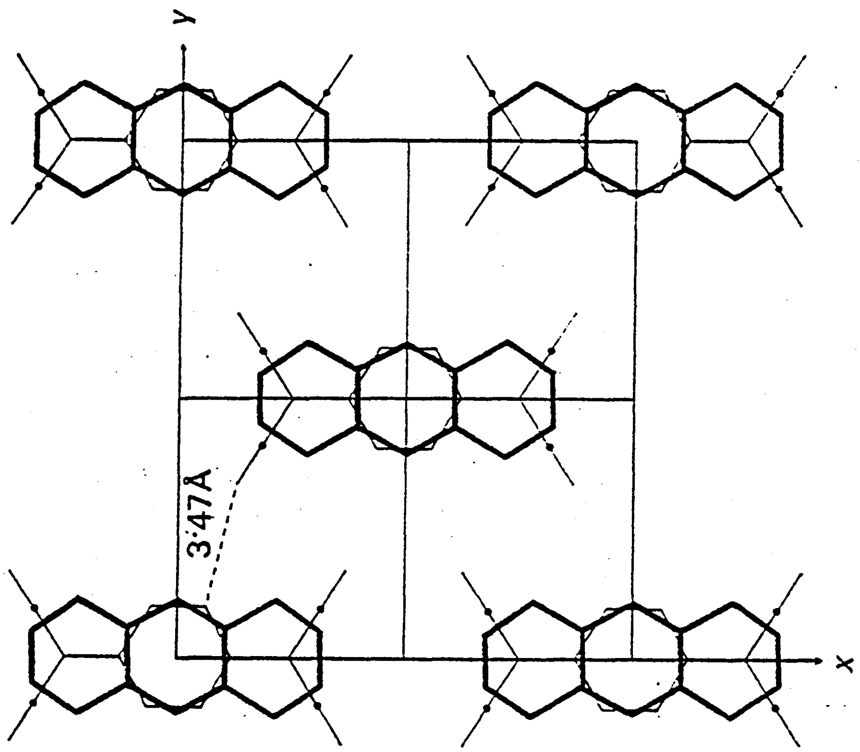

Figure 1.6 Anthracene - TCNQ; view showing the overlap of the constituent molecules and the rather loose packing arrangement.

(i)

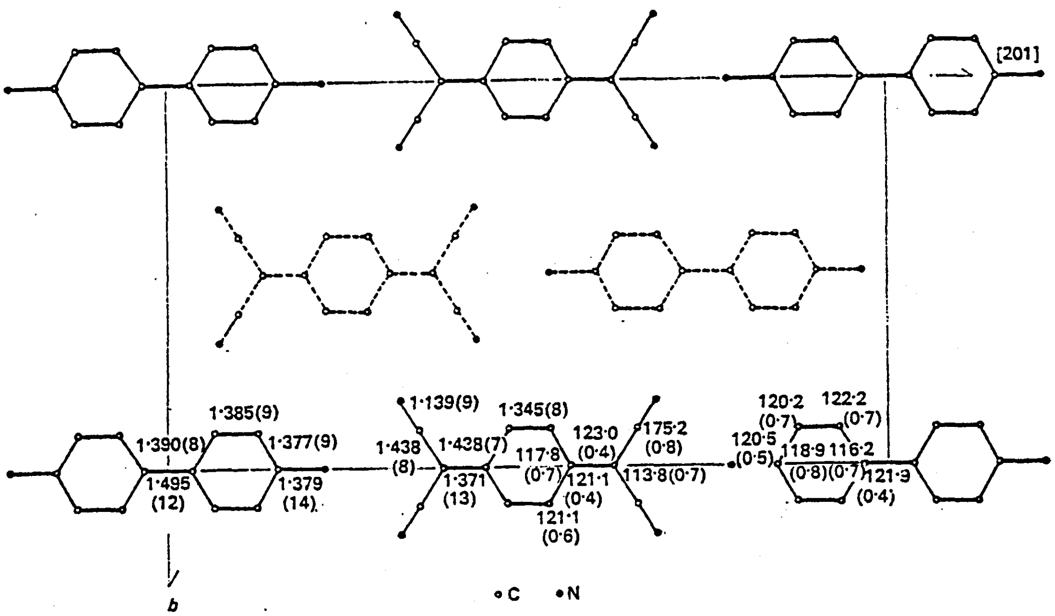

(ii)

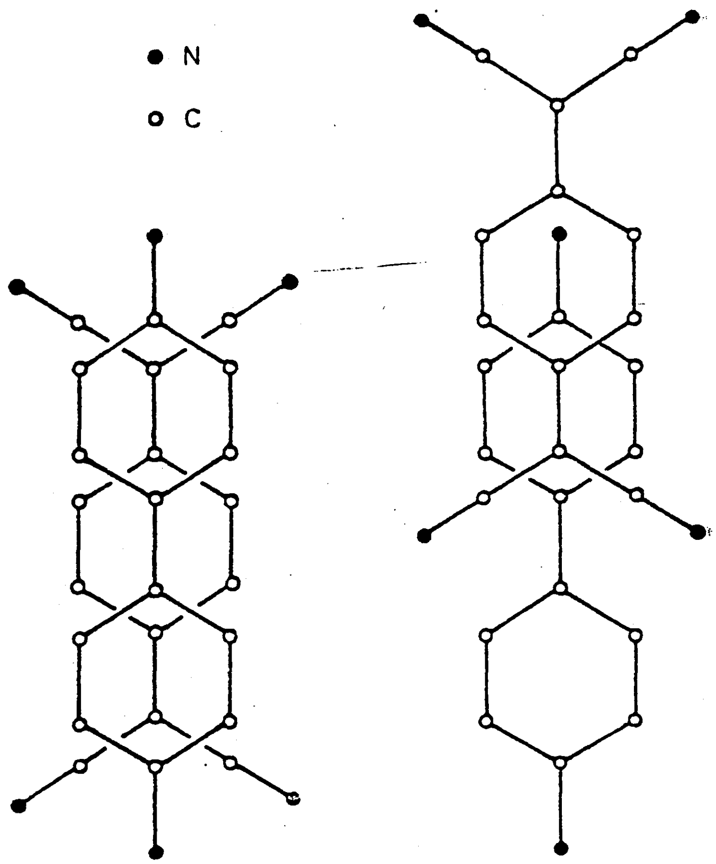

(a) (b)

Figure 1.7 (i) Benzidine - TCNQ ,(BD)(TCNQ)
(ii) Types of overlap observed in the 1:1 (benzidine)(TCNQ) complexes

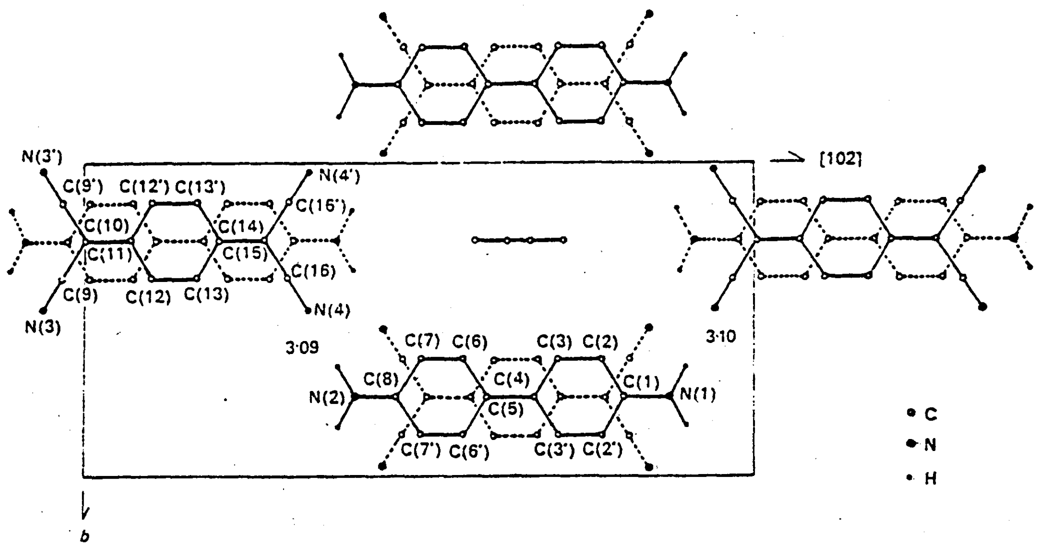

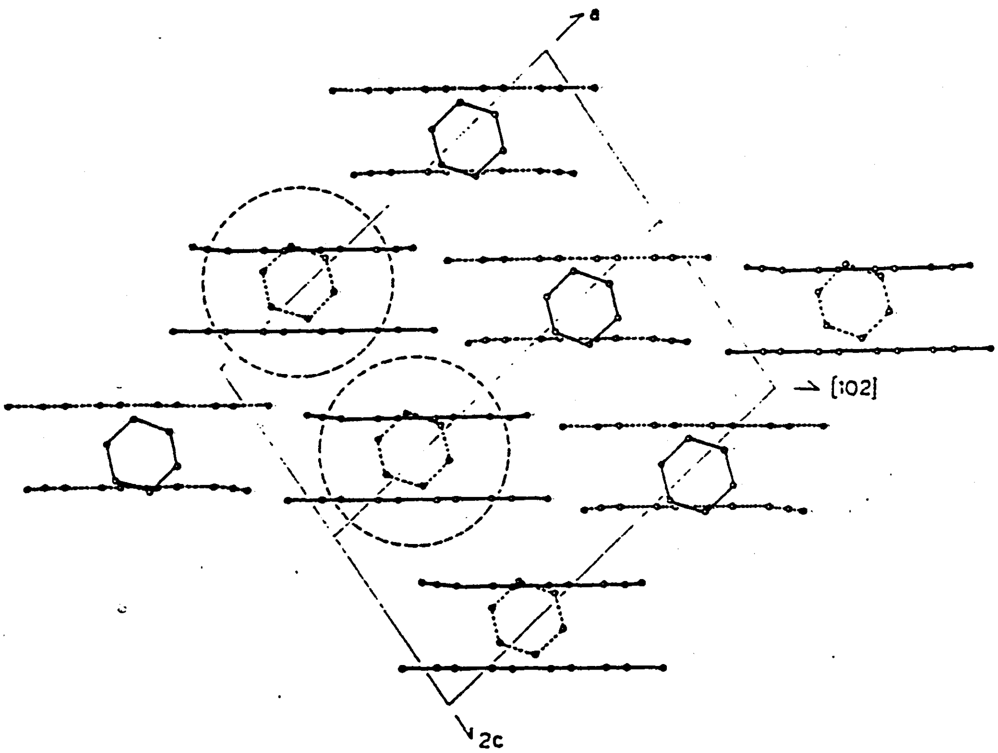

Figure 1.8 Packing diagrams for (BD)(TCNQ)(C_6H_6)

to semi-conducting range, the exact magnitude depending upon:

(a) the degree of overlap between the donor and acceptor moieties;

(b) the extent of charge-transfer;

(c) the extent of hydrogen bonding;

(d) the presence of inclusion molecules.

(iii) The homosoric class of TCNQ complexes

Most of the known TCNQ complexes fall into the homosoric and heterosoric classes. The homosoric complexes give rise to good electrical properties whilst the heterosoric and nonsoric complexes give rise to poor electrical properties. Consequently, it is the homosoric complexes which have received most interest and the structural features of representative examples are summarized in Table 1.1.

To be truly homosoric a TCNQ complex must exhibit six structural features:

(a) segregated stacks of TCNQ moieties and of cations, (Figure 1.5);

(b) a plane-to-plane stacking of the TCNQ molecules in columns (Figure 1.9);

(c) a regular interplanar spacing (d-spacing) of approximately 3.2Å, i.e. a monadic arrangement;

(d) good exocyclic double bond to quinonoid ring overlap, (Figure 1.10);

(e) the longitudinal staggering of adjacent TCNQ molecules must be in a consistent direction throughout the stack, (Figure 1.9);

(f) charge transfer must be incomplete between the TCNQ moieties in a given stack.

In most cases not all these conditions are satisfied and such complexes are often referred to as pseudosoric TCNQ complexes. The TCNQ molecules in a given column may stack for example not in the required monadic manner but rather group together to form diads, triads, tetrads or pentads, with irregular spacing between the constituent molecules. The modes of overlap within such pseudosoric structures vary from the

TCNQ complexes containing 'organic cations'.

Complex	TCNQ-TCNQ′ interplanar distances (Å)	Type of overlap	Type of TCNQ stacking	Ref.
(MEM)$(TCNQ)_2$ @ 113K	3.15 (in diads) 3.27 (between diads)	good poor	D sheet	65
(MEM)$(TCNQ)_2$ @ 348K	3.29 (average)	(good ((nearly good	D/M sheet	81
(TMPD)$(TCNQ)_2$	3.24 (average)	good	M sheet	42
(NH_4)(TCNQ)	3.31 (average)	good	M	68
$(MePh_3P)(TCNQ)_2$ @ 300K	3.20 (in tetrads) 3.58 (between tetrads)	good	T	48
(DMM)$(TCNQ)_2$	3.25 (in diads) 3.29 (between diads)	poor v.poor	D sheets	78
(Q)$(TCNQ)_2$	3.22 (average)	good	M	47
(HEM)$(TCNQ)_2$	3.23))(in tetrads) 3.31) 3.42 (between tetrads)	good poor good	T sheets	79
(DEM)$(TCNQ)_2$	3.14))(in diads) 3.19) 3.36))(between diads) 3.41)	good good good poor	D sheets	77

Complex	TCNQ-TCNQ′ interplanar distances (Å)	Type of overlap	Type of TCNQ stacking	Ref.
$(TEA)(TCNQ)_2$	3.22) (in tetrads)	good	T	57
	3.32)	good		
	3.34 (between tetrads)	poor		
$(M)_2(TCNQ)_3$	3.25 (in diads)	good	D	49
	3.24 (between diads)	poor		
$(TMA)(TCNQ)(I_3)_{\frac{1}{3}}$	3.23	good	M	69
$(NMETh)(TCNQ)_2$	3.30	good	T	60
$(NEMTh)(TCNQ)_2$	3.06 (in diads)	good	D	66
	3.22 (between diads)	poor		
$(DMPA)(TCNQ)_4$	3.20	good	T	90
	3.29	poor		
$(DPMBz)(TCNQ)_4$	3.22	good	T	83
	3.39	poor		
	3.40	poor		
$(DBzBP)(TCNQ)_4$	3.16) (in tetrads)	good	T	82
	3.23)			
	3.62 (between tetrads)			
$(DBzPE)(TCNQ)_5$	3.20) (in pentads)	good	P	88
	3.23)			
	3.40 (between pentads)			

Notes:

(i) Stacking

M - monadic

D - diadic

D/M - almost monadic

Sheet - TCNQ stacks arranged in two-dimensional sheets.

T - tetradic

P - pentadic stacking

(ii) Type of overlap

good - exocyclic double bond to quinonoid ring type.

nearly good - shifted ring-to-shifted ring, nearly exocyclic double bond to quinonoid ring type.

poor - ring to ring, little direct overlap.

(i)

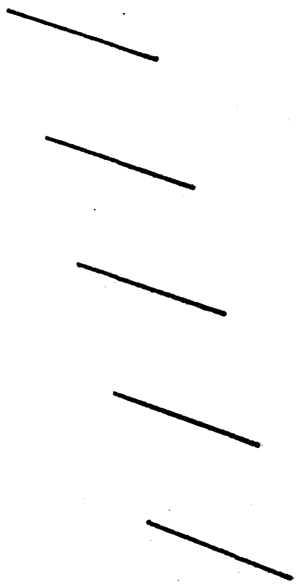

Longitudinal staggering of TCNQ molecules in a consistent direction and, a parallel plane-to-plane stacking of the TCNQ moieties in a given stack.

(ii)

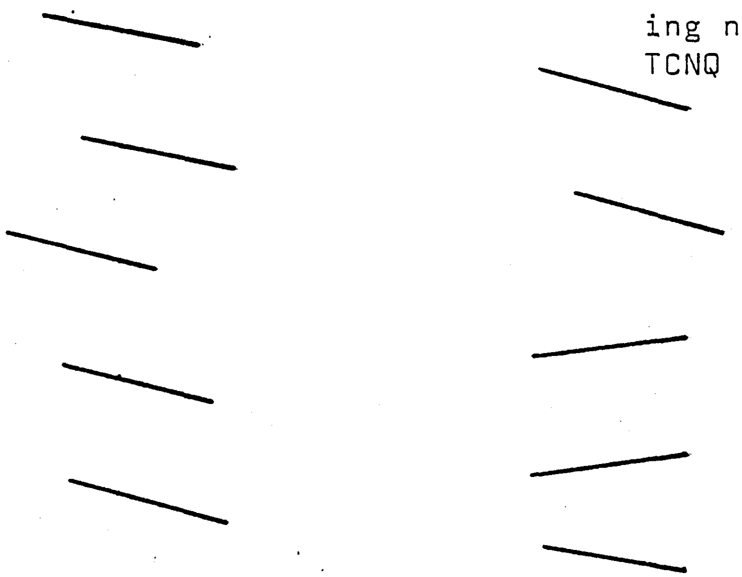

Longitudinal staggering not consistent and TCNQ moieties not stacked plane to-plane.

——— represents a side-on view of a TCNQ molecule

Figure 1.9 (i) Homosoric requirements fulfilled
(ii) homosoric requirements not fulfilled

(i)good exocyclic double-bond to quinonoid ring

(ii)shifted ring-to-ring, little direct overlap

(iii)ring-to-ring

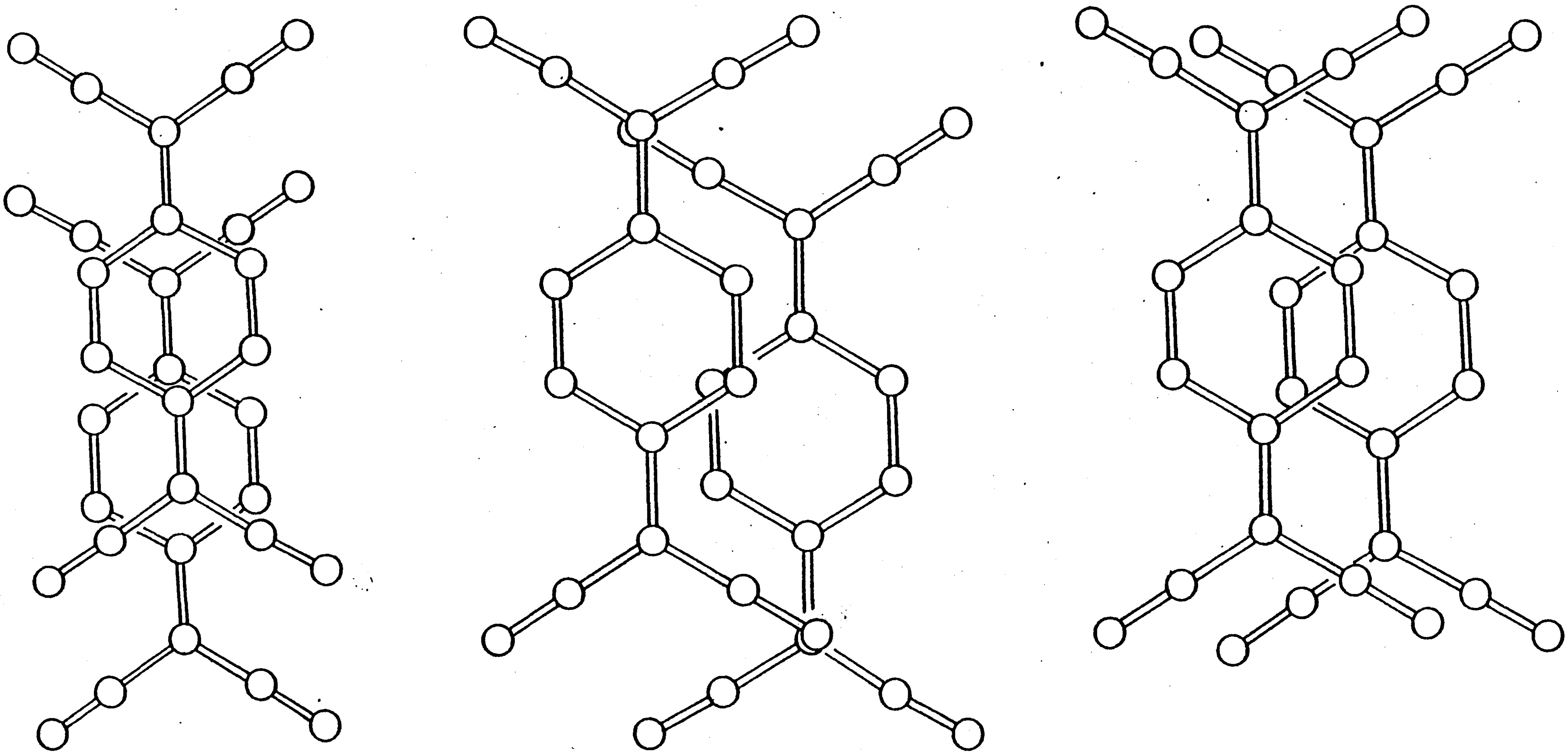

Figure 1.10 Types of overlap observed in TCNQ complexes belonging to the homosoric category

(homosoric) good eclipsed double bond to quinonoid ring type, to a ring-to-shifted-ring type, to very little direct overlap between adjacent molecules (Figure 1.10). It is primarily the nature of the TCNQ stack in these complexes which determines the conductivity. There are numerous factors which may influence the nature of the stacking in homosoric complexes.

(a) <u>The role of the cation</u>

The major role of the cation appears to be that of providing an attractive potential along the stack. There are two types of cation associated with homosoric TCNQ complexes; the closed-shell donor (e.g. NMP,[40,55,59] quinolinium ion[47]), and the open-shell radical which, when complexed with TCNQ, gives rise to partial charges on both moieties (e.g. TTF).[99-102,105,111,130] The closed-shell cation does not contribute to the electrical conductivity of a particular complex in a direct way and the electronic conduction occurs only in the TCNQ stacks. The open-shell radical cation functions in a more direct manner in that conduction processes occur along the cationic stack (movement of positive holes) as well as along the TCNQ stack (movement of electrons). The most highly conducting complexes of TCNQ have been shown to be those of a 1:1 stoichiometry, and especially those containing open-shell radical cations, with an average extent of charge-transfer of 0.5-0.6 from the radical cation to the TCNQ molecule e.g. (TTF)(TCNQ)[99-102,105,111,130], (TMTTF)(TCNQ).[115]

A number of complexes formed between TCNQ and various bipyridinium cations fall into the homosoric and pseudosoric categories.[82-97] The overall length of the cation in these salts is said to influence the mode of stacking within the TCNQ columns and consequently influence the conductivity.

(b) <u>The role of interstack interactions</u>

For a TCNQ complex to be a good conductor the TCNQ stacks are required to be as one-dimensional as possible. A noticeable feature of the complexes of TCNQ are the interactions between the cation stacks and the TCNQ stacks, involving both hydrogen bonding and also dipole-dipole interactions. The greater are such interactions, the less one-dimensional the TCNQ stacks become with a consequent lowering of the conductivity of the complex. In addition the presence of weak electrostatic (CN - - - - HC) interactions between TCNQ molecules in adjacent columns is often found to stabilize two-dimensional TCNQ sheets. The presence of such sheets, as opposed to monadic columns also leads to a reduction in conductivity. In $(M)_2(TCNQ)_3$ [49] hydrogen bonding exists between both the morpholinium ions (M) and also between the morpholinium ions and the TCNQ stacks.

(c) The role of disorder

A number of TCNQ complexes are said to be 'disorder-stabilized', whereby the presence of appropriate random disorder stabilizes the periodic lattice distortions associated with the TCNQ stacking. The latter distortions are inherent in quasi-one-dimensional systems and effectively lead to a reduction in conductivity. There are two major ways in which disorder may be introduced into TCNQ complexes:

(i) incorporation of a statistically-disordered cation,

(ii) inclusion of small molecules e.g. solvent molecules, into the lattice.

The extent of disorder introduced by a statistically-disordered cation is often found to be temperature dependent. As the temperature is raised the cation is able to become more disordered and this allows the TCNQ stacks to become more ordered and homosoric e.g. $(TEA)(TCNQ)_2$,[75] wherein the TEA cation has twofold disorder and is a good semiconductor.[76]

Consider disorder introduced by the inclusion of small molecules. Such molecules are normally present in the lattice in non-stoichiometric quantities e.g. $(TMA)(TCNQ)(I_3)_{\frac{1}{3}}$ [70,73] (Figure 1.11), $(DEPE)(TCNQ)_4(H_2O)_x$ [91,92,94]

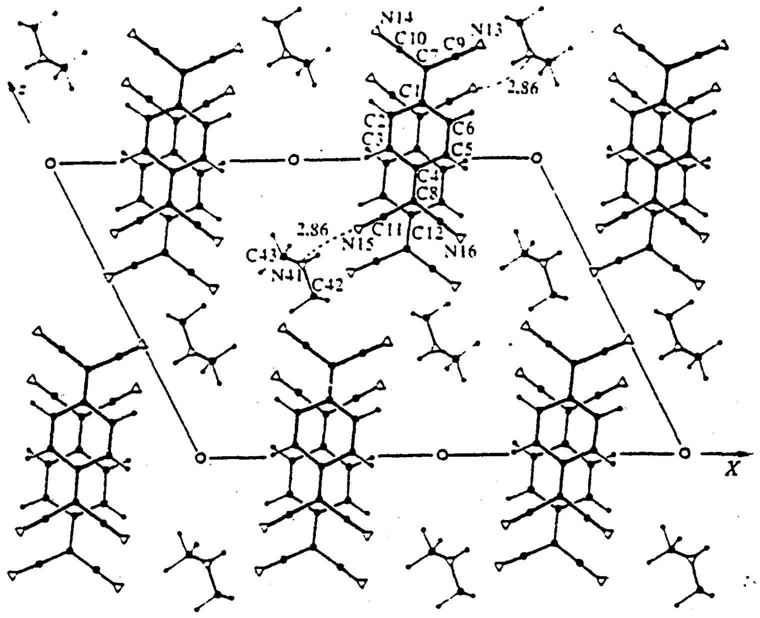

Figure 1.11 View down the y-axis in (TMA)(TCNQ)$(I_3)_{1/3}$

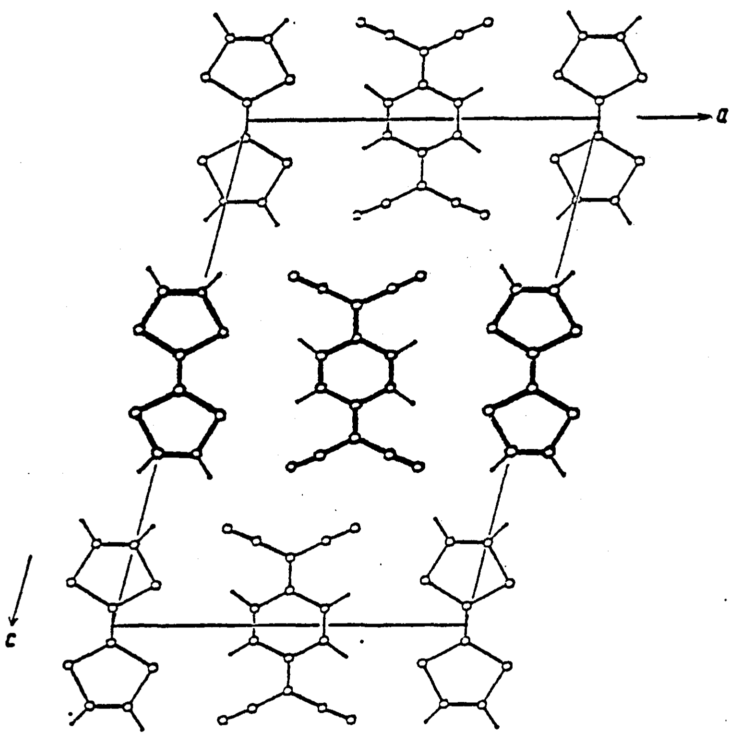

Figure 1.13 View down the b-axis in (TTF)(TCNQ)

where x is a small number. The disorder imparted by the inclusion of small quantities of such molecules is an important factor in suppressing one-dimensional transitions to a less conducting state i.e. Peierls transitions. Another factor to be considered is whether the inclusion molecules are formally neutral or charged. If charged, as in typical semi-conductors, they will help to enhance the conductivity by providing extra electrons with associated energy levels which fit into the band gap and thus create a favourable conduction pathway. A significant amount of disorder implies a significant density of states at the Fermi level and hence an enhancement of conductivity.

(d) <u>The influence of temperature and pressure</u>

The crystal structures of many TCNQ complexes have been carried out over a range of temperatures. The effect of increasing temperature is often to enhance the homosoric character of the complex. As previously seen, increasing the temperature may lead to disorder of the cation and a consequent reduction of cation-TCNQ interstack interactions, thereby increasing the uni-dimensionality and conductivity of the complex. This is discussed in more detail in Chapter 3.

Studies have been carried out to determine the influence of pressure upon the solid state structures of TCNQ complexes. (HMTTF)(TCNQ) shows the most dramatic effect of varying pressure.[124] The temperatures of the two phase transitions (43 and 49K) decrease when pressure is increased and conductivity is also found to be pressure dependent. At 10 k-bar the complex becomes metallic at low temperatures. At normal pressure a maximum conductivity is reached near 75K, and the phase transition at 43K is associated with the appearance of a periodic lattice distortion of HMTTF chains. Thus when pressure and low temperatures are applied the system changes from a good semi-conductor to a metallic conductor. Likewise in the complex (TSeF)(TCNQ) the phase transition observed at 29K, at atmospheric pressure, is strongly sensitive to the effect of pressure.[118] In (TTF)(TCNQ) the main effect of pressure is to

3.104(2)Å] and the TTF[3.476(2) → 3.417(1)Å] stacks.[105]

It is feasible that one of the effects of high pressure in TCNQ complexes could be the formation of TCNQ dimers containing a σ-bond (Figure 1.12) as found for example in $(NEP)_2(TCNQ_2)$[151] and $Pt(2,2'\text{-}dipy)_2^{2+}\ (TCNQ)_2^{2-}$.[139]

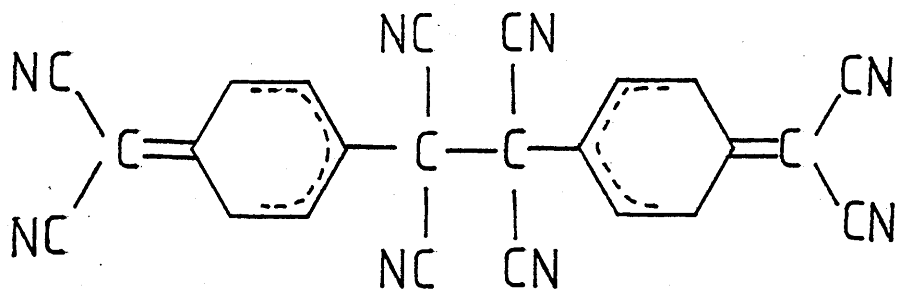

Figure 1.12 $(TCNQ)_2$dimer

1.2.5 Structures of selected homosoric and pseudosoric TCNQ complexes

The TCNQ complexes which have homosoric or pseudosoric structures may be divided into three groups:

(i) 'organic' complexes;[40-97]

(ii) complexes containing TTF and its cogeners;[98-132]

(iii) complexes containing cationic metal species.[133-150]

(i) 'Organic' complexes[40-97]

Structural details for selected structures of this type are given in Table 1.1. Few of the complexes formed by organic cations and TCNQ are truly homosoric. Some of the most highly conducting are (NMP)(TCNQ),[40,55,59] $(Q)(TCNQ)_2$[47] and $(DEPE)(TCNQ)_4\ (H_2O)_x$.[92] These have monadic stacks of TCNQ molecules with short interplanar spacings and good exocyclic double bond to quinonoid ring overlap. In $(Q)(TCNQ)_2$[47] the cation is disordered, thereby enhancing the conductivity, while in $(DEPE)(TCNQ)_4$-$(H_2O)_x$[92] the presence of non-stoichiometric amounts of water increases both the disorder in the system and also the electrical conductivity (compared with the anhydrous salt).

In 1973 the structure and electronic properties of a new type of complex, (TTF)(TCNQ),[99-102] were reported, (Figure 1.13). The complex is very one-dimensional and exhibits a high electrical conductivity. The TCNQ complexes formed by TTF and its cogeners (e.g. TMTTF,[115] HMTTF,[120] TSeF,[126] DTTSeF[113] etc.) give rise to some of the most one-dimensional organic conductors known, nearly all belonging to the homosoric (pseudosoric) category. It is interesting to note that the complexes in which selenium atoms are incorporated generally exhibit better electrical properties, (Table 1.2).

In this class of complex both the cationic and the anionic stacks are thought to be responsible for the high conductivities observed. Both the intermolecular TCNQ-TCNQ distances and also the cation-cation stacking distances are shorter than the van der Waals' distances. The overlap between consecutive molecules is of a ring-to-double bond type for both TCNQ moieties and also for TTF radical cations (and analogues), (Figure 1.14). While the packing may be regular in many of these complexes, the distances between consecutive anions or cations can vary considerably from structure to structure (Table 1.3). The relative arrangement of neighbouring stacks may vary also. Thus the structures of (TTF)(TCNQ)[102] and (TSeF)(TCNQ)[126] are isostructural but the structure of the closely related (HMTSeF)(TCNQ)[110] differs significantly (Figure 1.15). In (TTF)(TCNQ)[102] and (TSeF)(TCNQ)[126] the TCNQ moieties form a two-dimensional array within which there are isolated columns. Parallel to this array is a sheet of TTF or TSeF moieties, (Figure 1.13). In (HMTSeF)(TCNQ)[110] however, rather than two-dimensional sheets of TCNQ being formed, each column of TCNQ moieties is surrounded by columns of HMTSeF moieties and vice versa. The (HMTSeF)(TCNQ)[110] complex shows a further difference in the structural arrangement adopted in that it adopts a 'parallel pattern' of stacking, while (TTF)(TCNQ)[102] and (TSeF)(TCNQ)[126] adopt a 'cross-like' pattern (Figure 1.14). The overall

Table 1.2 Conductivity data for charge-transfer systems of the TTF family of TCNQ complexes

Complex	$\sigma_{//}$(300K)/S^{-1} cm^{-1}	Ref.
(TTF)(TCNQ)	600	111
(DMTTF)(TCNQ)	50	119
(TMTTF)(TCNQ)	350	117
(TTTF)(TCNQ)	400	128
(HMTTF)(TCNQ)	500	116
(TSeF)(TCNQ)	800	103
(TMTSeF)(TCNQ)	1200	127
(HMTSeF)(TCNQ)	2000	107
(DTTSeF)(TCNQ)	600	113
(DEDMTSeF)(TCNQ)	500	127
(DSeDTF)(TCNQ)	500	106
(TTT)(TCNQ)	20-160	104
(TMTTF)(DMTCNQ)	120	127
(TMTSeF)(DMTCNQ)	400-600	121,127

Notes: $\sigma_{//}$ (300K) is the conductivity in the stacking direction at 300K.

in the cationic stacks in the TTF-family of charge-transfer complexes

Complex	Distances between		Ref.
	Cations (Å)	Anions (Å)	
(TTF)(TCNQ)	3.47	3.17	102
(TMTTF)(TCNQ)	3.53	3.27	115
$(TMTTF)_{1.3}(TCNQ)$	3.59	3.24	109
(TTTF)(TCNQ)	3.58	3.20	122
(HMTTF)(TCNQ)	3.57	3.23	120
(DEDMTTF)(TCNQ)	3.62	3.31	129
(METTF)(TCNQ)	3.58	3.32	125
$(TTT)(TCNQ)_2$	3.52	3.18	104,108
(TSeF)(TCNQ)	3.52	3.21	126
(TMTSeF)(TCNQ)	3.60	3.26	114
(HMTSeF)(TCNQ)	3.61	3.21	110
(TMTSeF)(DMTCNQ)	3.64	3.31	121

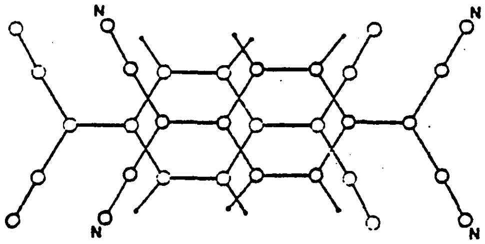

(a) Overlap between TCNQ moieties

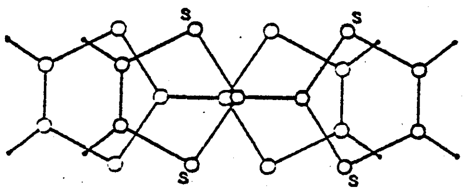

(b) Overlap between cationic moieties in (TTF)(TCNQ)
and analogues of TTF

represents a side-on view of a TCNQ molecule

represents a side-on view of a TTF or TTF analogue

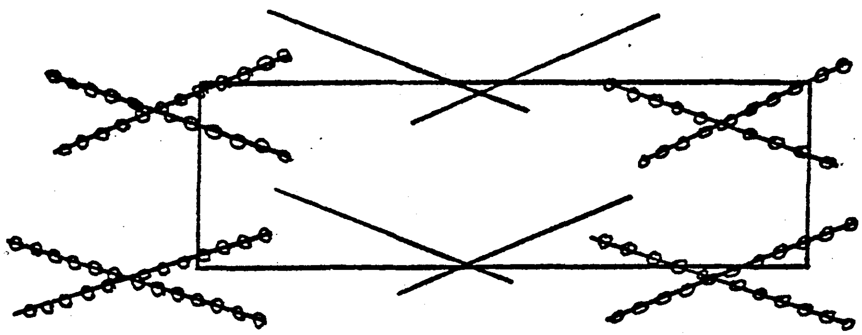

(c) 'Cross-like' pattern

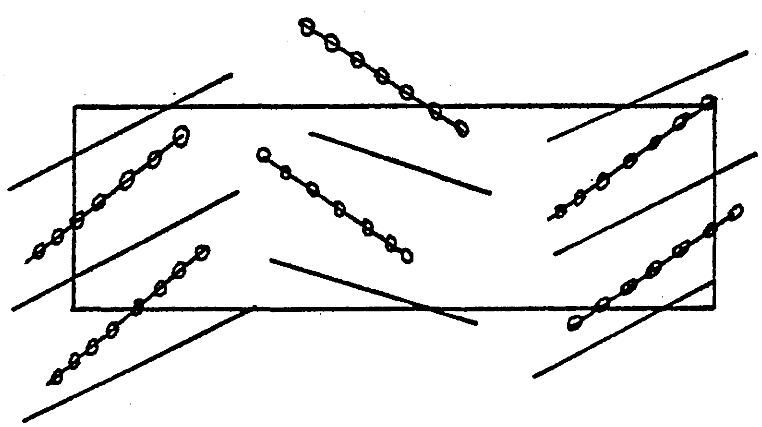

(d) 'Parallel-pattern'

Figure 1.14 Overlaps and mode of stacking in the complexes of TCNQ with members of the TTF-family of radical cations

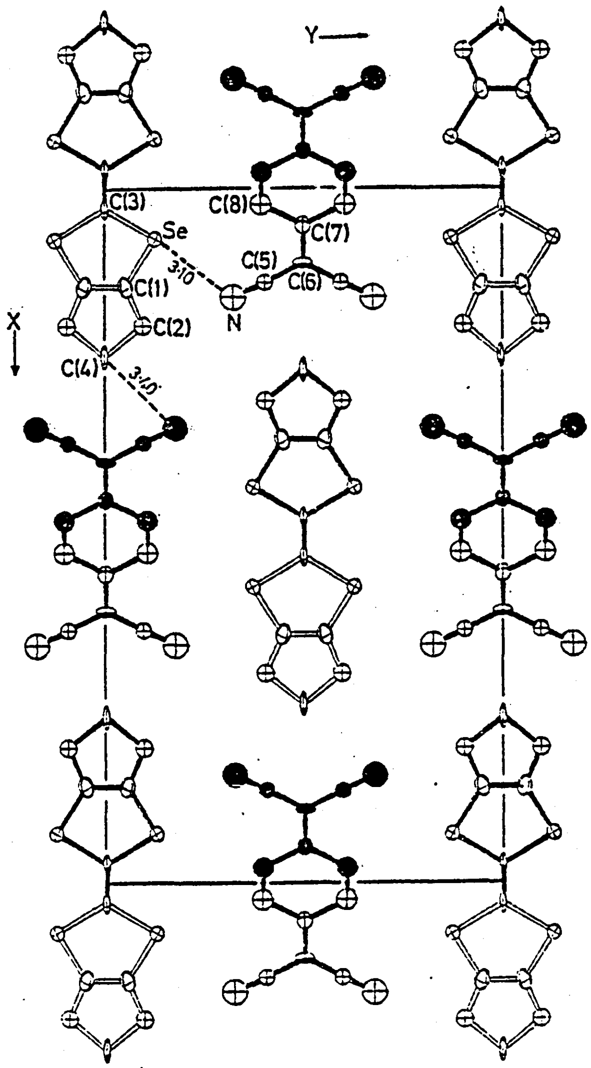

Figure 1.15 View down the z-axis for
(HMTSeF)(TCNQ)

arrangement adopted by the (HMTSeF)(TCNQ) complex appears to favour a higher electrical conductivity (Table 1.3).

(iii) <u>TCNQ complexes containing cationic metal species</u>

Complexes of TCNQ containing cationic metal species have recently been reported.[133-150] It is well established that square-planar complexes of $[Pt(CN)_4]^{n-}$ with halogen counter-ions form lustrous, homogeneous materials of stoichiometry, $K_2Pt(CN)_4X_{0.3}(H_2O)_3$, [X = Br, Cl].[133] These complexes have a partially-filled electron energy band, arising from the overlap of d_z2 atomic orbitals on adjacent platinium atoms. It is reasonable to assume that complexes comprising square-planar cationic functions and planar TCNQ anionic functions should be capable of quasi-one-dimensionality and thus high conductivity, with both the cationic and anionic stacks involved in the conduction process.

Complexes have been prepared which do exhibit homosoric characteristics. $[Pt(dipy)_2](TCNQ)_3$[143] for example comprises segregated stacks of $[Pt(dipy)_2]^{2+}$ ions and TCNQ moieties. The latter are grouped in triads with favourable overlap within each triad but poor overlap between adjacent triads.[143] The unit cell parameters of $[Pt(dipy)_2](TCNQ)_3$ are similar to those found in [1,4-di-(N-quinolinium methyl)benzene]-$(TCNQ)_3$,[138] and the nature of the stacking in both complexes is effectively the same.

$[Pd(CNMe)_4](TCNQ)_4 \cdot 2MeCN$[137] is an example of a homosoric salt with solvent molecules trapped in the crystal lattice. The TCNQ stacks comprise tetradic groups of molecules with irregular interplanar spacings of 3.29, 3.32 and 3.15Å within each tetrad, and 3.69Å between adjacent tetrads. The conductivity measurements made on both pressed pellet and single-crystal samples are consistent with a quasi-two-dimensional semi-conductor.

Several complexes formed between metal sandwich complexes and TCNQ have been prepared and their structures reported. Thus the chromium-arene complexes $[(\eta^6\text{-}C_6H_5Me)_2Cr](TCNQ)_2$ and $[(\eta^6\text{-}C_6H_5Me)_2Cr](TCNQ)$[134]

A number of ferrocene derivatives have been complexed with TCNQ to give one-dimensional charge-transfer complexes of which [$Fe(\eta^5-C_5H_4Me)_2$]-$(TCNQ)_2$ [148] is conducting and belongs to the homosoric category, as does $[Fe(\eta^5-C_5H_4)_2(CH_2)_3](TCNQ)_2$.[150]

In recent years, direct methods of phase determination in X-ray crystal structure analysis have come to the fore. Powerful computer programs for aiding analysis and refinement, such as SHELX[153] and MULTAN,[154] have made possible the routine solution by direct methods techniques of both centro- and non-centrosymmetric problems. An outline of crystal structure analysis and the application of direct methods is given in the following sections.

2.2 Diffraction of X-rays by Single Crystals

A single crystal is the most highly-ordered state of a solid in which the atoms, or ions, or molecules are arranged in a regular three-dimensional manner. Such regularity allows a single crystal to act as a diffraction grating for radiation of an appropriate wavelength. Cu-Kα and Mo-Kα X-radiation are commonly used in single crystal studies since the wavelengths (1.5418 and 0.71069Å respectively) are of the same order as the interatomic distances within a crystal. The scattering matter i.e. the atoms, or ions, or molecules may be represented in a fundamental block, termed the unit cell, which repeats itself in all directions. The unit cell is characterized by three non-coplanar axial lengths, denoted a, b, c, and three interaxial angles, denoted α, β, γ.

There are seven crystal systems, each described by different combinations of the axial lengths and interaxial angles of the unit cell. There are fourteen types of lattice, primitive and non-primitive, belonging to the seven crystal systems. These lattices are known as Bravais[155] lattices. Combining the thirty-two possible point groups and the fourteen Bravais lattices gives rise to the two hundred and thirty unique space groups, which are described in detail in 'The International Tables for X-ray Crystallography, Volume I'.[156]

Crystal and molecular structures may be elucidated using collected diffraction data. The electrons in the atoms are capable of scattering X-rays and Bragg[157] noted that the diffracted radiation behaves as if it had been reflected. It is for the latter reason that the X-ray diffraction maxima from single crystals are generally called reflections. The diffraction occurs when a set of planes are suitably orientated with respect to the incident beam of X-radiation. Each set of planes is characterized by Miller indices, (hkl), defined such that one of the set of planes intersects the three axes of the unit cell at the points a/h, b/k, c/l. The conditions necessary for diffraction

$$n\lambda = 2d_{hkl}\sin\theta \tag{2.1}$$

where d_{hkl} is the interplanar spacing, Θ is the angle of the incident radiation to the set of planes, λ is the wavelength of the radiation, and n is the order of diffraction (i.e. the difference in path length for waves reflected by successive planes).

2.3 Structure Factors

For a given diffraction maximum, arising from reflection off a set of planes with Miller indices (hkl), the resultant of adding the N waves scattered in that direction by the N atoms in the unit cell, is known as the structure factor, F_{hkl}. The structure factor is related to the positions of the atoms in the unit cell by;

$$F_{hkl} = \sum_{j=1}^{N} f_j \exp[2\pi i(hx_j + ky_j + lz_j)] \tag{2.2}$$

where f_j is the scattering factor for the j^{th} atom and x_j, y_j, z_j are its fractional co-ordinates in the unit cell.

The scattering factor of an atom depends upon the total number of electrons that the atom contains and upon $\sin\theta/\lambda$. At $\sin\theta/\lambda = 0$ the value of the scattering factor is equal to the total number of electrons in the atom, but as $\sin\theta/\lambda$ increases so the scattering factor decreases since the finite size of the electron cloud causes the scattering in one part of the electron density to be out of phase with that scattered in another part. The scattering factors are thus calculated on the basis of the electron distribution in a stationary atom. However, in practice, the atoms in crystals are always vibrating about their mean points and the effect of such vibration is to smear the electron cloud over a largervolume thereby reducing the scattering power of the atom. Thus, the scattering factor for a stationary atom, f_o, is modified to give the actual value f;

$$f = f_o \exp[-8\pi^2 U(\sin^2\theta)/\lambda^2] \tag{2.3}$$

isotropic temperature factor.

Towards the end of a structure analysis a more sophisticated description of thermal vibration is often used. The assumption of spherical symmetry is abandoned and the single isotropic temperature factor is replaced by an anisotropic temperature factor. The latter consists of six parameters which describe the magnitude and orientation of a vibration ellipsoid. The atomic scattering factor for atoms considered to be anisotropic is given by;

$$f = f_o \exp[-2\pi^2(U_{11}h^2a^{*2} + U_{22}k^2b^{*2} + U_{33}l^2c^{*2} + 2U_{12}hka^*b^* + 2U_{13}hla^*c^* + 2U_{23}klb^*c^*)] \qquad (2.4)$$

where the U_{ij} values are related to the vibrations in particular directions in the crystal.

2.4 Structure Amplitudes

The structure factor, F_{hkl}, is a complex quantity and has both a magnitude, known as the structure amplitude, $|F_{hkl}|$, and also a phase, ϕ_{hkl}. The structure amplitude is related to the intensity of the reflection by;

$$I_{hkl} \propto |F_{hkl}|^2 \qquad (2.5)$$

where I_{hkl} is the intensity. The expression for the structure factor can be resolved into its real and imaginary components,

A_{hkl} and B_{hkl} where;

$$A_{hkl} = \sum_{j=1}^{N} f_j \cos[2\pi(hx_j + ky_j + lz_j)] \qquad (2.6)$$

and,

$$B_{hkl} = \sum_{j=1}^{N} f_j \sin[2\pi(hx_j + ky_j + lz_j)] \qquad (2.7)$$

so that $F_{hkl} = A_{hkl} + iB_{hkl}$. The phase angle, ϕ_{hkl}, is given by;

$$\phi_{hkl} = \tan^{-1}(B_{hkl}/A_{hkl}) \qquad (2.8)$$

the above expressions in that for each fractional co-ordinate (x, y, z), there is an associated fractional co-ordinate (-x, -y, -z), and examination of the expressions shows that the sine terms cancel and the structure factor expression reduces to;

$$F_{hkl} = 2 \sum_{j=1}^{N/2} f_j \cos 2\pi(hx_j + ky_j + lz_j) \qquad (2.9)$$

where the summation is now over an acentric half of the atoms in the unit cell. The phase angle is then either 0 or 180° corresponding to the assignment of a positive or negative sign to the structure amplitude $|F_{hkl}|$.

2.5 Data Collection and Processing

For all structures in this thesis, the unit cell dimensions have been obtained from preliminary X-ray photographs using Weissenberg and precession goniometers. From these photographs, information may be obtained about the possible space group, by examination of the systematic absences.

The intensity measurements for four structures were made on a Stöe Stadi-2 two-circle diffractometer. The latter is essentially a Weissenberg camera with a scintillation counter replacing the film cylinder. The background-ωscan-background technique was used for data collection, whereby the counter remains stationary, set at a particular 2θ value for the layer being collected, and the crystal rotates by small steps in ω (0.01 per second). Background measurements were made at each extremity of the scan. The scan range, $\Delta\omega$, selected was dependent upon the equi-inclination angle, μ, and upon θ as given by;

$$\Delta\omega = A + B \sin\mu/\tan\theta \qquad (2.10)$$

The values of A and B were optimized by step scanning a number of reflections prior to data collection.

The intensity of a reflection, I_{hkl}, is given by;

2t

where T is the scan count, B_1, B_2 are the background counts at either end of the scan, C is the scan time and t is the time for the background measurements (normally thirty seconds). The error in the measurement of I_{hkl}, $\sigma(I_{hkl})$ is given by;

$$\sigma(I_{hkl}) = \left[T + \frac{(B_1 + B_2)C^2}{4t^2}\right]^{\frac{1}{2}} \qquad (2.12)$$

The reflections used for structure analysis are based upon the value of $I_{hkl}/\sigma(I_{hkl})$, so that, in many instances only those reflections having $I_{hkl}/\sigma(I_{hkl}) \geqslant 3.0$ are included in subsequent structure analyses.

Intensity data for one crystal were collected[158] on an Enraf-Nonius four-circle diffractometer using a variable scan speed and an $\omega - 4/3\,\theta$(goniometer-counter) scanning ratio, as optimized by peak-analysis routines. The scan interval was given by;

$$\Delta\omega = (1.5 + 0.525 \tan\theta) \qquad (2.13)$$

The net intensity is given by;

$$I_{hkl} = T - 2(B_1 + B_2) \qquad (2.14)$$

where B_1, B_2 are the background counts measured during the first and last sixths of the $\Delta\omega$-scan. The error in the measured intensity is given by;

$$\sigma(I_{hkl}) = [T + 4(B_1 + B_2) + 0.0009\, I_{hkl}^2]^{\frac{1}{2}} \qquad (2.15)$$

The intensity data collected from the Stöe Stadi-2 two-circle diffractometer must be corrected for several non-structure dependent effects, namely Lorentz, polarization and absorption effects.

2.5.1 Lorentz Effects

The Lorentz factor, L, depends on the measurement technique employed and compensates for the differing lengths of time that a set of planes are in the diffraction position. For Weissenberg geometry, with equi-inclination angle, μ, the correction factor is given by;

and the intensity data are corrected by multiplying by the reciprocal of L.

2.5.2 Polarization Effects

The polarization effect is independent of the method of data collection and arises from the fact that upon diffraction X-rays are polarized and this causes a reduction in intensity. Polarization arises from two sources;

(i) the crystal itself does not reflect waves vibrating in all directions with equal efficiency so that the reflected beam is partially polarized. The correction factor is given by;

$$p = (1 + \cos^2 2\theta)/2 \qquad (2.17)$$

and the intensity data corrected by multiplying by the reciprocal of p.

(ii) The Mo-Kα radiation used with the Stöe Stadi-2 two-circle diffractometer is monochromated using a graphite crystal monochromator rather than a zirconium filter. The graphite also partially polarizes the X-ray beam leading to a more complex expression for the overall polarization effects.

2.5.3 Absorption Effects

For structures containing no heavy atoms, as in the present work, the absorption effect are generally negligible since the absorption coefficient, μ, depends on the number and types of atoms present in the unit cell. If t is the integral path length, then the intensity of the beam, I'_{hkl}, after passing through the crystal is given by;

$$I'_{hkl} = I_{hkl} \exp(-\mu t) \qquad (2.18)$$

For the structures reported here only Lorentz and polarization factors were applied thus,

$$I_{hkl} = \frac{K^2 \, |F_{hkl}|^2}{LP} \qquad (2.19)$$

these correction factors a set of observed structure amplitudes, $|F_o|$, may be obtained and these may be used in the subsequent structure analyses.

2.6 Fourier Syntheses

Since it is the electrons in a crystal structure which scatter the X-rays, a single crystal may be considered as a periodic three-dimensional distribution of electron density. Periodicity may be expressed as a Fourier series, such that the electron density at the point (x, y, z), $\rho(x, y, z)$, is given by;

$$\rho(x, y, z) = \frac{1}{V_c} \sum_h \sum_k \sum_l |F_{hkl}| \cos[2\pi(hx + ky + lz) - \phi_{hkl}] \qquad (2.20)$$

where $|F_{hkl}|$ is the experimentally determined structure amplitude, $|F_o|$, and ϕ_{hkl} is the associated phase. While $|F_o|$'s are readily obtained from the experimentally measured intensities, the phases, ϕ_{hkl}, are not experimentally determined and this constitutes the 'phase problem' i.e. only when sufficient phases are known can Fourier syntheses be calculated and hence atoms located.

The Fourier synthesis given by equation 2.20 is referred to as an observed Fourier and is generally used in the early stages of analysis. In the later stages difference Fourier syntheses are often employed;

$$\rho(x, y, z) = \frac{1}{V_c} \sum_h \sum_k \sum_l (|F_o| - |F_c|) \cos[2\pi(hx + ky + lz) - \phi_{hkl}] \qquad (2.21)$$

where $|F_o|$ is the observed structure amplitude and $|F_c|$ is the calculated structure factor. $|F_c|$ is calculated from the positions of the atoms already located;

$$|F_c| = |F_{hkl}| = (A_{hkl}^2 + B_{hkl}^2)^{\frac{1}{2}} \qquad (2.22)$$

A_{hkl} and B_{hkl} are calculated using the equation 2.6 and 2.7.

The atom positions located by Fourier techniques are only approximate and refinement is carried out using least-squares techniques. The function mimimized is,

$$D = \sum_{hkl} w_{hkl}(|F_o| - |kF_c|)^2 \tag{2.23}$$

$$= \sum w\Delta^2$$

where w_{hkl} is the weight applied to each $|F_o|$ and k is the scale factor to put $|F_o|$ and $|F_c|$ on the same scale. In the early stages of refinement unit weights ($w = 1$) are used but in the final stages non-unit weights are applied;

$$w = a/[\sigma^2(|F_o|) + b(|F_o|)^2] \tag{2.24}$$

a and b are refined so as to minimize the variation of $w\Delta^2$ over ranges of $|F_o|$. The minimization of D is achieved by differentiating the right-hand side of equation 2.23 with respect to each of the structural parameters in turn and setting the derivative to zero. This produces a set of n equations in n unknowns called the 'normal' equations, having the form,

$$\sum_{hkl} w_{hkl}(|F_o| - |kF_c(p_1, p_2, \ldots, p_n)| \frac{\partial |kF_c(p_1, \ldots, p_n)|}{\partial pj} = 0$$

$$(j = 1, 2, \ldots, n) \tag{2.25}$$

However, the functional form of the structure factor is non-linear and so the 'normal' equations are not directly solvable. In such cases $|F_c|$ is expanded as a Taylor series and terms higher than the first are ignored so that;

$$|kF_c(p_1, \ldots, p_n)| = |kF_c(a_1, \ldots, a_n)| + \frac{\partial |kF_c|}{\partial p_1}\Delta p_1 + \ldots$$

$$\ldots + \frac{\partial |kF_c|}{\partial p_n}\Delta p_n \tag{2.26}$$

where $p_1, \ldots, p_n$ may be any of the scale, positional, or thermal 'normal' equations then become linear in the shifts of each parameter,

Δp_j;

$$\sum_{hkl} w_{hkl}\{|F_o| - |kF_c(a_1, \ldots\ldots, a_n)| - \frac{\partial|kF_c|}{\partial p_1}\Delta p_1 - , \ldots$$

$$\ldots - \frac{\partial|kF_c|}{\partial p_n}\Delta p_n\}\frac{\partial|kF_c|}{\partial p_j} = 0 \qquad (2.27)$$

$(j = 1, 2, \ldots\ldots, n)$

$$\sum_{hkl} w_{hkl}\left[\frac{\partial|kF_c|}{\partial p_1}\right]^2 \Delta p_1 + \sum_{hkl} w_{hkl}\frac{\partial|kF_c|}{\partial p_1}\,\frac{\partial|kF_c|}{\partial p_2}\Delta p_2 + \ldots$$

$$\ldots + \sum_{hkl} w_{hkl}\frac{\partial|kF_c|}{\partial p_1}\,\frac{\partial|kF_c|}{\partial p_n}\Delta p_n = \sum_{hkl} w_{hkl}\{|F_o| - |kF_c|\}\frac{\partial|kF_c|}{\partial p_1}$$

$$\vdots \qquad\qquad\qquad\qquad \vdots$$

$$\sum_{hkl} w_{hkl}\frac{\partial|kF_c|}{\partial p_n}\,\frac{\partial|kF_c|}{\partial p_1}\Delta p_1 + \sum_{hkl} w_{hkl}\frac{\partial|kF_c|}{\partial p_n}\,\frac{\partial|kF_c|}{\partial p_2}\Delta p_2 + \ldots$$

$$\ldots + \sum_{hkl} w_{hkl}\left[\frac{\partial|kF_c|}{\partial p_n}\right]^2 \Delta p_n = \sum_{hkl} w_{hkl}\{|F_o| - |kF_c|\}\frac{\partial|kF_c|}{\partial p_n}$$

$$\begin{bmatrix} a_{11} & a_{12} & \cdots & a_{1n} \\ a_{21} & a_{22} & \cdots & a_{2n} \\ \vdots & \vdots & & \vdots \\ a_{n1} & a_{n2} & \cdots & a_{nn} \end{bmatrix} \begin{bmatrix} \Delta p_1 \\ \Delta p_2 \\ \vdots \\ \Delta p_n \end{bmatrix} = \begin{bmatrix} V_1 \\ V_2 \\ \vdots \\ V_n \end{bmatrix} \qquad (2.29)$$

where,

$$a_{ij} = \sum_{hkl} w_{hkl} \frac{\partial |kF_c|}{\partial p_i} \frac{\partial |kF_c|}{\partial p_i} \qquad (2.30)$$

and,

$$V_i = \sum_{hkl} w_{hkl} \{ |F_o| - |kF_c| \} \frac{\partial |kF_c|}{\partial p_i} \qquad (2.31)$$

i.e.

$$[A][\Delta P] = [V] \qquad (2.32)$$

which if multiplied by the inverse matrix of $[A]$ gives;

$$[A^{-1}][A][\Delta P] = [A^{-1}][V] \qquad (2.33)$$

Thus the required shifts are given by;

$$[\Delta P] = [A^{-1}][V] \qquad (2.34)$$

These equations are linear and solvable for the shifts, Δp_j. Combination of these with the a_j's gives improved values for the various parameters. The process is repeated until suitable convergence is attained and successive cycles produce no further significant change.

The correctness of a trial structure is given by a reliability index, R;

$$R = \frac{\Sigma \, \big| \, |F_o| - |F_c| \, \big|}{\Sigma \, |F_o|} \qquad (2.35)$$

where $|F_o|$ and $|F_c|$ are on the same scale. $|F_o|$ is the observed structure amplitude and $|F_c|$ is the structure amplitude calculated from the trial structure and hence the lower the R-value, the greater the confidence that can be placed in the trial structure. Once a non-unit uated;

$$R_w = \frac{\Sigma \mid |F_o| - |F_c| \mid w^{\frac{1}{2}}}{\Sigma |F_o| w^{\frac{1}{2}}} \qquad (2.36)$$

2.8 Overcoming the Phase Problem

The aim of single crystal X-ray analyses is to determine the molecular and crystal structure. Since X-rays cannot be focused by a lens, an image of the structure cannot be obtained directly. The way in which the diffraction data are collected results in the loss of all phase information. This loss of phases is commonly referred to as the 'Phase Problem' and there are two main ways in which the problem may be overcome:

(i) Patterson Syntheses

(ii) Direct methods techniques

2.8.1 Patterson Syntheses[159-161]

The Patterson function, P(u,v,w,) may be calculated at any point (u,v,w) in the unit cell and does not depend upon a knowledge of the phases of the reflections:

$$P(u,v,w) = \frac{1}{V_c} \sum_h \sum_k \sum_l |F_{hkl}|^2 \cos 2\pi(hx + ky + lz) \qquad (2.37)$$

The three-dimensional function gives rise to a 'Patterson map' containing positive regions (peaks) which correspond to the vectors between the atoms in the unit cell. The height of the vector is proportional to $z_i z_j$, where z_i and z_j are the atomic numbers of the two atoms involved.[159-160] The method is particularly applicable to structures incorporating heavy atoms for vectors involving such atoms are easily identified and enable the positions of the heavy atoms to be evaluated.

2.8.2 Direct Methods of Phase Determination

In recent years the use of direct methods techniques has become an indispensible tool for crystal structure analyses. These methods involve probability techniques and the most commonly used programs employed are MULTAN[154] and SHELX.[153]

In the development of inequalities and probability functions it became necessary to have structure factors expressed in a form which optimizes the reliability of relationships and led to the use of normalized structure factors,[162] E_{hkl}, given by,

$$|E_{hkl}|^2 = \frac{|F_{hkl}|^2}{\varepsilon \sum_{i=1}^{N} f_i^2} \qquad (2.38)$$

where ε is an integer which depends upon the reflection and the space group symmetry.[163] The statistical distribution[164] of the $|E|$ values often provide a useful test for distinguishing between centrosymmetric and non-centrosymmetric crystals. Centrosymmetric crystals tend to display a large proportion of both very weak and very strong reflections whilst those for non-centrosymmetric crystals tend to be distributed much more closely about their mean value (Table 2.1). If the fraction, N(Z) of the reflections less than a specified fraction of the average intensity, I/<I>, is plotted against I/<I>, then the theoretical curves for the two types of structure are shown as in Figure 2.1.

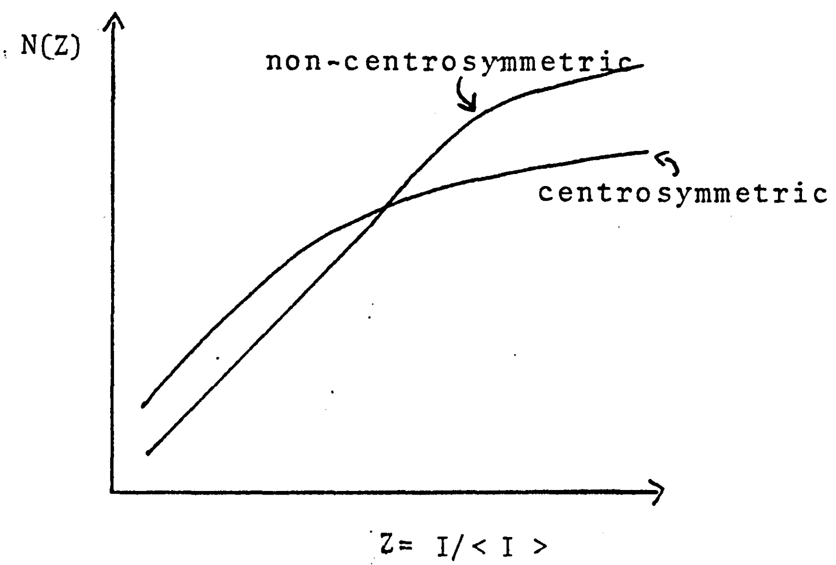

Figure 2.1

Theoretical curves of N(Z) versus Z=I/<I>

Table 2.1 $|E|$-statistics

	Centrosymmetric	Non-centrosymmetric
$\langle \lvert E\rvert^2 \rangle$	1.000	1.000
$\langle \lvert E\rvert \rangle$	0.798	0.886
$\langle \lvert E^2 - 1\rvert \rangle$	0.968	0.736
% $\lvert E\rvert > 1$	32.0	36.8
% $\lvert E\rvert > 2$	5.0	1.8
% $\lvert E\rvert > 3$	0.3	0.01

The most commonly used phase determining formula for centrosymmetric structures is the Σ_2 relationship:[165,166]

$$s(E_{\underline{h}}) \simeq s\Big(\sum_{\underline{k}} E_{\underline{k}} E_{\underline{h}-\underline{k}}\Big) \tag{2.39}$$

where s means 'the sign of', $\underline{h},\underline{k}$ represent the Miller indices (h,k,l) and (h',k',l') respectively and $\underline{h}-\underline{k}$ is the triplet (h-h', k-k', l-l'). This is a more general form of the Sayre[167] relationship,

$$s(F_{\underline{h}}) \simeq s(F_{\underline{k}} F_{\underline{h}-\underline{k}}) \tag{2.40}$$

The probability[166,168,169] that the sign of $E_{\underline{h}}$ is positive, $P_+(\underline{h})$, is given by,

$$P_+(\underline{h}) = \tfrac{1}{2} + \tfrac{1}{2}\tanh\Big\{\sigma_3 \sigma_2^{-3/2} |E_{\underline{h}}| \sum_{\underline{k}} E_{\underline{k}} E_{\underline{h}-\underline{k}}\Big\} \tag{2.41}$$

where $\sigma_n = \sum_i^N z_i^n$ and z_i is the atomic number of the i^{th} atom.

For non-centrosymmetric crystals, the most common phase determining formula is the tangent formula;[162]

$$\tan\phi_{\underline{h}} = \frac{\sum_{\underline{k}} |E_{\underline{k}} E_{\underline{h}-\underline{k}}| \sin(\phi_{\underline{k}} + \phi_{\underline{h}-\underline{k}})}{\sum_{\underline{k}} |E_{\underline{k}} E_{\underline{h}-\underline{k}}| \cos(\phi_{\underline{k}} + \phi_{\underline{h}-\underline{k}})} \tag{2.42}$$

where $\phi_{\underline{h}}$ is the phase angle being determined. The reliability in the determination of a phase angle, $\phi_{\underline{h}}$, from the tangent formula is indicated by the quantity $\alpha_{\underline{h}}$, where,

$$\alpha^2_{\underline{h}} = \{\sum_{\underline{k}} \kappa_{\underline{h}\,\underline{k}} \cos(\phi_{\underline{k}} + \phi_{\underline{h}-\underline{k}})\}^2 + \{\sum_{\underline{k}} \kappa_{\underline{h}\,\underline{k}} \sin(\phi_{\underline{k}} + \phi_{\underline{h}-\underline{k}})\}^2 \qquad (2.43)$$

$$\text{where } \kappa_{\underline{h}\,\underline{k}} = 2\,\sigma_3\,\sigma_2^{-3/2}|E_{\underline{h}}E_{\underline{k}}E_{\underline{h}-\underline{k}}| \qquad (2.44)$$

and $\sigma_n = \sum_{j=1}^{N} z_j^n$ and z_j is the atomic number of the j^{th} atom

The higher the value of $\alpha_{\underline{h}}$ so the greater the reliability of $\phi_{\underline{h}}$. In the initial stages of phase determination, α cannot be evaluated for no phase information is available, and an estimated or expected value, $\alpha^{est}_{\underline{h}}$, is employed.[171] This is given by,

$$\{\alpha^{est}_{\underline{h}}\}^2 = \sum_{\underline{k}} \kappa^2_{\underline{h}\,\underline{k}} + 2 \sum_{\underline{k}} \sum_{\substack{\underline{k}' \\ \underline{k} \neq \underline{k}'}} \kappa_{\underline{h}\,\underline{k}} \kappa_{\underline{h}\,\underline{k}'} \frac{I_1(\kappa_{\underline{h}\,\underline{k}})}{I_o(\kappa_{\underline{h}\,\underline{k}})} \cdot \frac{I_1(\kappa_{\underline{h}\,\underline{k}'})}{I_o(\kappa_{\underline{h}\,\underline{k}'})} \qquad (2.45)$$

where I_o and I_1 are modified Bessel functions. An approximation is often used,[172]

$$\{\alpha^2_{\underline{h}}\}^{\frac{1}{2}} = \sum_{\underline{k}} \kappa_{\underline{h}\,\underline{k}} \frac{I_1(\kappa_{\underline{h}\,\underline{k}})}{I_o(\kappa_{\underline{h}\,\underline{k}})} \qquad (2.46)$$

During the course of a direct methods determination, phases of reflections are evaluated and these depend ultimately on the positions of the atoms expressed relative to a unit cell origin. The centrosymmetric space groups, for example, have eight permissible origins, corresponding to the eight centres of symmetry in the primitive unit cell. The possible origins are not necessarily all equivalent, as they may be situated differently with respect to the symmetry elements. However, a change of origin from one centre to another will affect only the phases and not the magnitudes of any calculated structure factors. Not all reflections are suitable for defining the origin since some have phases which are the same for more than one origin choice and are called seminvariants.

In a non-centrosymmetric space group, not only must the origin determining reflections be chosen but, in addition, a reflection must be selected which will fix the enantiomorph. This is necessary since in the absence of anomalous dispersion, the structure factor magnitudes do not distinguish between the two possible enantiomorphous structures.

The choice of the reflections for fixing the origin and the possible enantiomorph is the most critical point of the entire procedure for phase determination and the manner in which it is done and the subsequent sign expansion pathway vary significantly from program to program. In the present work two direct methods multisolution procedures have been adopted:

(i) SHELX 'automatic direct methods'-only suitable for centrosymmetric crystals.

(ii) SHELX and MULTAN multisolution tangent refinement.

(i) <u>SHELX 'automatic direct methods'</u>

Origin determining reflections are selected from those having E values greater than a minimum value (normally $\geqslant 1.2$). The sign expansion is based on the Σ_2 relationship, equation 2.39, with unknown phases being allocated multisolution values of 0 or 180°. The introduction of such 'multisolution symbols' gives rise to a large number of phase sets (2^{12} being the maximum value normally allowed). To reduce the number of possible phase sets a rejection test[173] based on the absolute figure of merit M (abs), is used during the expansion pathway.

$$M\ (abs) = \frac{\sum_{\underline{h}} \alpha_{\underline{h}} - \sum_{\underline{h}} \alpha_{\underline{h}}^{rand.}}{\sum_{\underline{h}} \alpha_{\underline{h}}^{est.} - \sum_{\underline{h}} \alpha_{\underline{h}}^{rand.}} \tag{2.47}$$

where (i) $\alpha_{\underline{h}}^{est.}$ is the estimated value of alpha and is given by equation 2.46 (ii) $\alpha_{\underline{h}}^{rand.}$ is the value for a randon set of phases and is defined by;

$$(\alpha_{\underline{h}}^{rand})^2 = \sum_{\underline{k}} \kappa^2_{\underline{h}\,\underline{k}} \qquad (2.48)$$

$$\text{(iii)} \quad \alpha_{\underline{h}} = 2\, \sigma_3\, \sigma_2^{-3/2} |E_{\underline{h}}| (T_{\underline{h}}^2 + B_{\underline{h}}^2)^{\frac{1}{2}} \qquad (2.49)$$

where, T_h, B_h are defined in equation 2.51.

At the end of the sign expansion the number of surviving permutations is further reduced by the use of phase information from low E values. The resulting phase sets are ordered in terms of a reliability index (based in part upon the M (abs) test and the associated E-maps are printed. Such E-maps use $|E_{hkl}|$ values rather than $|F_{hkl}|$ as Fourier coefficients in equation 2.20.

(ii) Multisolution tangent refinement

The procedures adopted by the SHELX and MULTAN programs share many similarities and the following outlines the steps adopted by the MULTAN program.

The first step is to work out all the triplet interactions of the type;

$$\phi_{\underline{h}} = \phi_{\underline{k}} + \phi_{\underline{h}-\underline{k}} \qquad (2.50)$$

which are known as the Σ_2 relationships. Many thousands of these are possible but only the 'strongest' relationships are used and the reliability of the Σ_2 relationships is indicated by a large value of the quantity κ defined in equation 2.44.

The next step is to find the best reflections to use for origin and enantiomorph fixing reflections in the case of a non-centrosymmetric crystal. The reliability in the determination of a phase angle, $\phi_{\underline{h}}$, from the tangent formula is indicated by the quantity α (equation 2.43). In the absence of phase information the value of $\alpha_{\underline{h}}$ can be estimated using Bessel functions as given by equations 2.45 and 2.46. Values of α are estimated for all reflections and the reflection with the smallest value is eliminated along with all the Σ_2 relationships in which it is involved. Revised estimated α's are calculated for the remaining reflections and the lowest is again eliminated. This process is repeated and converges on that group of reflections which are linked together best of all. The necessary origin and multisolution phases are then chosen from this group of reflections, the whole process being known as the convergence procedure.[173]

Phases are then determined using the tangent formula; the order in which phases are calculated is the reverse of that found during the convergence procedure. The origin defining phases are used, with the multisolution phases being allocated values of 45, 135, 225 and 315° in a weighted form of the tangent formula;

$$\tan \phi_{\underline{h}} = \frac{\sum_{\underline{k}} w_{\underline{k}} w_{\underline{h}-\underline{k}} |E_{\underline{k}} E_{\underline{h}-\underline{k}}| \sin(\phi_{\underline{k}} + \phi_{\underline{h}-\underline{k}})}{\sum_{\underline{k}} w_{\underline{k}} w_{\underline{h}-\underline{k}} |E_{\underline{k}} E_{\underline{h}-\underline{k}}| \cos(\phi_{\underline{k}} + \phi_{\underline{h}-\underline{k}})} = \frac{T_{\underline{h}}}{B_{\underline{h}}} \tag{2.51}$$

where $w_{\underline{h}} = \tanh\{\sigma_3 \sigma_2^{-3/2} |E_{\underline{h}}| (T_{\underline{h}}^2 + B_{\underline{h}}^2)^{\frac{1}{2}}\}$

The weighting enables all reflections to be included, as poorly determined phases have little effect on the determination of other phases. The tangent formula procedure is repeated so that phases are refined, but the multisolution phases are kept constant until this convergence is nearly complete and they are then allowed to refine to their final values.

Several phase sets are produced and figures of merit are used to determine the phase set with the optimum phases, although E-maps are normally computed for a number of phase sets.

<u>Figures of Merit</u>

(i) <u>M (abs)</u> as defined in equation 2.47, and often called the absolute figure of merit (ABSFOM). Values for ABSFOM should be close to unity.

(ii) <u>PSIZERO</u>, defined by,

$$\Psi_o = \sum_{\underline{h}} \Big| \sum_{\underline{k}} E_{\underline{k}} E_{\underline{h}-\underline{k}} \Big| \tag{2.52}$$

where the inner summation is over the determined phases and the outer summation is over the $|E_{\underline{h}}|$'s with small or zero values. Ψ_o should be as low as possible for a good phase set.

(iii) RESID, the residual which is a measure of how well the Σ_2 relationships have followed the statistical expectations and is calculated as;

$$\mathrm{RESID} = \frac{100 \sum_{\underline{h}} |S\alpha_{\underline{h}}^{est} - \alpha_{\underline{h}}|}{\sum_{\underline{h}} \alpha_{\underline{h}}^{est}} \tag{2.53}$$

where S is a scale factor and $\alpha_{\underline{h}}$ is defined in equation 2.49.

After all the sets of phases have been generated, MULTAN outputs a summary of the figures of merit along with a 'combined figure of merit' calculated from;

$$w_1 \frac{AF - AF(min)}{AF(max) - AF(min)} + w_2 \frac{PS(max) - PS}{PS(max) - PS(min)} + w_3 \frac{R(max) - R}{R(max) - R(min)} \tag{2.54}$$

where w_1, w_2, w_3 are weights, and AF is ABSFOM, PS is PSIZERO and R is RESID.

When a suitable phase set has been chosen from consideration of the figures of merit, the $|E_{\underline{h}}|$ values are used as coefficients in a Fourier synthesis to produce an E-map. Experience has shown that the figures of merit are usually reliable in indicating the correct phase set for a centrosymmetric structure but for a non-centrosymmetric structure the figures of merit can be misleading. The MULTAN package incorporates a fast Fourier transform program coupled to a peak search program so that a large number of possible phase sets may be examined without producing the E-maps. Allied to this is a procedure which examines the electron density peaks found to look for a known structural fragment or molecule.

Computing

All calculations were carried out either on the Sheffield City Polytechnic IBM 370/145 computer or on the IBM 370/165 at the SERC Daresbury Computing Laboratory.

CHAPTER THREE

Structural studies of Dimethyldibenzophospholium Bis-7,7,8,8 - tetracyanoquinodimethanide, (DMBP)$(TCNQ)_2$, and the phosphonium complexes $(R_1R_2Ph_2P)(TCNQ)_2$, where R_1, R_2 = Et; R_1, R_2 = Me; R_1 = Me, R_2 = Et.

Contents

3.1 Introduction

The crystal structures of the 1:2 phosphonium TCNQ complexes $(Ph_3RP)(TCNQ)_2$ where R = Ph,Me,Et, are known to exhibit subtle changes in the stacking of TCNQ molecules, depending upon the cation present.[43,48,53,72] To examine further the influence upon TCNQ stacking of phosphorus containing cations, structural studies of 1:2 salts containing the dimethyldibenzophospholium cation (I) and a series of phosphonium cations (II) have been examined.

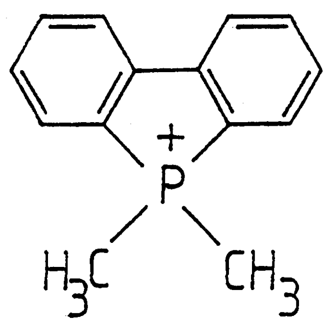

(I)

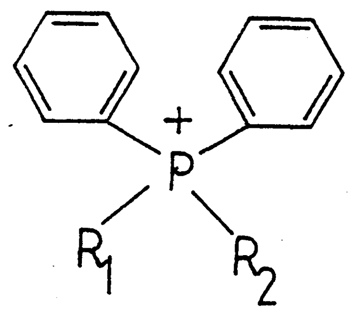

(II)

3.2 Crystal Data

$(DMBP)(TCNQ)_2$, $C_{38}H_{22}N_8P$, M_r = 621.5, monoclinic, a = 7.547(4), b = 30.189(19), c = 7.863(5) Å, β = 115.86(7)°, U = 1612.1 Å^3, μ(Mo-Kα) = 0.89cm^{-1}, Z = 2, D_m = 1.31(2), D_c = 1.29 Mgm^{-3}, F(000) = 642.

$(Me_2Ph_2P)(TCNQ)_2$, $C_{38}H_{24}N_8P$, M_r = 623.6, monoclinic, a = 32.01(2), b = 6.56(1), c = 15.72(2)Å, β = 107.4(8)°, U = 3149.9Å^3, D_m = 1.30, D_c = 1.32 Mgm^{-3}, Z = 4, μ(Mo - Kα) = 0.91cm^{-1}, F(000) = 1292.

3.3 Crystal Structure Analysis of Dimethyldibenzophospholium Bis - 7,7,8,8 - tetracyanoquinodimethanide, (DMBP)$(TCNQ)_2$

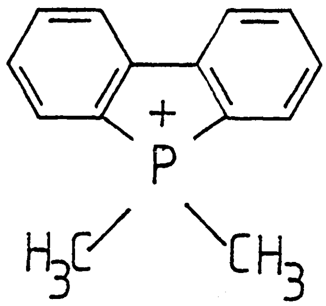

(DMBP)

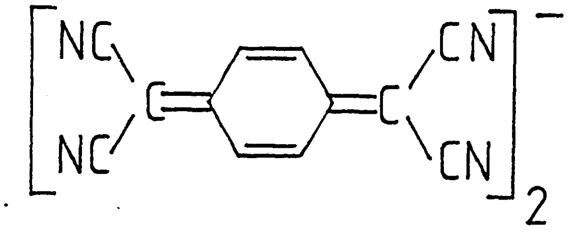

$(TCNQ)_2$

3.3.1 Determination of the Space Group

The systematic absences noted on the Weissenberg and precession photographs, [hkl, h + l = 2n + 1; 0k0, k = 2n + 1;] are consistent with two monoclinic space groups, $B2_1$ or $B2_1/m$. Both are non-standard space groups and it was decided to convert the unit cell and space groups to the corresponding primitive ones. The unit cell parameters obtained from the preliminary photographs were a = 7.547, b = 30.189, c = 14.189Å, β = 92.88°. $B2_1$ and $B2_1/m$ are non-standard settings of $P2_1$ and $P2_1/m$ respectively and the unit cell dimensions for the standard primitive cell were calculated to be a = 7.547, b = 30.189, c = 7.863Å, β = 115.86°. The reflections were reindexed using the matrix:

$$\begin{pmatrix} h \\ k \\ l \end{pmatrix} = \begin{pmatrix} -1 & 0 & 0 \\ 0 & 1 & 0 \\ 0.5 & 0 & 0.5 \end{pmatrix} (h' \; k' \; l')$$

where (hkl) are the indices based on the primitive cell and (h'k'l') are those from the B-centered cell. In the centrosymmetric space group $P2_1/m$, the asymmetric unit would contain one independant TCNQ molecule and half a DMBP ion, i.e. pairs of TCNQ molecules would be related to each other through mirror planes at 0.25b and 0.75b, while the phosphorus atom and the methyl carbon atoms of the cation would actually lie on the mirror plane. In the non-centrosymmetric space group $P2_1$, the cation is not required to lie on a special position and the asymmetric unit would contain one DMBP ion and two independant TCNQ species.

3.3.2 Data Collection

A crystal of approximate dimensions 0.36 x 0.07 x 0.48mm was selected and mounted with the a-axis coincident with the rotation (ω) axis of the Stöe Stadi 2-two circle diffractometer. Data were collected using monochromated Mo - K_α radiation and the background-ω-scan-background technique previously described. Corrections for Lorentz and polarization effects were made but not for absorption effects. The crystal was weakly diffracting and of the 3061 unique reflections measured only 1081 had $I \geqslant 2\sigma(I)$ and were used for subsequent analysis.

3.3.3 Structure Solution and Refinement

Structure solution was initially attempted in the non-centrosymmetric space group $P2_1$, by multisolution direct methods using the SHELX package. The starting set was chosen from the convergence mapping:

(i) Three origin determining reflections whose phase angles are restricted and set at 0°. For $P2_1$, two of these reflections must be of the form h0l (one of these must have an even value of l), and these fix the ac plane perpendicular to the b-direction. The third origin determining reflection is of the form hkl, where hkl must be non-zero. h and l must be even and if $k \neq 1$ then at least one other reflection in the starting set must have k = 1. This reflection fixes a point along the b-direction.

(ii) For a non-centrosymmetric space group, as in this case, a reflection must be chosen which fixes the enantiomorph. This must be a general reflection, and the phase angles chosen must be in the range 0 to $\mp \pi$

(iii) All other reflections, at which the expansion pathway is broken must be included in the starting set and unless the phase angles are given restricted values they are given four possible phase angles 45, 135, 225 and 315°.

For the present structural analysis the following starting set was utilized:

h	k	l	phase angles (°)	
-5	17	2	0	origin determining reflections
5	0	4	0	
-2	0	5	0	
-1	11	4	45, 135	enantiomorph fixing reflection
0	19	4	45, 135, 225, 315	multi-solution set of reflections
-1	9	8	45, 135, 225, 315	
-2	14	6	45, 135, 225, 315	
-2	0	4	0, 180	
2	0	7	0, 180	

All the non-hydrogen atom positions were readily located from an E-map calculated for the solution with the third largest figure-of-merit. Large correlations between positional parameters of the TCNQ molecules were evident in the subsequent least-squares refinement, resulting in distortions of the geometrical arrangements and unrealistic thermal parameters. In view of these high correlations and the fact that two independant TCNQ molecules located were so closely related by a mirror plane passing through the cation, it was decided to continue the analysis in the centrosymmetric space group $P2_1/m$.

The four E-maps with the highest parachor values were produced, Table 3.1. One TCNQ molecule and two possible phosphorus atom positions were located from the E-map with the third largest figure-of-merit. Subsequent least-squares refinement indicated the correct position for the phosphorus atom. Successive Fourier difference maps enabled the hydrogen atoms to be located and they were included in the refinement in positions calculated from the geometry of the molecule (C - H = 1.08Å). Common isotropic temperature factors were applied to methyl and phenyl-type hydrogen atoms and refined to final values of $U = 0.062(19)$ and $0.066(17)\text{Å}^2$ respectively. The weighting scheme $w = 5.3159/[\sigma^2(F_o) + 0.0010(F_o)^2]$ was adopted. Full matrix refinement with anisotropic temperature factors for all non-hydrogen atoms gave the final $R = 0.095$ and $R_w = 0.080$.

The large errors of the positional parameters and the associated bond distances and angles led to a further attempt at a solution in the non-centrosymmetric space group $P2_1$. However, the final R-value showed no significant improvement at 0.095. If the non-centrosymmetric solution was correct one would expect a lower R-value because twice as many independent parameters were being refined. In the light of the observation that both of the R-values were comparable, and the unrealistic anisotropic temperature factors for many of the atoms and the unsatisfactory geometry of the TCNQ groups associated with refinement in $P2_1$, it seemed likely that $P2_1/m$ was the more appropriate space group. The $|E|$-statistics appeared to support the centrosymmetric solution:

$\sin\theta/\lambda$	0.14 - 0.21	- 0.28	- 0.35	- 0.42	- 0.49	- 0.56	- 0.63	
$\|E\|$	0.613	0.955	0.901	0.952	0.961	1.034	1.000	1.000
$\|E^2 - 1\|$	0.818	1.053	0.903	1.025	0.820	0.943	0.833	0.723

The final positional and thermal parameters are given in Appendix A1.1, structure factor tables in Appendix A3.1, equations for mean planes in Appendix A2.1, with bond distances and angles in Table 3.2.

3.3.4 Description of the Structure

The structure comprises segregated stacks of TCNQ molecules and DMBP ions. A projection of the structure along a^* (Figure 3.1) and b (Figure 3.2) shows the TCNQ molecules to be located in columns parallel to the c-axis, grouped into diadic units with mean inter- and intradimer separations of 3.44(2) and 3.17(2) Å respectively. The overlap of TCNQ molecules within each diad is of the desired exocyclic double-bond to quinonoid ring type but between diads there is little overlap (Figure 3.3). The direction of staggering of the TCNQ molecules within each column is constant and the TCNQ columns form a herringbone pattern. A similar arrangement has been observed in $(morpholinium)_2(TCNQ)_3$.[49]

Short N - - - H distances exist between the TCNQ columns (Table 3.3) which are within the sum of the van der Waals' radii[175] for nitrogen and hydrogen. This type of N - - - H interaction has been attributed to Coulomb attractive forces[79] where the nitrogen of the terminal cyano group on a TCNQ may have a small negative charge and the C - H of the quinonoid ring of an adjacent TCNQ may have a small positive charge, hence facilitating weak electrostatic interactions. In the present complex these weak interactions between diadic units lead to the formation of sheets of TCNQ molecules which are parallel to the ac plane (Figure 3.2). There is only one type of sheet within the structure, successive sheets being related to each other by the two-fold screw axis along b, and being separated by the DMBP ions (Figure 3.1). The TCNQ moieties are not quite planar and adopt a slight boat form[77] (Appendix A2.1). The structural features observed in the present complex may be compared and contrasted to known complexes which also exhibit irregular stacking of TCNQ columns e.g. $(DEM)(TCNQ)_2$,[77] $(TEA)(TCNQ)_2$,[57,75] $(DMPA)(TCNQ)_4$.[89]

The geometry of the DMBP ion (Figure 3.4, Table 3.2) closely resembles that of 5-(p-bromobenzyl)-5-phenyldibenzophospholium bromide (III).[176] The phosphorus atom lies 0.0066Å out of the C13, C14, C14′, C13′ mean plane and the six-membered rings are inclined at an angle of 2.04° to this plane, and 3.72° to each other (Appendix A2.1). The exocyclic bond angles at phosphorus lie in the range 107.6(9) to 114.2(6)°, while the endocyclic angle is found to be only 95.6(4)°. The latter may be compared to values of 93.9(9) and 93.4° found in the 5-(p-bromobenzyl)-5-phenyldibenzophospholium bromide (III)[176] and in the 5-hydroxydibenzo-5-H-phosphole-5-oxide (IV).[177] This small endocyclic angle at phosphorus implies the existence of bond angle strain within the dibenzophospholium cation.[176]

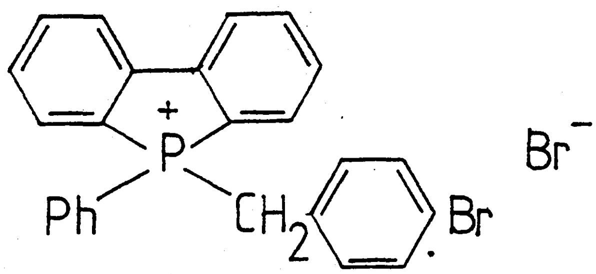

(III)

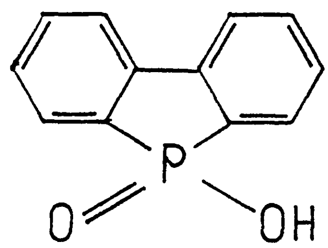

(IV)

3.3.5 Relationship Between the Crystal Structure of $(DMBP)(TCNQ)_2$ and its Conductivity

Conductivity measurements show the complex to be a poor semi-conductor (Table 3.4, Figure 3.5) with no phase transitions apparent over the measured temperature range of 150 - 430K. The room temperature conductivity is $\sigma_{RT} = 5 \times 10^{-4}$ ohm^{-1} cm^{-1}, and the activation energy $E_a = 0.2eV$. The poor conductivity can be readily related to the crystal structure of the complex. The first limiting factor, as regards a high conductivity, is the rigidity of the cation. There appears to be a direct relationship between the shape and flexibility of the cation and the nature of the stacking adopted by the TCNQ molecules. In particular, the presence of a cation capable of crystallising in a disordered manner often leads to a more ordered TCNQ stacking and in the extreme, to a true homosoric arrangement. In the present complex, the phospholium ion is so rigid and planar that disorder does not occur and localised attractions between the cation and TCNQ molecules in adjacent columns develop, thereby leading to the formation of sheets containing TCNQ diadic units. While the type of overlap within a given diad is of the desired quinonoid ring to exocyclic double bond type, the overlap between adjacent diads is poor (Figure 3.3). This non-uniformity in one-dimensionality produces a reduction in mobility of the charge carriers in the conduction process, and hence a low conductivity. Similar effects are observed in the $(\text{morpholinium})_2(\text{TCNQ})_3$[49] and (TEA[57,75])$(\text{TCNQ})_2$ complexes where the stacks are also non-uniform. In both of these complexes there is hydrogen bonding between the cations and the TCNQ molecules. Such hydrogen bonding facilitates the formation of pseudosoric arrangements in the TCNQ stacks.

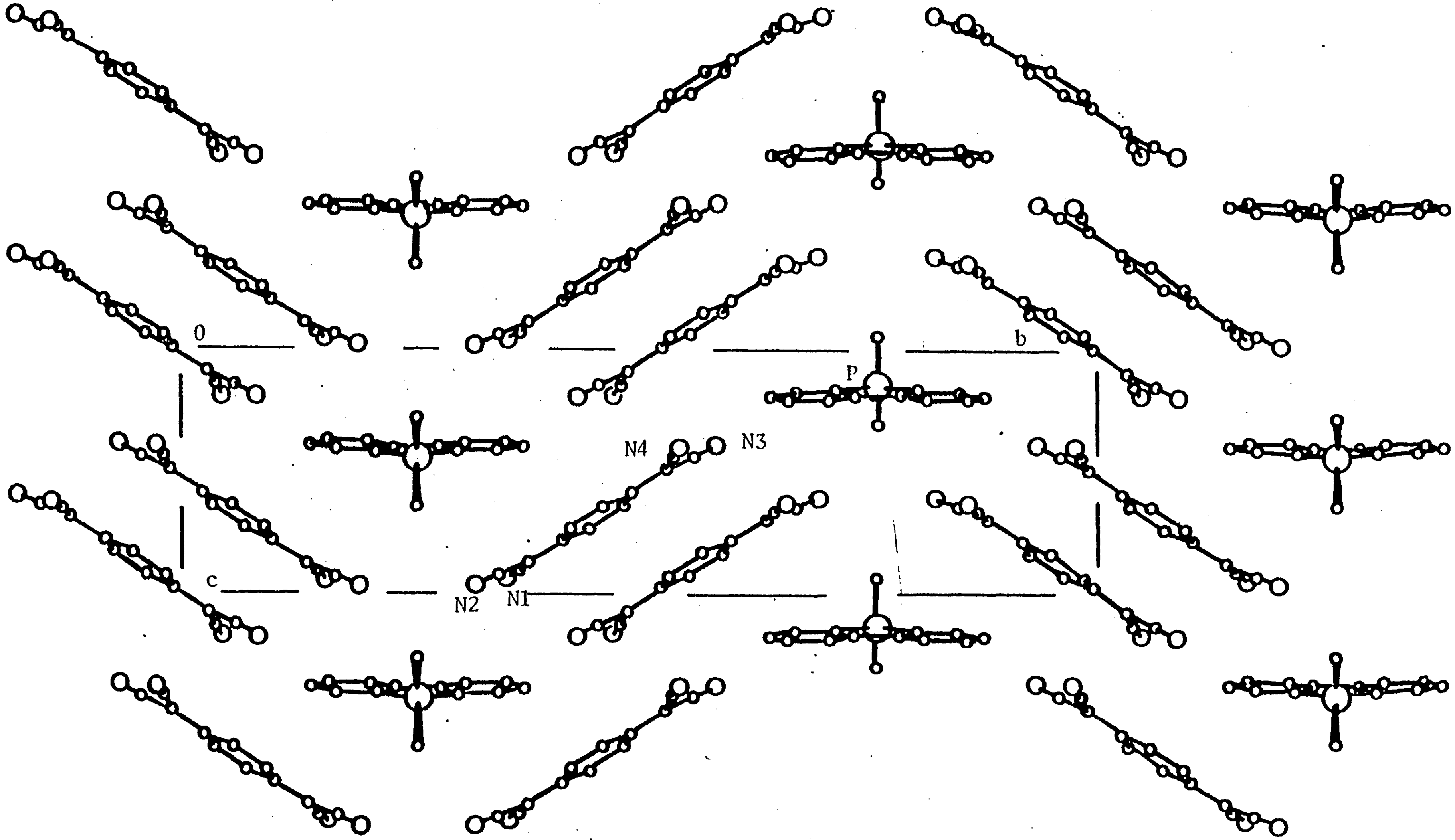

Figure 3.1 (DMBP)(TCNQ)$_2$, Projection down the a* -direction

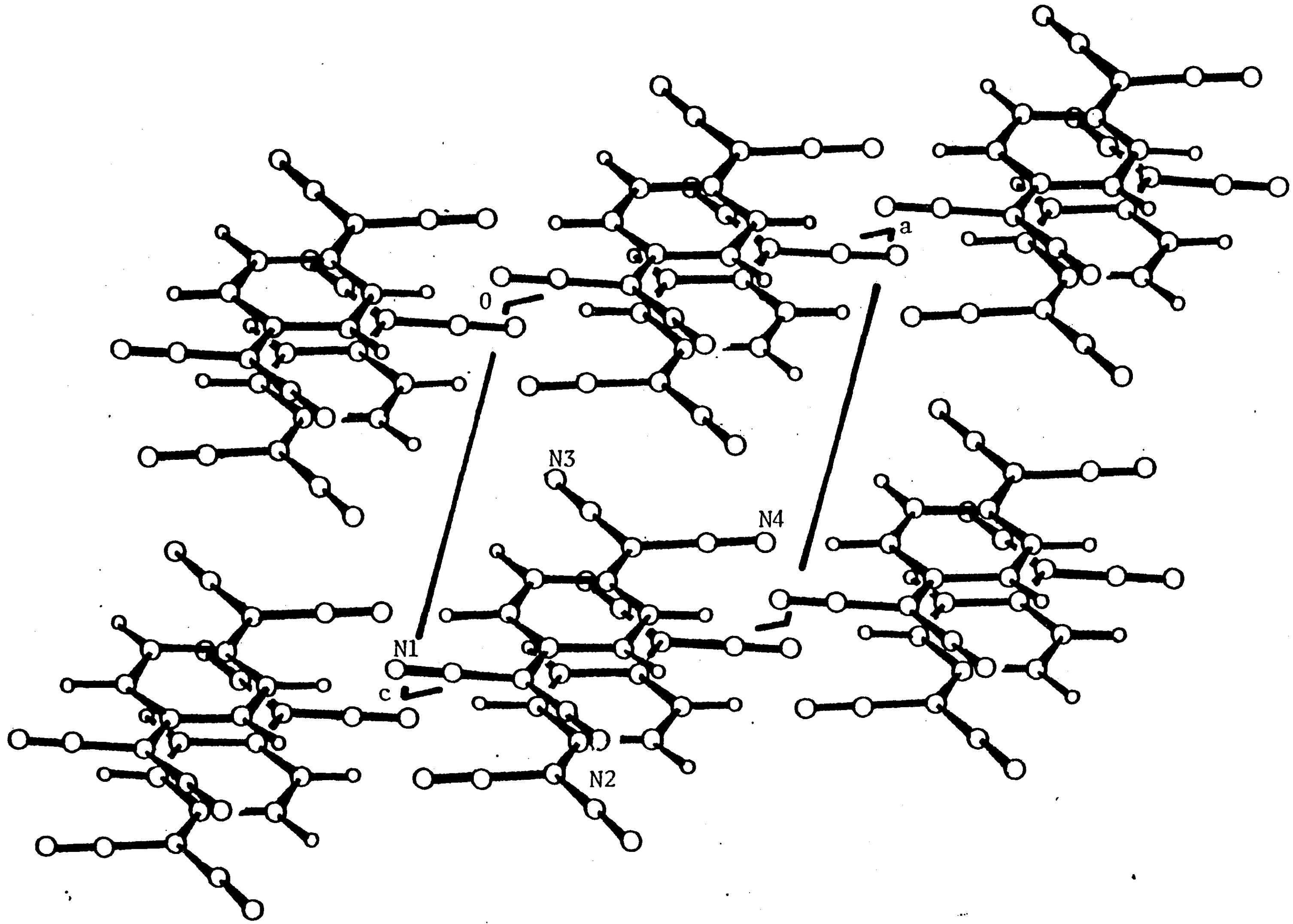

Figure 3.2 (DMBP)$(TCNQ)_2$, Projection down the b-axis, omitting the cation for clarity.

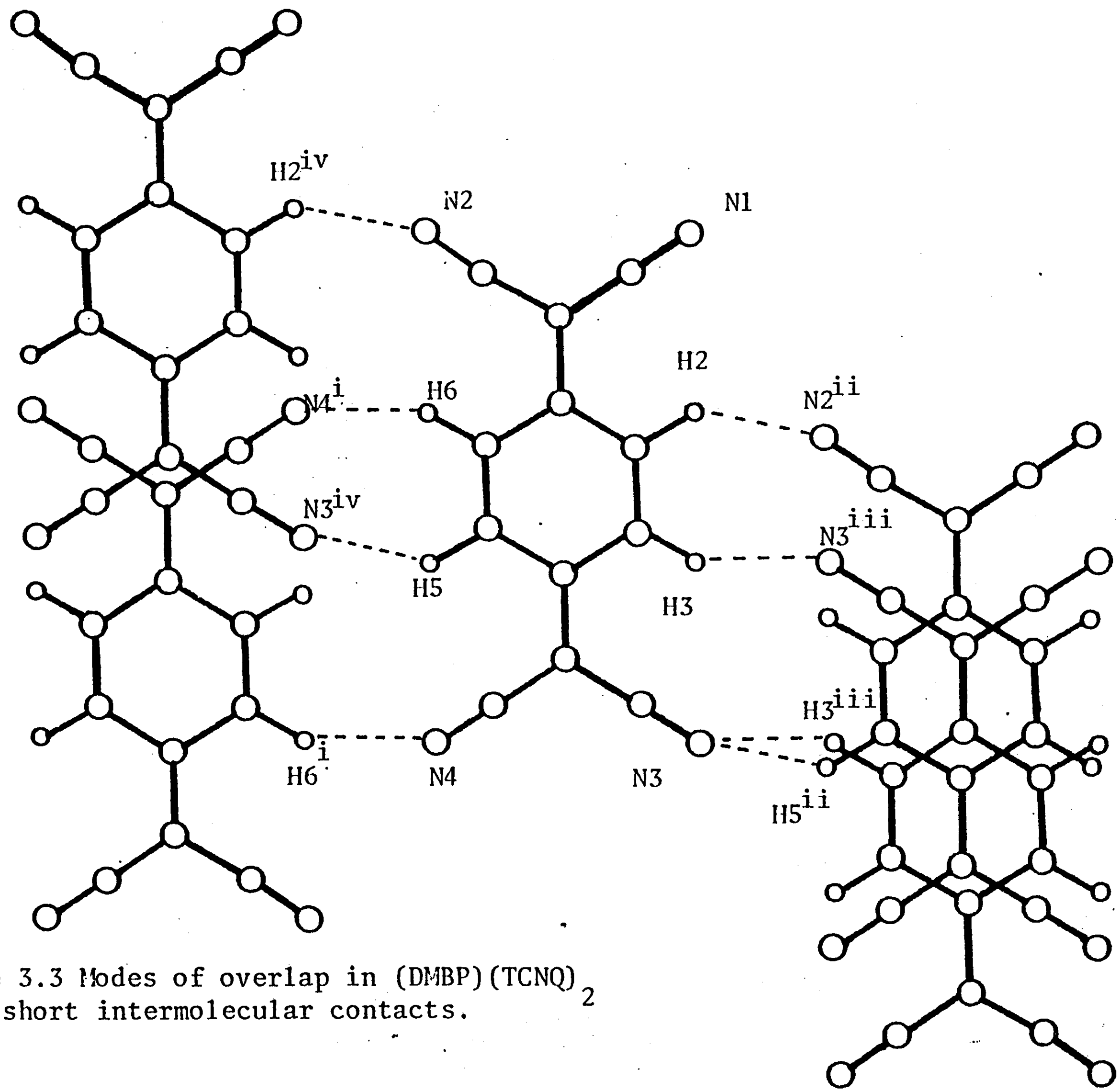

Figure 3.3 Modes of overlap in (DMBP)(TCNQ)$_2$ and short intermolecular contacts.

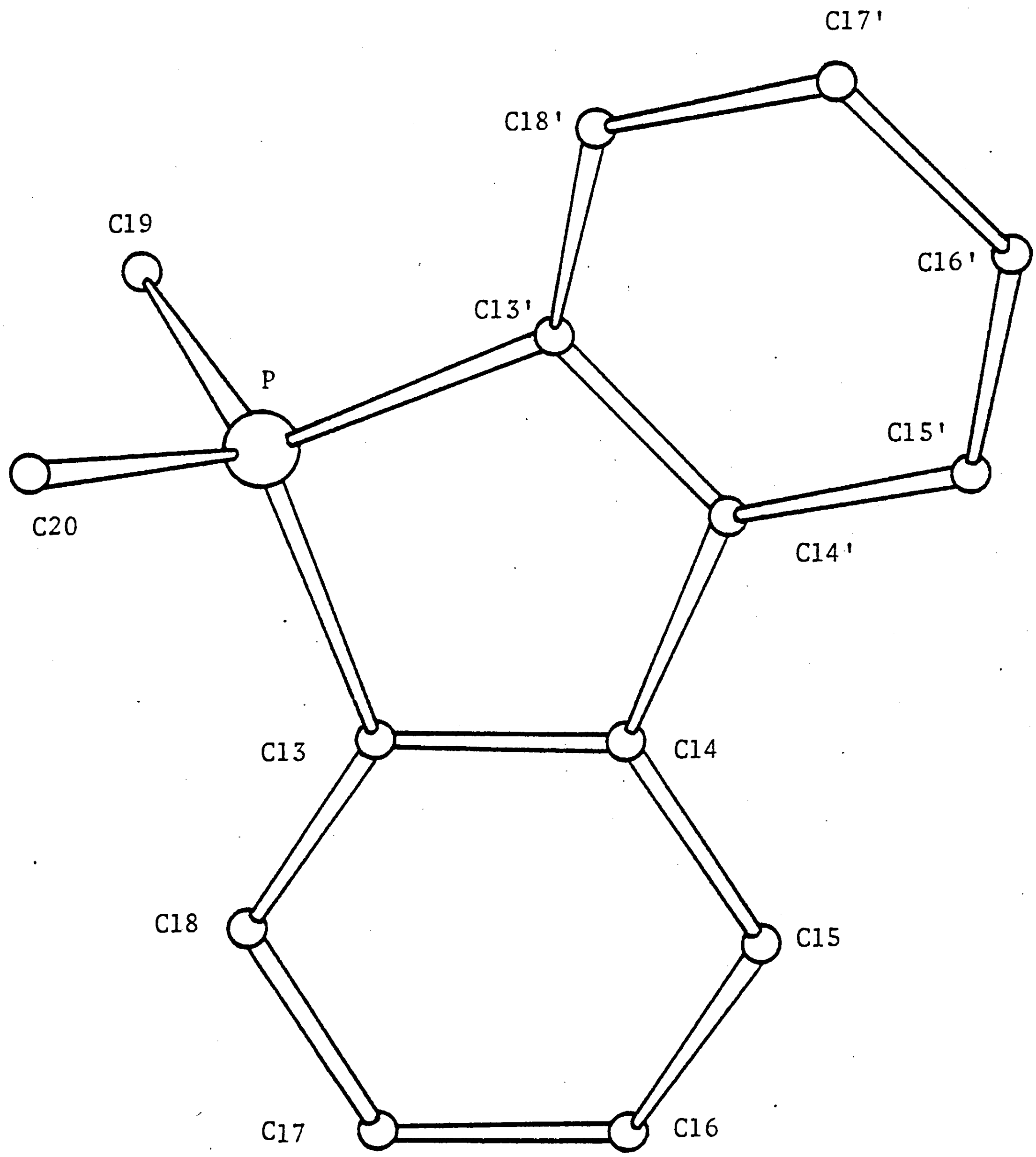

Figure 3.4 DMBP cation

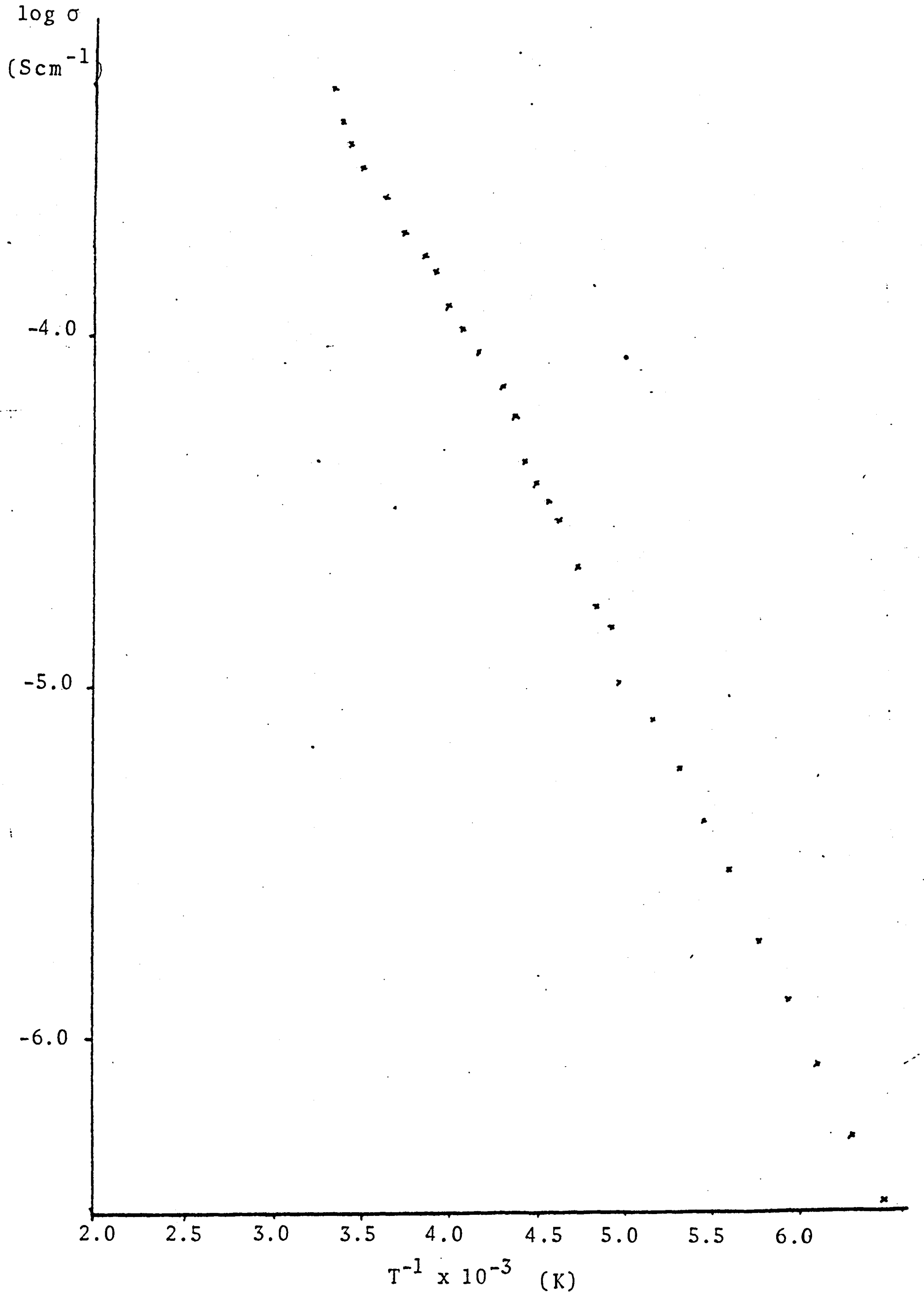

Figure 3.5 Conductivity versus temperature for $(DMBP)(TCNQ)_2$

Table 3.1 Starting Sets for Solution of $(DMBP)(TCNQ)_2$ in $P2_1/m$

(i) Reflections, E-value and phase angles:-

h	k	l	Phase Angle°	
-5	1	2	0	origin determining reflections
0	19	4	0	
0	4	2		Multisolution set of reflections Phase Angles 0 or 180°
6	9	0		
0	14	2		
-1	9	2		
-2	14	6		
-1	9	8		
5	3	2		
5	2	2		
-1	11	4		
0	22	2		
-6	6	6		
1	11	0		

(ii) Figures-of-merit

E-map	Parachor	M(abs)	NQT	Phase Angle*
1	1.928	0.810	-0.128	+ + − + + + − + − + + + − −
2	1.884	0.729	-0.163	+ + − + + − − − + − − + − +
3	1.876	1.018	0.064	+ + − − + − − − − + − + + +
4	1.843	1.018	0.082	+ + + − − + + + − + + − − −

* The order of the reflections is the same as that given in (i), with + and − corresponding to a phase angle of 0 and 180° respectively.

Table 3.2 Bond Distances (Å) and Angles (°) with Estimated Standard Deviations in Parentheses

(i) DMBP ion

Symmetry code: none x,y,z; (′) x,0.5-y,z

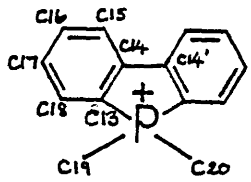

Bond Distances (Å)

P-C13	1.812(11)	C14-C14′	1.502(20)
P-C19	1.796(25)	C14-C15	1.400(18)
P-C20	1.782(14)	C15-C16	1.383(18)
C13-C14	1.396(17)	C16-C17	1.388(19)
C13-C18	1.341(16)	C17-C18	1.395(19)

Bond Angles (°)

C13-P-C13′	95.6(4)	C13-C14-C14′	115.1(11)
C13-P-C19	114.2(6)	C13-C14-C15	119.1(10)
C13-P-C20	112.5(6)	C14′-C14-C15	125.9(10)
C19-P-C20	107.6(9)	C14-C15-C16	115.3(12)
P-C13-C14	107.1(7)	C15-C16-C17	124.7(12)
P-C13-C18	127.7(11)	C16-C17-C18	118.8(11)
C14-C13-C18	125.0(11)	C13-C18-C17	116.8(3)

(ii) TCNQ

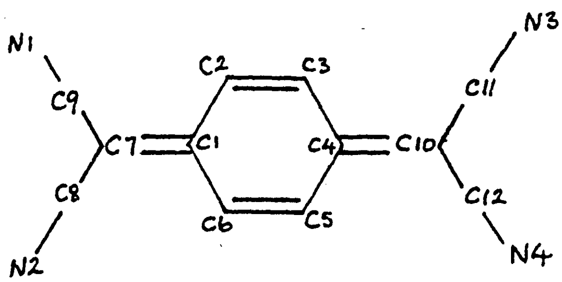

Table 3.2 (ii) contd.

Bond Distances (Å)

N1-C9	1.145(18)	C3-C4	1.410(15)
N2-C8	1.154(28)	C4-C5	1.452(21)
C7-C8	1.420(26)	C5-C6	1.370(20)
C7-C9	1.412(18)	C10-C4	1.410(19)
C7-C1	1.392(19)	C10-C11	1.440(23)
C1-C2	1.457(21)	C10-C12	1.421(18)
C1-C6	1.411(16)	N3-C11	1.149(24)
C2-C3	1.350(19)	N4-C12	1.149(17)

Bond Angles (°)

N1-C9-C7	179.8(7)	C4-C5-C6	121.3(11)
N2-C8-C7	173.1(15)	C5-C6-C1	120.1(14)
C8-C7-C9	117.4(13)	C6-C1-C2	118.3(12)
C8-C7-C1	119.4(11)	C10-C4-C3	121.3(13)
C9-C7-C1	123.0(15)	C10-C4-C5	120.8(10)
C7-C1-C2	120.7(11)	C11-C10-C4	121.3(11)
C7-C1-C6	120.9(14)	C12-C10-C4	122.4(14)
C1-C2-C3	121.2(11)	C12-C10-C11	116.2(14)
C2-C3-C4	121.1(13)	N3-C11-C10	176.3(15)
C3-C4-C5	117.9(12)	N4-C12-C10	178.2(15)

Table 3.3 Short Intermolecular Contacts (Å) in $(DMBP)(TCNQ)_2$

$N4 ---- H6^{i}$	2.656	$H5^{ii} ---- N3$	2.808
$H5 ---- N3^{iv}$	2.808	$H3^{iii} ---- N3$	2.634
$H6 ---- N4^{i}$	2.656	$N3^{iii} ---- H3$	2.634
$N2 ---- H2^{iv}$	3.049	$N2^{ii} ---- H2$	3.049

Symmetry code:

none x,y,z (i) -x,1-y,1-z (ii) -1+x,y,z (iii) 2-x,1-y,2-z

(iv) -x,y,z

Table 3.4 Conductivity Data for (DMBP)(TCNQ)$_2$

$\log \sigma = \log (^1/R \times {}^L/A)$

where

σ = conductivity (Scm^{-1})

R = resistance (S)

L = thickness of the crystal (cm)

A = area of crystal surface (cm^2)

1000/T (K^{-1})	log σ (Scm^{-1})	1000/T (K^{-1})	log σ (Scm^{-1})
3.34	-3.29	4.56	-4.47
3.38	-3.39	4.61	-4.55
3.44	-3.45	4.72	-4.66
3.50	-3.52	4.82	-4.77
3.63	-3.61	4.90	-4.83
3.74	-3.71	4.95	-4.98
3.85	-3.77	5.15	-5.09
3.92	-3.85	5.29	-5.24
3.99	-3.91	5.43	-5.38
4.07	-3.97	5.58	-5.55
4.16	-4.05	5.75	-5.73
4.29	-4.15	5.92	-5.90
4.37	-4.23	6.09	-6.08
4.42	-4.37	6.29	-6.29
4.48	-4.43	6.49	-6.49

3.4 Crystal Structure Analysis of Dimethyldiphenylphosphonium Bis-7,7,8,8-tetracyanoquinodimethanide, $(Me_2Ph_2P)(TCNQ)_2$

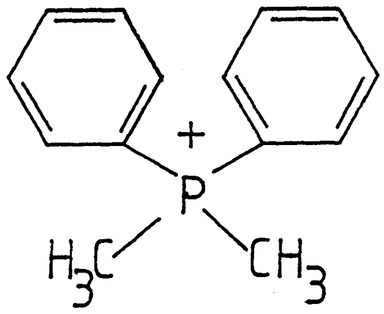

(Me_2Ph_2P)

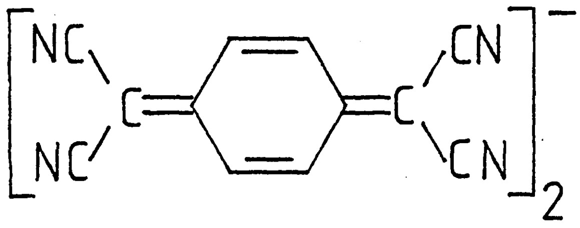

$(TCNQ)_2$

3.4.1 Determination of the Space Group

From Weissenberg and precession photographs, the following systematic absences were noted: [hkl, $h+k = 2n + 1$; h0l, $l = 2n + 1$ ($h = 2n + 1$)] These absences are consistent with two monoclinic space groups, Cc and C2/c. In the centrosymmetric space group, C2/c, the asymmetric unit would contain one TCNQ molecule and half a (Me_2Ph_2P) ion, i.e. the cation would be required to lie on a special position. Two types of special position are available, such that the cation would contain either a centre of symmetry or a two-fold rotation axis. While the cation could contain a two-fold axis, a centre of symmetry is only possible if the cation is statistically disordered. In the non-centrosymmetric space group the cation is not required to lie on a special position as the asymmetric unit would contain one (Me_2Ph_2P) ion and two independent TCNQ molecules.

3.4.2 Data Collection

A crystal of approximate dimensions 0.5 x 0.2 x 0.2mm was selected and mounted with the b-axis coincident with the rotation axis of the Stöe Stadi 2 two-circle diffractometer. 2360 unique reflections were collected of which 1292 had $I \geq 2\sigma(I)$ and were used for subsequent analysis.

3.4.3 Structure Solution and Refinement

The $|E|$- statistics for ranges of $\sin\theta/\lambda$ were examined and these indicated the structure to be centrosymmetric:

$\sin\theta/\lambda$	0.07 - 0.14	- 0.21	- 0.28	- 0.35	- 0.42	- 0.49	- 0.56	-
$\lvert E \rvert$	1.016	0.950	0.973	0.987	1.027	1.000	1.000	1.000
$\lvert E^2-1 \rvert$	1.389	0.973	1.020	1.029	1.153	1.126	1.046	1.031

Initial attempts at solution using the centrosymmetric automatic direct methods faculty in SHELX did not prove successful and the data were converted into a format suitable for use in the MULTAN package. Attempts at finding a solution in the centrosymmetric space group were again unsuccessful; the lowest R-value for the many solutions refined being above 0.60. A three-dimensional sharpened-Patterson was computed but an unambiguous interpretation could not be obtained and efforts were then concentrated in the use of direct methods in the non-centrosymmetric space group Cc. MULTAN gave six phase sets, of which only two are independent (Table 3.5). Computation of an E-map based on the phase set having the largest figures-of-merit and lowest residual enabled two independent TCNQ molecules to be readily located. While the phosphorus atom of the cation was readily located, considerable difficulty was found in finding the phenyl and methyl carbon atoms. Successive difference-Fourier maps enabled two phenyl rings to be eventually located and their relative positions indicated that the cation did not contain a two-fold rotation axis but was disordered.

The phosphorus atom was refined with a population parameter of 1.0, but in view of the apparent disorder of the cation, the associated carbon atoms were all given population parameters of 0.50. While least-squares refinement of the two independent TCNQ molecules and the disordered cation led to an acceptable reduction in the R-value (to below

20%), there were considerable correlations between positional parameters of the two independent TCNQ molecules and there was obvious distortion within the geometries of both molecules. Examination of the atomic co-ordinates of the two independent TCNQ molecules indicated them to be almost related by a two-fold screw axis along the b-direction. Attempts were then made to make this 'apparent' symmetry exact, by changing the origin of the unit cell and refining in C2/c. Subsequent refinement did not prove acceptable as the R-value increased substantially and it was decided to finish the refinement in the non-centrosymmetric space group. A number of atoms within the TCNQ molecules could not be given anisotropic temperature factors for they became non-positive definite. This was attributed to the pseudo-symmetry relating the two independent TCNQ molecules and the atoms concerned, along with most of the located carbon atoms of the cation, were given isotropic temperature factors. It was possible to obtain a minimum R-value of 0.12, but the associated geometry of the TCNQ molecules was quite unacceptable. Refinement was consequently attempted using damping factors so as to minimize the correlation effects, and the two phenyl rings were given idealised geometries with C-C = 1.395Å and C-C-C bond angles = 120°. A final R-value, using this approach, of 0.148 was obtained, although parts of the TCNQ geometries were still rather distorted. The weighted R-value (R_w), refined to a final value of 0.154 with the final weighting scheme adopted being: $w = 8.9262/[\sigma^2(F_o) + 0.0006(F_o)^2]$. Final positional and thermal parameters are given in Appendix A.1.2, structure factor tables in Appendix A.3.2, equations of mean planes in Appendix A.2.2, with bond distances and angles in Table (3.6).

3.4.4 Description of the Structure

The structure comprises segregated stacks of TCNQ molecules and (Me_2-Ph_2P) ions (Figure 3.6) The cation is represented by the phosphorus atom position . The TCNQ molecules stack in a monadic/diadic manner such that the interplanar TCNQ spacings are alternately 3.25 and 3.30A within each column. The overlap of TCNQ molecules within each stack is of the exocyclic double bond to quinonoid ring type (Figure 3.7) and, this, together with the uniformity of the stacking, puts $(Me_2$-$Ph_2P)(TCNQ)_2$ within the homosoric category of TCNQ complexes.

Adjacent columns of TCNQ moieties are displaced by 0.25b, forming sheets parallel to the bc plane (Figure 3.8). Successive sheets are separated by the disordered (Me_2Ph_2P) cations. This homosoric arrangement is in contrast to that observed for the related complexes $(Ph_3RP)(TCNQ)_2$ where R = Ph,Et,Me:[43,48,53,72]

(i) $(Ph_4P)(TCNQ)_2$[43] contains segregated stacks of TCNQ molecules and (Ph_4P) cations. The anionic stacks are made up of TCNQ dimers which form sheets interleaved with cations. The overlap within each dimer is good but poor between adjacent dimers (Figure 3.9).

(ii) $(MePh_3P)(TCNQ)_2$ and $(MePh_3As)(TCNQ)_2$ are found to be isomorphous and both contain segregated stacks of cations and TCNQ molecules.[48] The TCNQ columns are made up of tetradic units, the overlap within the tetrads being good and that between adjacent tetrads being poor.

(iii) $(EtPh_3P)(TCNQ)_2$[72] contains segregated stacks of TCNQ molecules and $(EtPh_3P)$ cations, the anionic stacks comprising tetradic units of TCNQ moieties, with good overlap within the tetrads, but a ring-to-shifted-ring type of overlap between adjacent tetrads.

(iv) $(TMA)(TCNQ)(I_3)_{\frac{1}{3}}$[70] exhibits many structural parameters similar to those found in $(Me_2Ph_2P)(TCNQ)_2$. Thus the complex contains segregated stacks of cations and TCNQ molecules (plus columns of iodine atoms) with the d-spacing in the TCNQ columns being strictly monadic.

3.4.5 Relationship Between the Solid State Structures of the Phosphonium Salts $(R_1R_2Ph_2P)(TCNQ)_2$ where $R_1,R_2 = Me$; $R_1,R_2 = Et$; $R_1 = Me,R_2 = Et$; and their Conductivities

Conductivity measurements have been made[178] on single crystals of all the complexes and the results are shown in Figure 3.10. These data indicate:

(i) The $(Me_2Ph_2P)(TCNQ)_2$ complex undergoes a semi-conductor-to-semi-conductor transition at approximately 320K, whilst $(Et_2Ph_2P)(TCNQ)_2$ and $(MeEtPh_2P)(TCNQ)_2$ do not exhibit any transitions over the temperature range studied.

(ii) The conductivities, for the temperatures studied, decrease in the order $(Et_2Ph_2P)(TCNQ)_2 \geq (Me_2Ph_2P)(TCNQ)_2 > (MeEtPh_2P)(TCNQ)_2$.

To aid an understanding of these conductivity data, preliminary X-ray photographs have been taken of $(MeEtPh_2P)(TCNQ)_2$ and $(Et_2Ph_2P)(TCNQ)_2$, in addition to the full structural study of $(Me_2Ph_2P)(TCNQ)_2$. Examination of the oscillation photographs for the latter complex shows two sets of layer lines about the b-axis (Figure 3.11). The strong layer lines correspond to a d-spacing of 6.50Å and the weak layer lines to a d-spacing of 13.07Å. Since b is the direction in which the TCNQ molecules stack, it is possible to understand the origin of the two sets of lines in terms of a Peierls-type distortion:

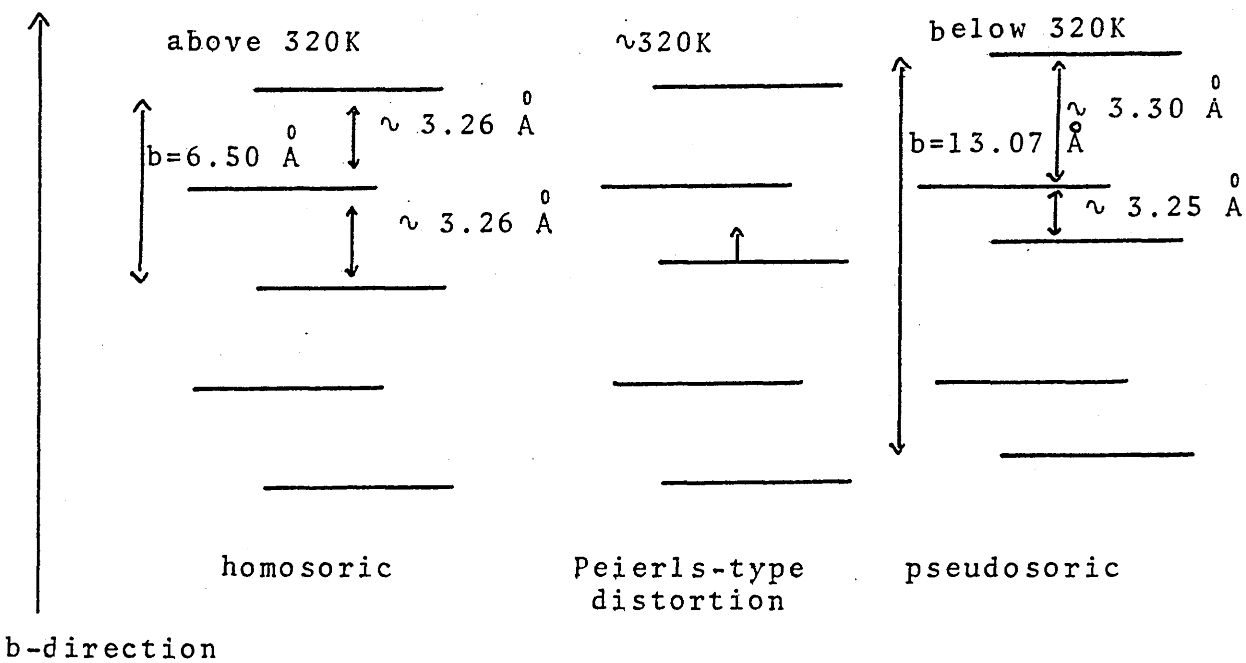

where ——— represents a side-on view of a TCNQ molecule. Thus, at the temperature at which the oscillation photographs were taken, and the intensity data collected, while the dominant arrangement is that of a homosoric system (strong layer lines), there is also an incipient Peierl's distortion present giving rise to the weak layer lines. The origin of the distortion can be related to the disorder associated with the cation. A completely disordered cation facilitates homosoric stacking and localised cation-stack interactions will be minimized. As the temperature is lowered, the cation becomes more ordered and, in order to balance charge and allow for incomplete charge-transfer, the TCNQ moieties must group together in a pseudosoric manner i.e. the charges become localised. Hence, the interplanar distances become unequal and the effect is to lower the conductivity. The X-ray analysis of $(Me_2Ph_2P)(TCNQ)_2$ has thus been conducted at a temperature in the range of the phase transition and this may account for the considerable difficulties in solving the structure.

Weak layer lines have been similarly observed in $(TMA)(TCNQ)(I_3)_{\frac{1}{3}}$,[70] $(NH_4)(TCNQ)$[68] and complexes belonging to the (TTF)(TCNQ) family.[123,110] The behaviour in the (TTF)(TCNQ) family has been attributed to inherent lattice instability. In $(NH_4)(TCNQ)$ the phenomenon is said to be associated with a monomer-dimer transition at 28°C and in $(TMA)(TCNQ)(I_3)_{\frac{1}{3}}$ it is attributed to a one-dimensional disorder in the iodine columns.

Oscillation and Weissenberg photographs show that the dimethyl- and diethyldiphenylphosphonium salts are isostructural having very similar unit cell dimensions and reflection intensities (Figures 3.11, 3.12, 3.13; Table 3.7). The most striking difference is seen on the oscillation photographs (Figure 3.11) where the weak layer lines observed in $(Me_2Ph_2P)(TCNQ)_2$ are no longer observed for $(Et_2Ph_2P)(TCNQ)_2$. Examination of the conductivity properties of the latter complex (Figure 3.10) offers an explanation. The indication is that the diethyl complex comprises a homosoric arrangement at the temperature at which the oscillation photographs were taken. Why should the $(Et_2Ph_2P)(TCNQ)_2$

salt give rise to a higher conductivity compared to $(Me_2Ph_2P)(TCNQ)_2$? An examination of the structures and conductivities of the following related phosphonium salts gives an insight:

	Reference
$(Ph_4P)(TCNQ)_2$	43
$(MePh_3P)(TCNQ)_2$	48,53
$(EtPh_3P)(TCNQ)_2$	72

$(Ph_4P)(TCNQ)_4$ contains the bulkiest phosphonium ion and the one least likely to be disordered. The TCNQ molecules are found to stack in dimer units, the overlap in the dimer units being good but that between adjacent dimer units being very slight (Figure 3.9). The room temperature X-ray analysis of $(MePh_3P)(TCNQ)_2$ shows it to contain tetradic stacks of TCNQ molecules. The mode of overlap and the spacing of 3.20Å in the tetrads are suitable for high conductivity but the overlap between adjacent tetrads is of the ring-to-ring type and the inter-tetrad spacing increases to 3.58Å. Thus the replacement of one phenyl group by a methyl group has enhanced the homosoric nature of the TCNQ stacks. It is interesting that the higher-temperature study of $(MePh_3P)(TCNQ)_2$[53] shows that while the mode of overlap within the tetrads has remained unchanged (i.e. is good), the inter-tetrad overlap has improved to become a ring-to-shifted-ring type (Figure 3.14). Moreover, the conformation of the phosphonium ion is disordered. Thus in this complex the homosoric character has been increased by a disordering of the phosphonium ion resulting from an increase in temperature.

The influence of increasing temperature upon cation disorder and subsequently upon stacking of TCNQ molecules is well illustrated by the methylethylmorpholinium complex, $(MEM)(TCNQ)_2$, which undergoes a semi-conductor-to-semi-conductor transition at 340K and whose structure has been determined[65,80,81] at 113, 294, 323 and 348K.

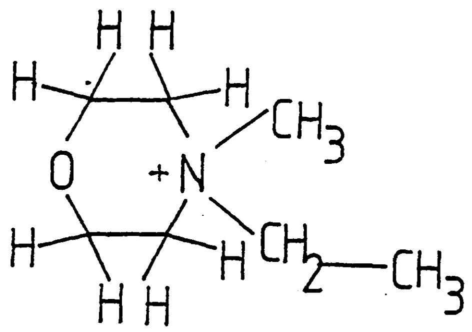

(MEM) .

The following structural changes are observed with increasing temperature:

(i) Studies[68,80] at 113, 294, 323K.

The structures consist of sheets of TCNQ dimers separated by MEM cations. While stacking of the TCNQ dimers hardly changes over the temperature range 113 to 323K, there is an increasing disorder of the MEM group with increasing temperature. With the assumption of two preferred orientations the 100% occupancy of the orientation observed at 113K decreases to 84% at 294K and 63% at 323K.

(ii) Study[81] at 348K.

The disorder of the MEM group is enhanced above the transition temperature and the strongly dimerised TCNQ stacks observed below the transition temperature become nearly regular.

The room-temperature crystal structure of $(EtPh_3P)(TCNQ)_2$[72] is found to be similar to the high-temperature form of $(MePh_3P)(TCNQ)_2$[53] in its mode of overlap within the tetrads, but the inter-tetrad overlap is even more of a shifted-ring-to-ring type (Figure 3.14). This replacement of a methyl substituent by an ethyl group appears, in these $(RPh_3P)(TCNQ)_2$salts, to enhance the homosoric stacking. Similar effects seem to be operating in the $(R_2Ph_2P)(TCNQ)_2$ complexes where the diethyl salt is more conducting than is the dimethyl salt.

Conductivity measurements indicate $(MeEtPh_2P)(TCNQ)_2$ to have a lower conductivity compared with either the dimethyl or the diethyl complexes studied (Figure 3.10). Unfortunately, while the oscillation photographs are easily measured, giving a rotation axis of 6.463Å, the Weissenberg photographs are complex and show the crystals to be disordered; a possible explanation is that there is a superimposition of an orthorhombic supercell on the monoclinic lattice.

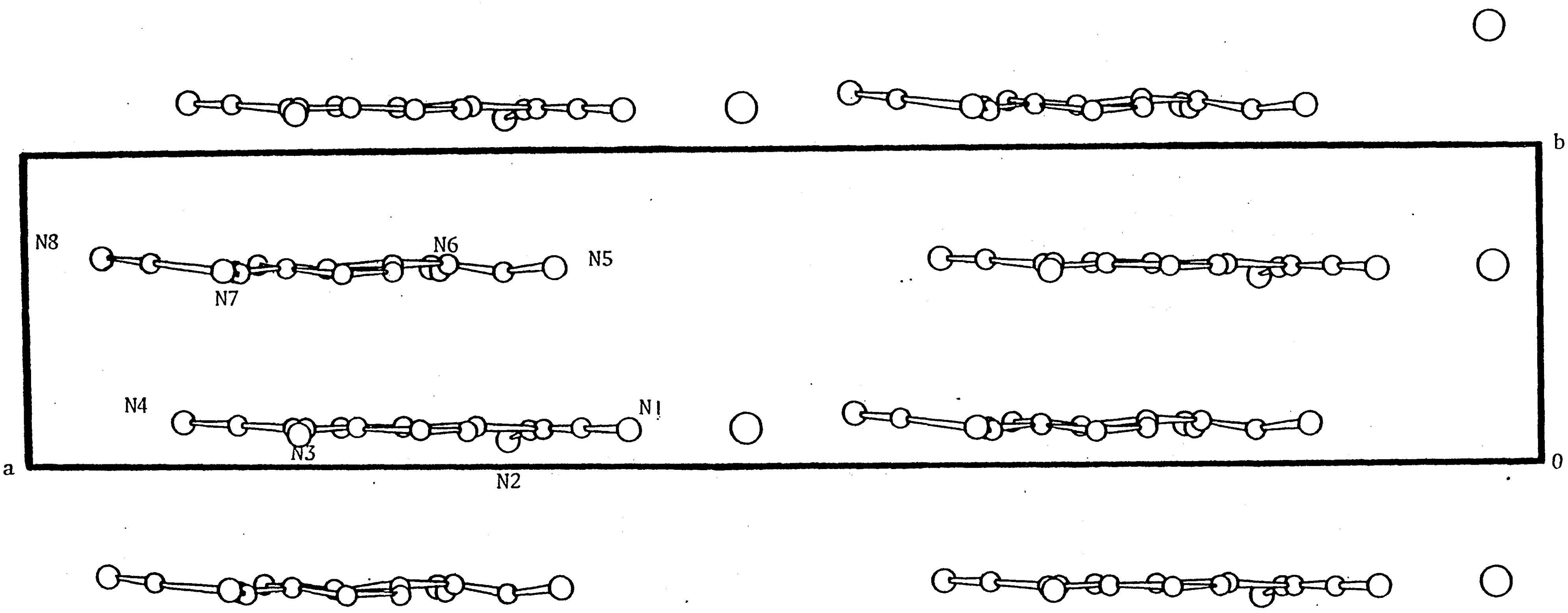

Figure 3.6 Projection down the c^*-axis for $(Me_2Ph_2P)(TCNQ)_2$

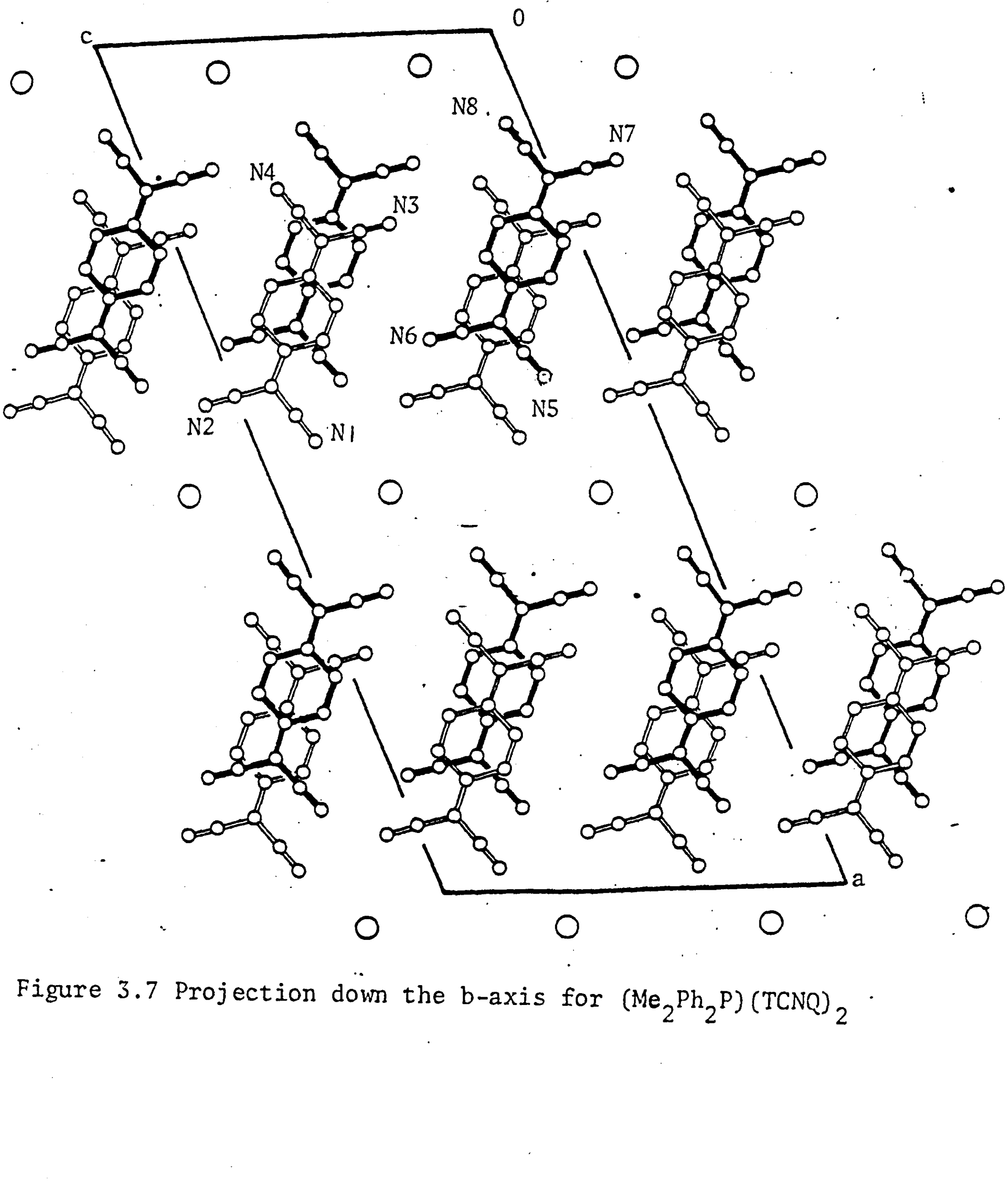

Figure 3.7 Projection down the b-axis for $(Me_2Ph_2P)(TCNQ)_2$

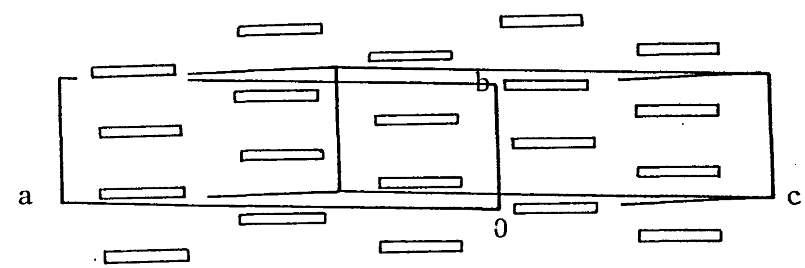

represents an end-on view of a TCNQ molecule

Figure 3.8 Projection along the C1-C7 bond showing the TCNQ moieties displaced by 0.25b thus forming sheets.

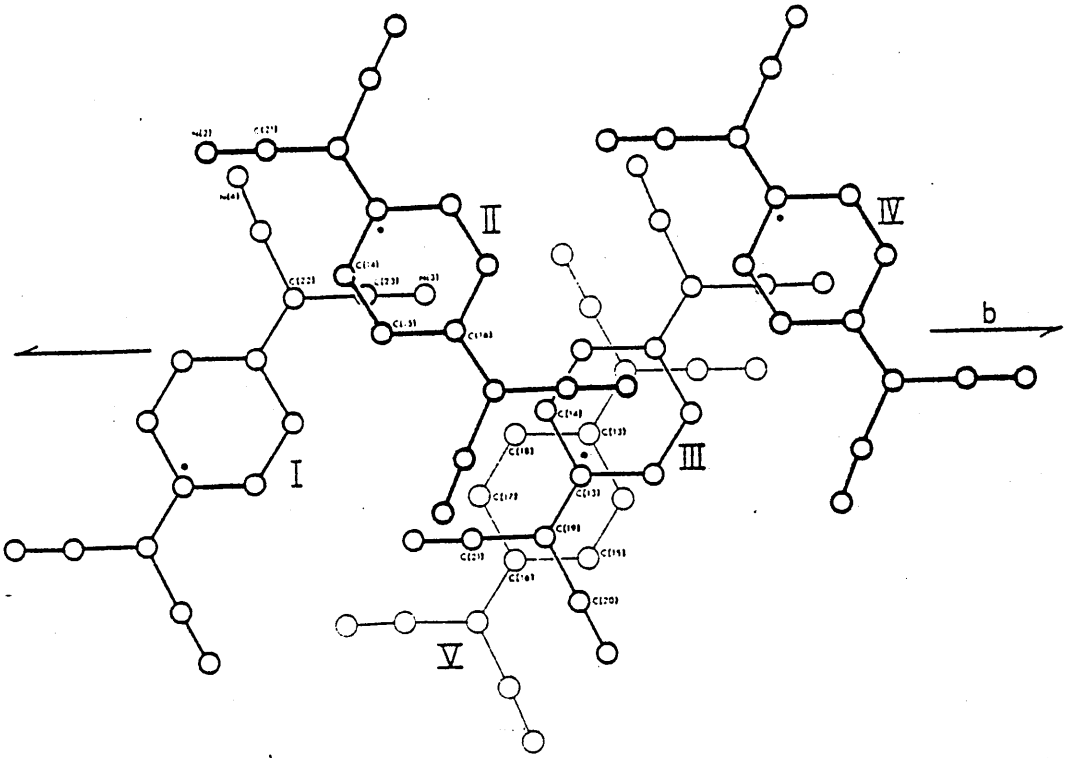

Figure 3.9 Mode of overlap in $(Ph_4P)(TCNQ)_2$

$(Me_2Ph_2P)(TCNQ)_2$ ooo 300K = 0.05 Scm^{-1}, E_a = 0.20 eV

$(Et_2Ph_2P)(TCNQ)_2$ □□□ 300K = 0.96 Scm^{-1}, E_a = 0.05 eV

$(MeEtPh_2P)(TCNQ)_2$ xxx 300K = 0.02 Scm^{-1}, E_a = 0.22 eV

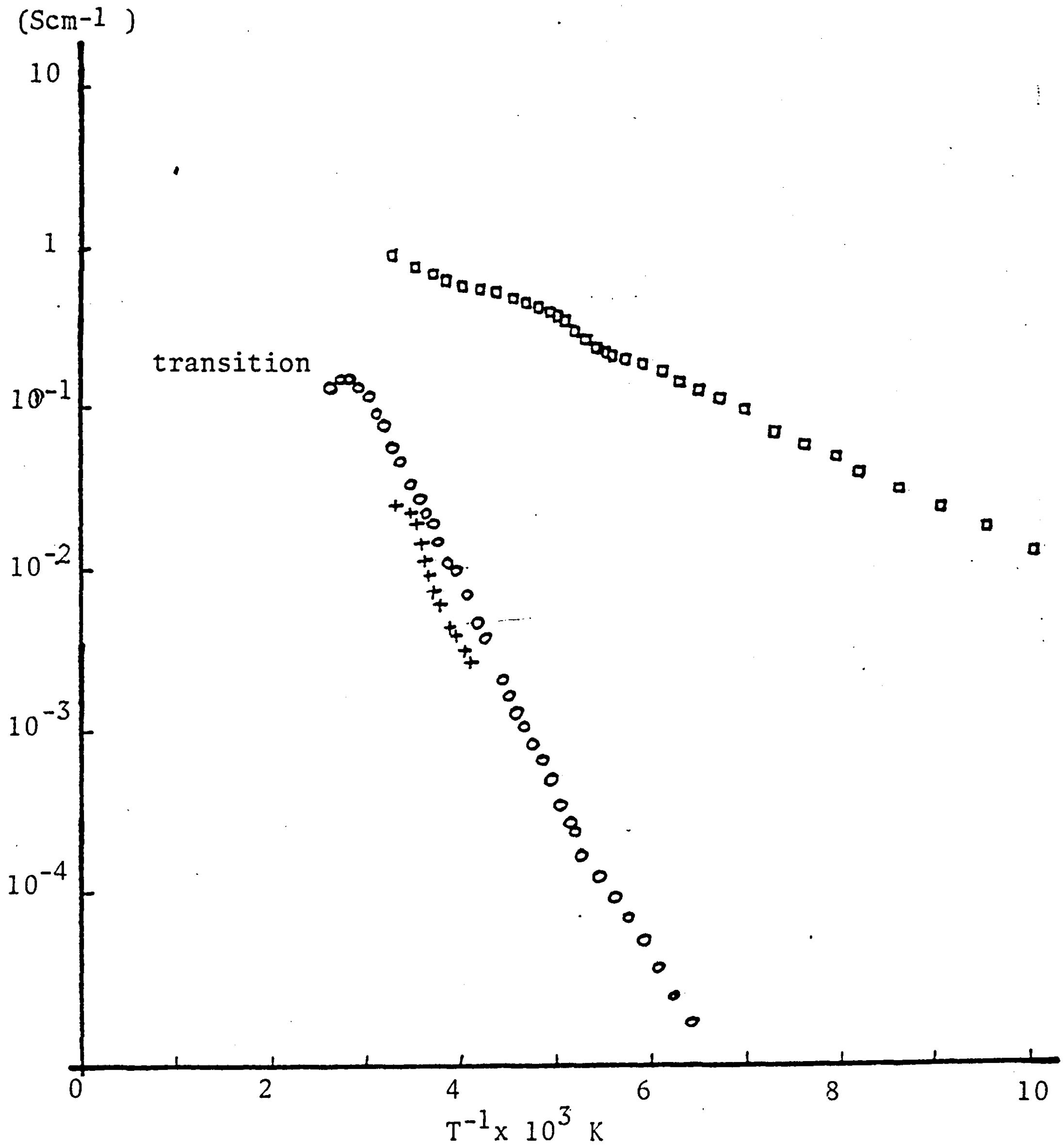

Figure 3.10 Conductivity data for $(R_2Ph_2P)(TCNQ)_2$ series

$(MeEtPh_2P)(TCNQ)_2$

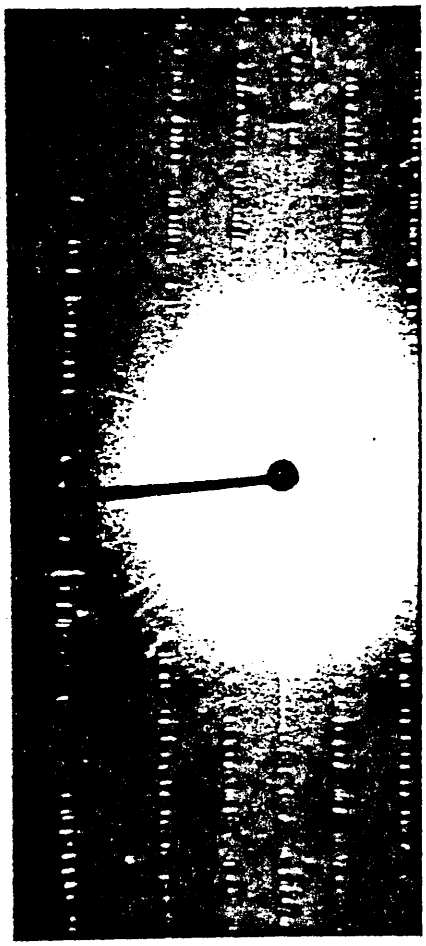

$(Et_2Ph_2P)(TCNQ)_2$

$(Me_2Ph_2P)(TCNQ)_2$

Figure 3.11 Oscillation photographs for $(R_2Ph_2P)(TCNQ)_2$ series

First Level Weissenberg

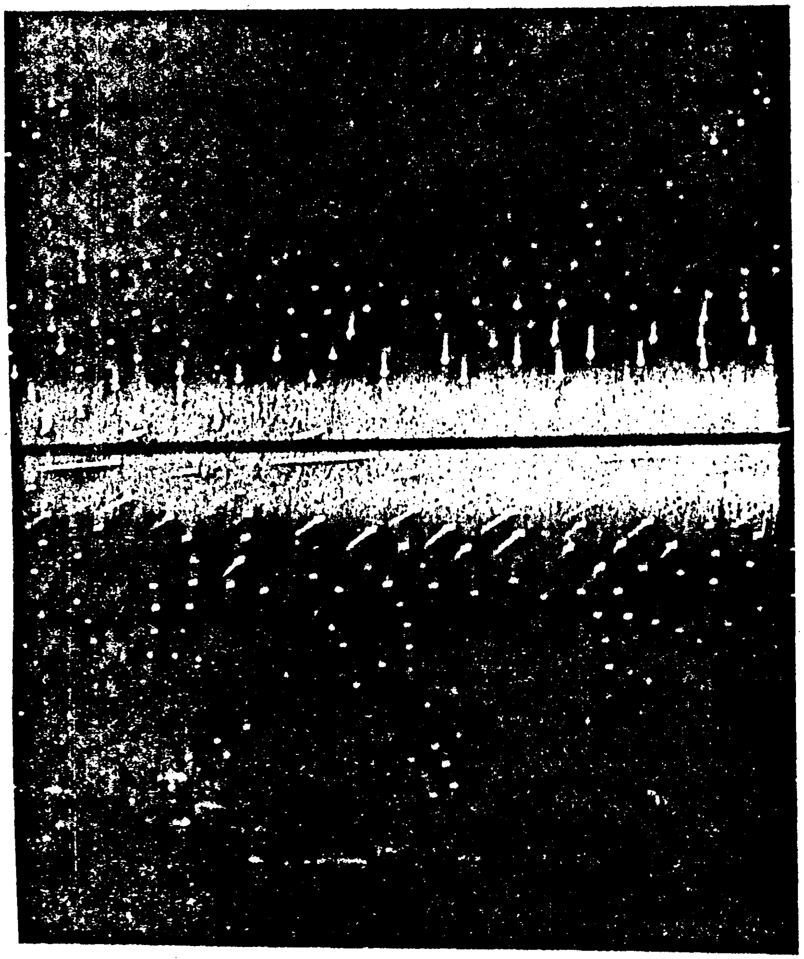

Zero Level Weissenberg

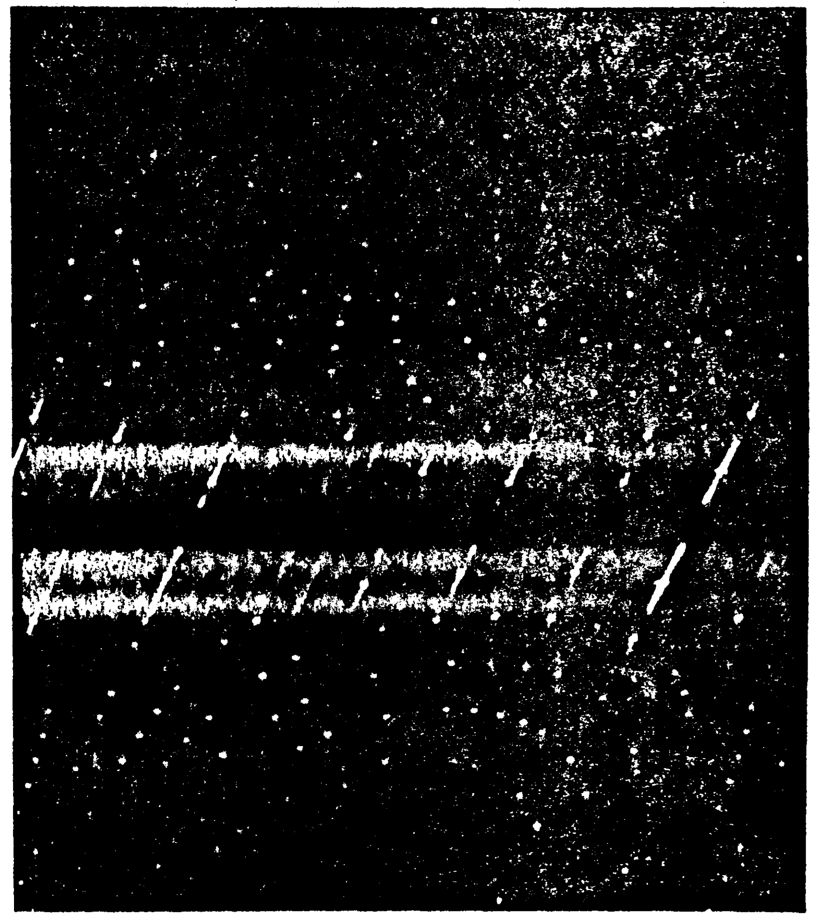

Figure 3.12 Weissenberg photographs for $(Me_2Ph_2P)(TCNQ)_2$

First Level Weissenberg

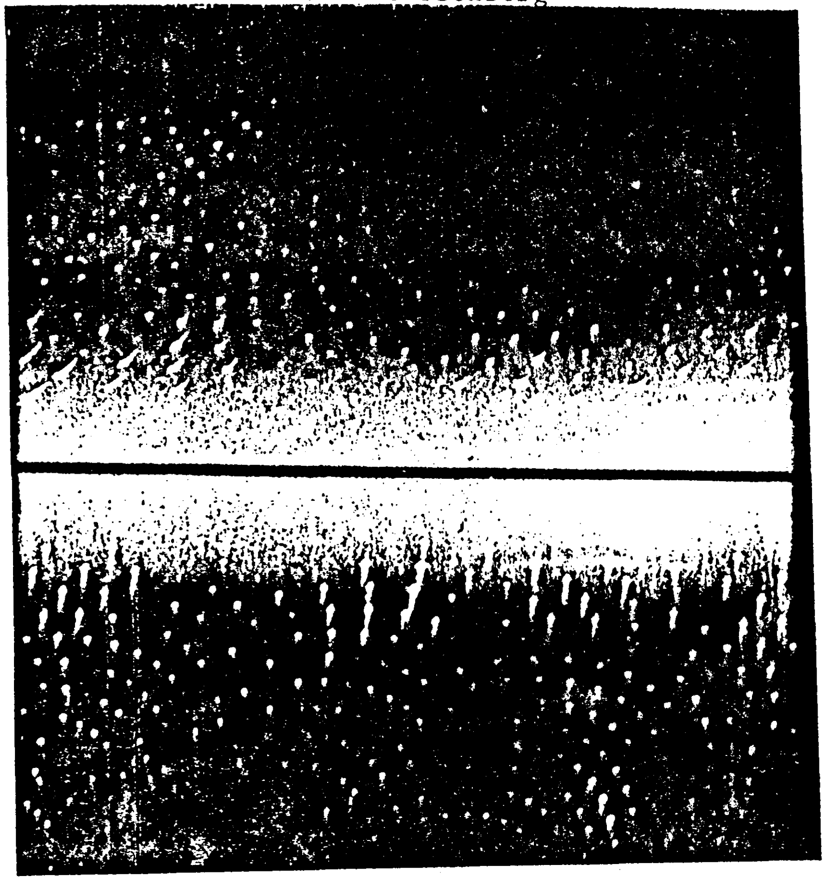

Zero Level Weissenberg

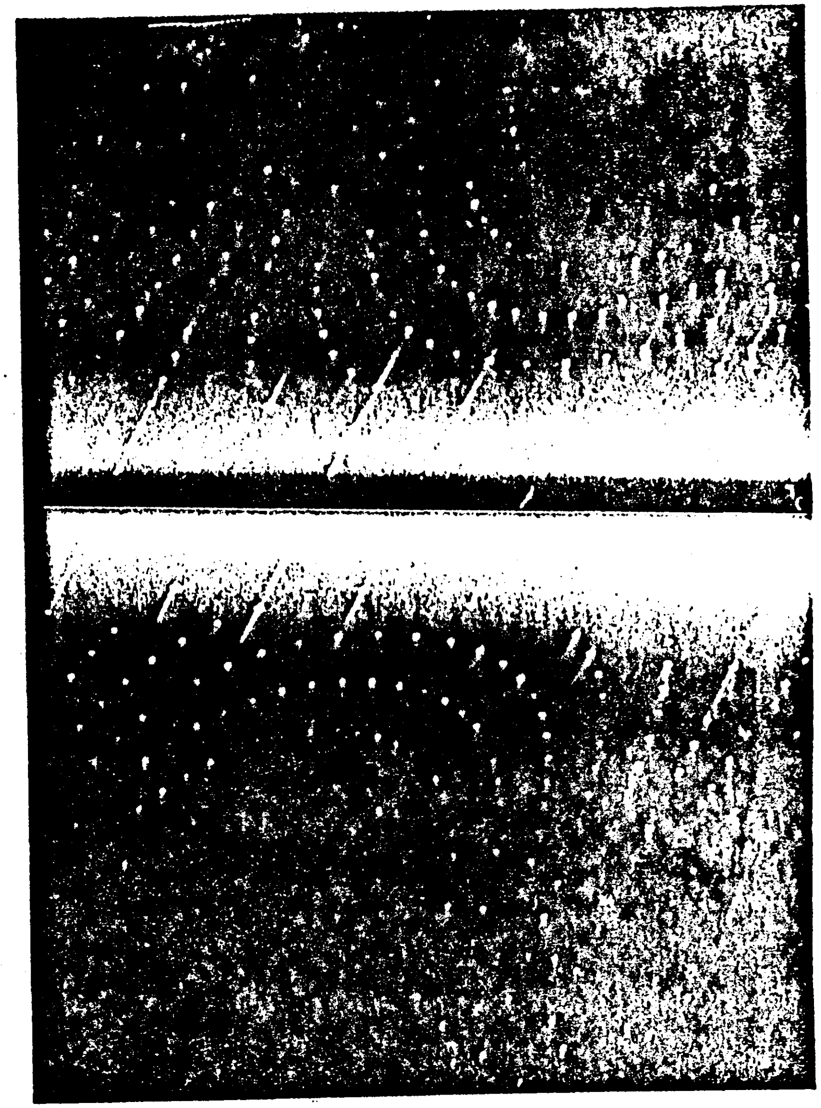

Figure 3.13 Weissenberg photographs for $(Et_2Ph_2P)(TCNQ)_2$

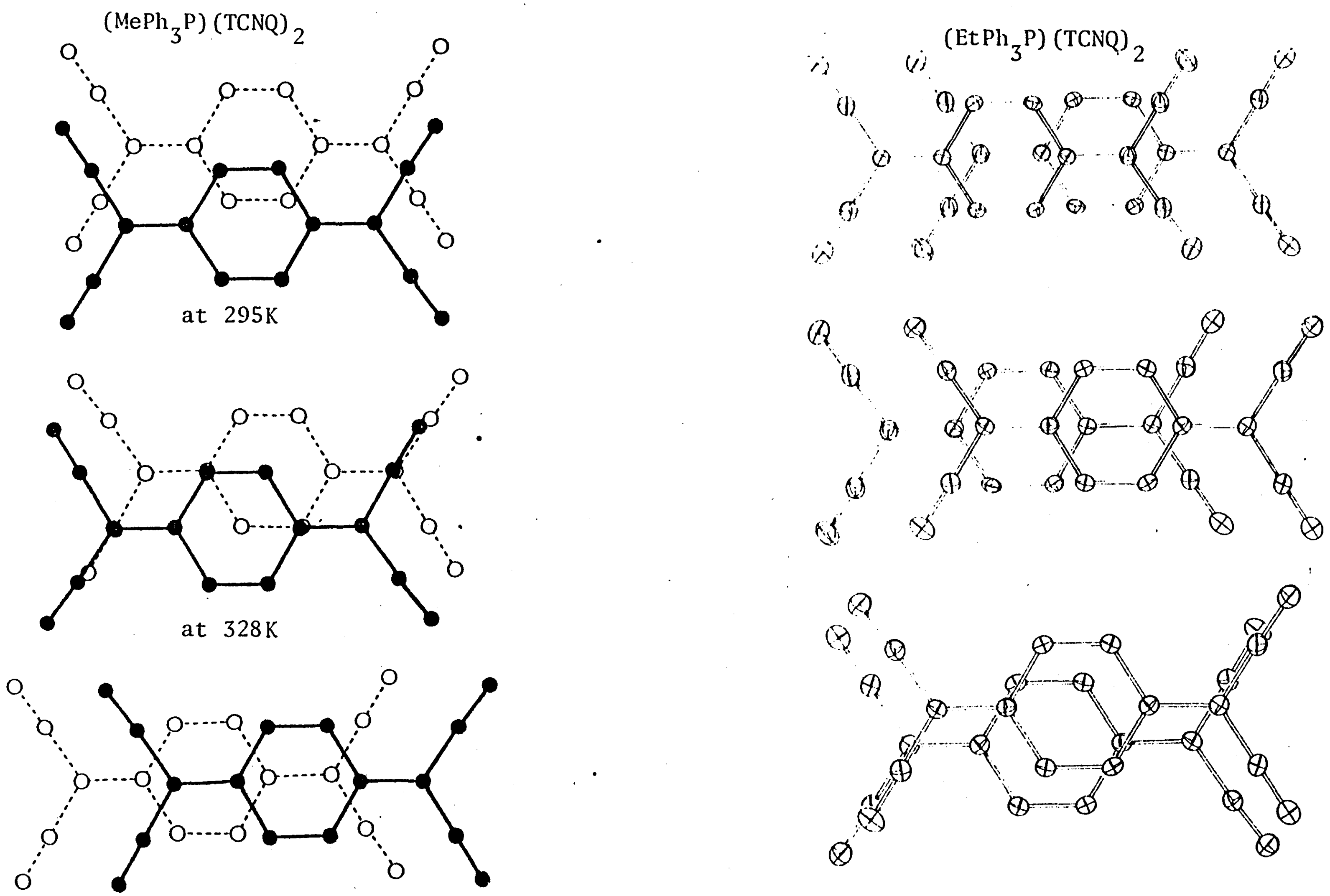

Figure 3.14 Mode of overlap in $(RPh_3P)(TCNQ)_2$ complexes

Table 3.5 Summary of Multan Output for Possible Phase Sets

Set	Abs FOM	Psi Zero	Residual	Combined FOM	Phase Angles for Reflections*(°)			
					a	b	c	d
1	1.3641	3.926	29.25	1.9998	360	360	45	30
2	1.3640	3.926	29.25	Set 1	360	360	135	90
3	1.3641	3.927	29.25	Set 1	360	360	45	270
4	1.3640	3.926	29.25	Set 1	360	360	135	330
5	1.1120	2.443	34.00	1.0000	360	360	45	135
6	1.3642	3.927	29.25	Set 1	360	360	135	210

*Reflections	a	10	2	13	Origin determining reflections
	b	7	1	-9	Origin determining reflections
	c	2	2	-1	Enantiomorph fixing reflection
	d	22	2	-11	General reflection

Table 5.6 Bond Distances (Å) and Angles (°) with Estimated Standard Deviations in Parentheses

Bond Distances (Å)

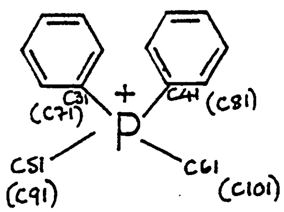

(Me_2Ph_2P) ion

P-C31	1.89(2)	P-C71	1.88(4)
P-C41	1.88(2)	P-C81	1.43(6)
P-C51	1.49(7)	P-C91	2.02(8)
P-C61	1.89(4)	P-C101	2.06(7)

TCNQ A

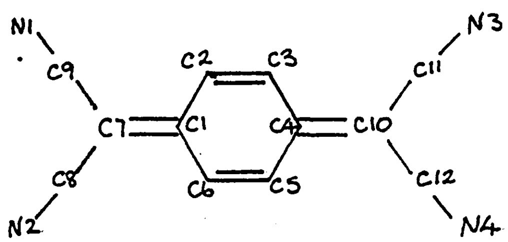

N1-C9	1.05(4)	C1-C6	1.59(4)
N2-C8	1.08(4)	C2-C3	1.30(3)
N3-C11	1.05(3)	C3-C4	1.36(3)
N4-C12	1.27(4)	C4-C5	1.48(4)
C7-C9	1.84(4)	C5-C6	1.62(4)
C7-C8	1.46(3)	C10-C4	1.48(2)
C7-C1	1.36(2)	C10-C11	1.42(3)
C1-C2	1.28(4)	C10-C12	1.22(4)

Table 3.6 contd.

TCNQ B

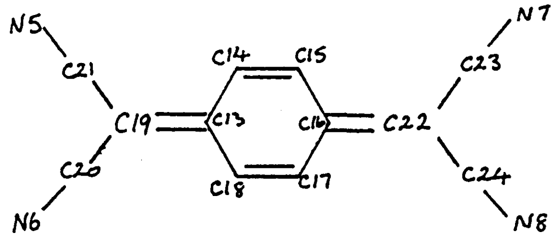

N5-C21	0.97(4)	C13-C18	1.67(3)
N6-C20	1.27(4)	C18-C17	1.42(4)
N7-C23	1.24(4)	C17-C16	1.57(4)
N8-C24	1.01(4)	C16-C15	1.54(3)
C19-C20	1.52(4)	C15-C14	1.22(3)
C19-C21	1.31(4)	C22-C16	1.54(3)
C19-C13	1.36(3)	C22-C23	1.51(4)
C13-C14	1.37(4)	C22-C24	0.96(4)

Bond Angles (°)

(Me_2Ph_2P) ion

C31-P-C41	161(1)	C51-P-C91	74(3)
C31-P-C51	165(2)	C51-P-C101	74(2)
C31-P-C61	79(2)	C61-P-C71	96(2)
C31-P-C71	55(1)	C61-P-C81	113(3)
C31-P-C81	86(2)	C61-P-C91	74(2)
C31-P-C91	111(1)	C61-P-C101	144(3)
C31-P-C101	95(1)	C71-P-C81	126(2)
C41-P-C51	21(2)	C71-P-C91	66(2)
C41-P-C61	103(1)	C71-P-C101	110(2)
C41-P-C71	106(1)	C81-P-C91	163(2)
C41-P-C81	110(2)	C81-P-C101	31(2)
C41-P-C91	53(2)	C91-P-C101	139(2)
C41-P-C101	94(1)	P-C31-C32	120(1)
C51-P-C61	116(2)	P-C31-C36	120(1)

Table 3.6 contd.

C51-P-C71	118(3)	P-C41-C42	113(2)
C51-P-C81	89(3)	P-C41-C46	126(1)

TCNQ A

N1-C9-C7	173(2)	C2-C3-C4	123(2)
N2-C8-C7	155(4)	C3-C4-C5	117(2)
C9-C7-C8	161(2)	C4-C5-C6	127(2)
C9-C7-C1	128(2)	C5-C6-C1	95(3)
C8-C7-C1	121(2)	C10-C4-C5	116(2)
C7-C1-C2	119(2)	C10-C4-C3	126(2)
C7-C1-C6	105(2)	C4-C10-C11	121(2)
C2-C1-C6	136(2)	C4-C10-C12	120(2)
C1-C2-C3	121(2)	C10-C11-N3	171(3)
C11-C10-C12	117(2)	C10-C12-N4	164(3)

TCNQ B

N5-C21-C19	178(3)	C15-C16-C17	100(2)
N6-C20-C19	169(4)	C16-C17-C18	137(2)
C20-C19-C21	116(2)	C17-C18-C13	106(3)
C20-C19-C13	106(3)	C22-C16-C15	123(2)
C21-C19-C13	137(2)	C22-C16-C17	137(2)
C19-C13-C14	139(2)	C16-C22-C24	123(2)
C19-C13-C18	102(2)	C16-C22-C23	107(3)
C14-C13-C18	119(2)	C23-C22-C24	130(3)
C13-C14-C15	126(2)	C22-C23-N7	167(3)
C14-C15-C16	133(2)	C22-C24-N8	170(3)

Table 3.7 Measurements of Cell Constants from Preliminary Photographs with Standard Deviations in Parenthesis

Complex	Oscillation Photographs		Zero-Level	Weissenberg Photographs	
	b/Å		a/Å	c/Å	β(°)
$(Me_2Ph_2P)(TCNQ)_2$	6.528(11)		15.239(7)	31.222(8)	106.1
	13.067(17)	Weak layer lines			
$(Et_2Ph_2P)(TCNQ)_2$	6.513(4)		15.475(7)	31.480(25)	104.2
$(MeEtPh_2P)(TCNQ)_2$	6.463(28)				

CHAPTER FOUR

Single crystal X-ray analyses of two bipyridinium-TCNQ complexes;

(i) N,N′-Dicyanophenyl-4,4′-bipyridylium Tetrakis-7,7,8,8-tetracyanoquinodimethanide, $(DC\emptyset BP)(TCNQ)_4$.

(ii) N,N′-Diethyl-4,4′-bipyridiniumethane Tetrakis-7,7,8,8-tetracyanoquinodimethanide, $(DEPA)(TCNQ)_4$.

Contents

Recently, structural studies have been carried out[82-97] on a series of TCNQ salts in which the cationic moiety comprises one of a series of di-substituted bipyridinium systems (I-III):

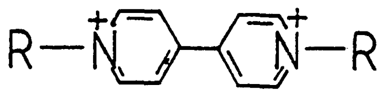

(I)

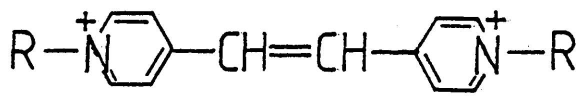

(II)

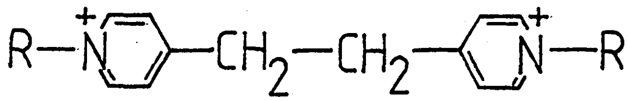

(III)

where R = alkyl, phenyl or benzyl.

The effect of the length of the cation upon the stacking of the TCNQ molecules and the stoichiometry have been studied in a bid to determine which features in the cation enhance the homosoric nature of TCNQ complexes and thus enable highly conducting systems to be designed. Two complexes belonging to the bipyridinium series have been examined in the present work, $(DC\emptyset BP)(TCNQ)_4$ (IV) and $(DEPA)(TCNQ)_4$ (V), and their crystal structures are herewith presented.

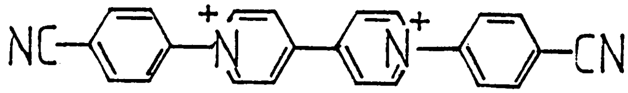

(IV)

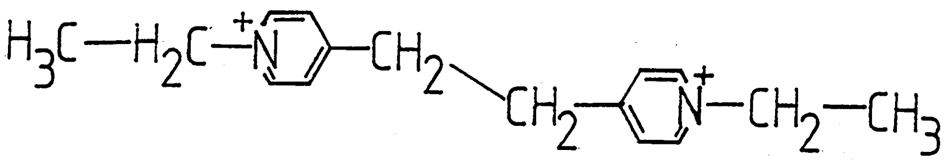

(V)

4.2 Crystal Data

(DCØBP)(TCNQ)$_4$, $C_{72}N_{20}H_{32}$, M_r = 1177.1, triclinic, a = 7.558(5), b = 13.501(4), c = 15.155(4)Å, α = 102.08(2), β = 100.60(4), γ = 98.43(4)° U = 1458.5Å^3, μ(Mo-Kα) = 0.49cm^{-1}, D_m = 1.36, D_c = 1.34gcm^{-3}, Z = 4, F(000) = 604.

(DEPA)(TCNQ)$_4$, $C_{64}N_{18}H_{38}$, M_r = 1058.97, monoclinic, a = 15.208(10), b = 25.97(6), c = 7.771(9)Å, β = 116.33(5)°, U = 2750.89Å^3, μ(Mo-Kα) = 0.46cm^{-1}, D_m = 1.33 D_c = 1.31 gcm^{-3}, Z = 4, F(000) = 1096.

4.3 Crystal Structure Analysis of N,N′-Dicyanophenyl-4,4′-bipyridylium Tetrakis-7,7,8,8-tetracyanoquinodimethanide, (DCØBP)(TCNQ)$_4$

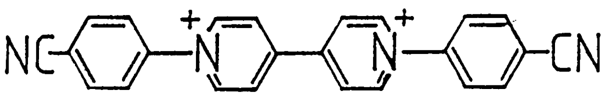

(DCØBP)

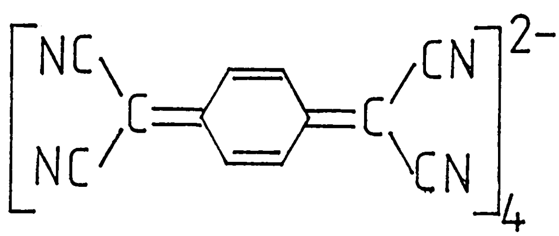

(TCNQ)$_4$

4.3.1 Determination of the Space Group

From Weissenberg and precession photographs, the crystal system was determined to be triclinic, the space group being either the centrosymmetric $P\bar{1}$, or the non-centrosymmetric $P1$.

In the centrosymmetric space group $P\bar{1}$, the asymmetric unit would contain two independent TCNQ molecules and half a (DCØBP) ion, i.e. the cation would be required to lie on a special position (a centre of symmetry), with the two independent TCNQ molecules being related to the remaining TCNQ molecules by centres of symmetry. In the non-centrosymmetric space group $P1$, the cation is not required to lie on a special position as the asymmetric unit would contain one (DCØBP) cation and four independent TCNQ molecules.

4.3.2 Data Collection

A crystal of approximate dimensions 0.25 x 0.15 x 0.10mm was selected Cell dimensions were calculated from the centred settings of 25 reflections with $7 < \theta < 13^{\circ}$ on an Enraf-Nonius CAD-4 diffractometer[158] with monochromated Mo-$K\alpha$ radiation. Intensities for reflections having θ in the range 1.35 - 20° were measured on the same instrument with a variable scan speed and a $\omega - {}^{4}/_{3}\,\theta$ (goniometer-counter) scanning ratio, as optimized by peak-analysis routines. A scan interval of $\Delta\omega = (1.5 + 0.525 \tan\theta)^{\circ}$ was employed. Of the 3799 unique reflections measured, 2338 had $I \geqslant 2\sigma(I)$ and were considered to be observed. The net intensity $I = T - 2B$, where T = measured intensity, B = sum of background counts measured during the first and last sixth of the $\Delta\omega$ scan; $\sigma(I) = (T + 4B + 0.0009I^{2})^{\frac{1}{2}}$. Corrections were made for Lorentz and polarization effects. The intensities of two central reflections were monitored and showed negligible deterioration.

4.3.3 Structure Solution and Refinement

The $|E|$ statistics for ranges of $\sin\theta/\lambda$ were examined and indicated the structure to be centrosymmetric:

$\sin\theta/\lambda$	0.07 - 0.14	- 0.21	- 0.28	- 0.35	- 0.42	- 0.49	- 0.56	- 0.63
$\lvert E \rvert$	0.794	1.024	0.969	0.987	0.986	1.021	1.000	1.000
$\lvert E^2-1 \rvert$	1.090	1.415	1.067	1.106	0.999	1.242	1.166	1.035

Initial attempts at solution using the centrosymmetric automatic direct methods facility in SHELX proved successful. The starting sets used by the multisolution expansion and convergence mapping are presented in Table 4.1.(i). The four $\lvert E \rvert$-maps with the highest figures-of-merit were produced [Table 4.1(ii)]. All the non-hydrogen atom positions were located from the E-map with the third largest figure-of-merit (parachor). Hydrogen atoms were included in positions calculated from the geometry of the molecules (C-H = 1.08Å). Common isotropic temperature factors were applied to the hydrogens and refined to final values of U_{cation} = 0.0798(38), $U_{TCNQ(A)}$ = 0.0708(50), $U_{TCNQ(B)}$ = 0.0617(54)$Å^2$. The weighting scheme adopted was $w = 1.0000/[\sigma^2(F_o) + 0.002346(F_o)^2]$. Full matrix refinement with anisotropic temperature factors for all non-hydrogen atoms gave a final R-value of 0.0481 with R_w = 0.0527. The final difference-Fourier map showed no peaks greater than 0.175e$Å^{-3}$. Final atomic parameters and temperature factors are listed in Appendix A1.3, mean plane data in Appendix A2.3, observed and calculated structure factors in Appendix A3.3, with bond distances and angles presented in Table 4.2.

4.3.4 Description of the Structure

The structure comprises segregated stacks of TCNQ molecules and (DCØBP) ions (Figure 4.1). There are two crystallographically independent TCNQ moieties present TCNQ (A), TCNQ (B), the dimensions of which are given in Table 4.2, and the distances of selected bonds are summarized and compared with neutral and charged TCNQ geometries in Table 4.3. The values of these bond distances for TCNQ (A) and TCNQ (B) are, within experimental error, identical and are similar overall to those observed for $TCNQ^{-\frac{1}{2}}$. Some dimensions of TCNQ (A) are similar to those observed for $TCNQ^{\circ}$, whilst some dimensions of TCNQ (B) are similar to those observed for $TCNQ^{-}$ (Table 4.3), but this is not considered to be strong evidence for charge localization, as the differences are not significant. The negative charge is more likely to be smeared evenly over the two independent moieties. A similar situation has been observed in the related complex $(DBzPE)(TCNQ)_5$.[88]

The TCNQ molecules are arranged in columns parallel to the b-axis and in sheets parallel to the ab-plane (Figure 4.1). The sheets are held together by a network of weak electrostatic interactions between the nitrogen of the terminal cyano-function of one TCNQ and the ring-hydrogen of another, (Figures 4.1, 4.2, Table 4.4). (DCØBP) ions are interleaved between the TCNQ sheets, and the whole three-dimensional array is held together by a series of weak electrostatic interactions between the cationic and anionic stacks (Table 4.4).

The TCNQ molecules in each column are arranged in tetrads, with mean interplanar spacings within a tetrad of 3.356(3) [TCNQ (A)-TCNQ (B)] and 3.005(3)Å [TCNQ (B)-TCNQ (B′)], and a mean spacing of 3.283(3)Å [TCNQ (A)-TCNQ(A″)] between adjacent tetrads (Figures 4.3, 4.4).

Within the tetrads two types of overlap are observed, a ring-to-ring type [TCNQ (A)-TCNQ (B)] and a very minimal side-to-side interaction [TCNQ (B)-TCNQ (B′)]. The overlap between adjacent tetrads is of the desired type: exocyclic double bond to quinonoid ring [TCNQ (A)-TCNQ (A″)], (Figure 4.5). Thus, within a tetrad, one can consider the arrangement as a pair of poorly overlapping diads.

In the (DCØBP) cation, the central bipyridylium function is required to be planar as the C34-C34′ bond lies on a center of symmetry (Figure 4.6). The terminal cyanophenyl groups are twisted out of the plane of the bipyridylium function by 38.7. The cyanide functions are displaced out of the plane of the phenyl ring by as much as 0.155Å (Appendix A2.3).

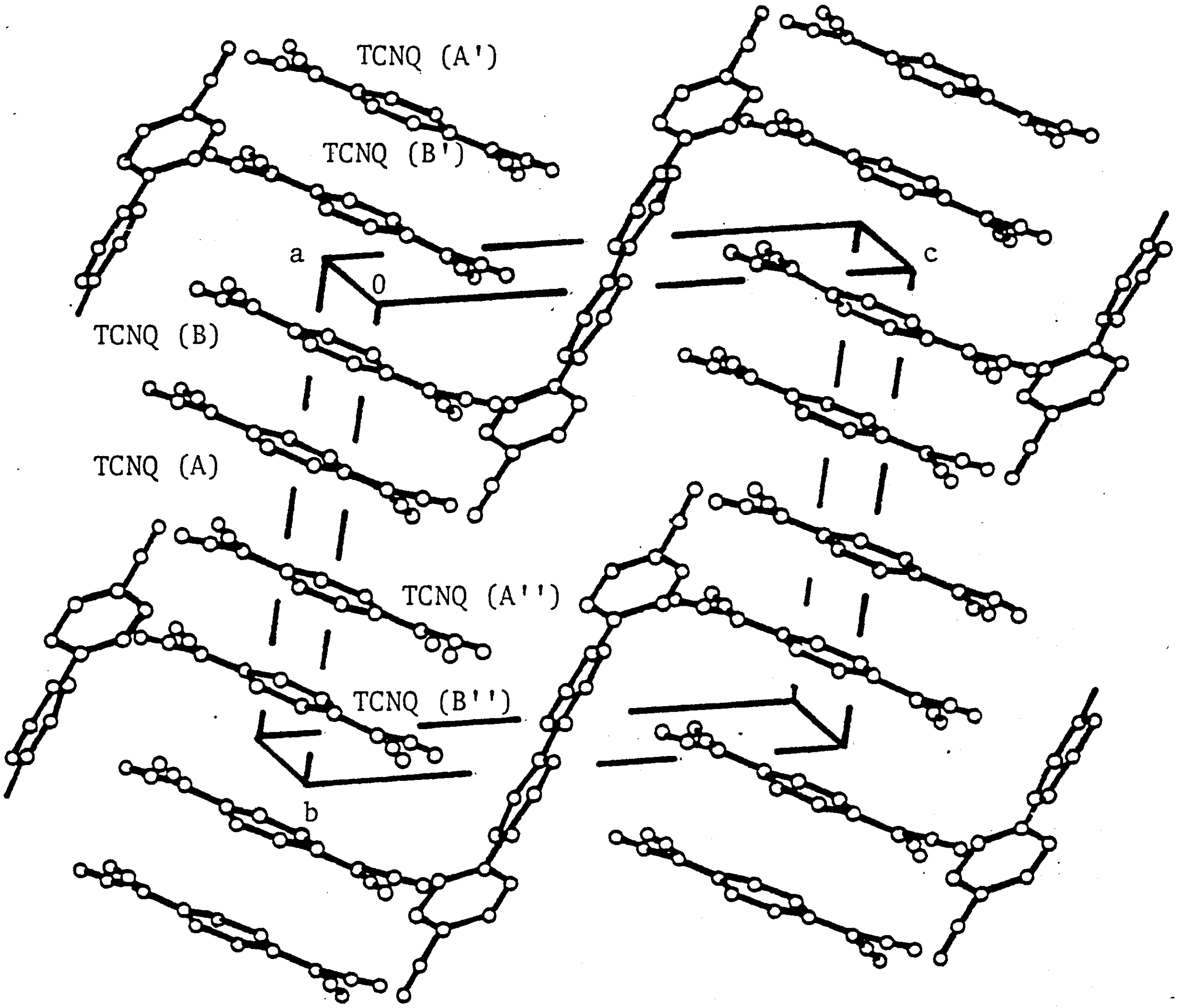

Figure 4.1 General view of the unit cell contents of (DCØBP)$(TCNQ)_4$

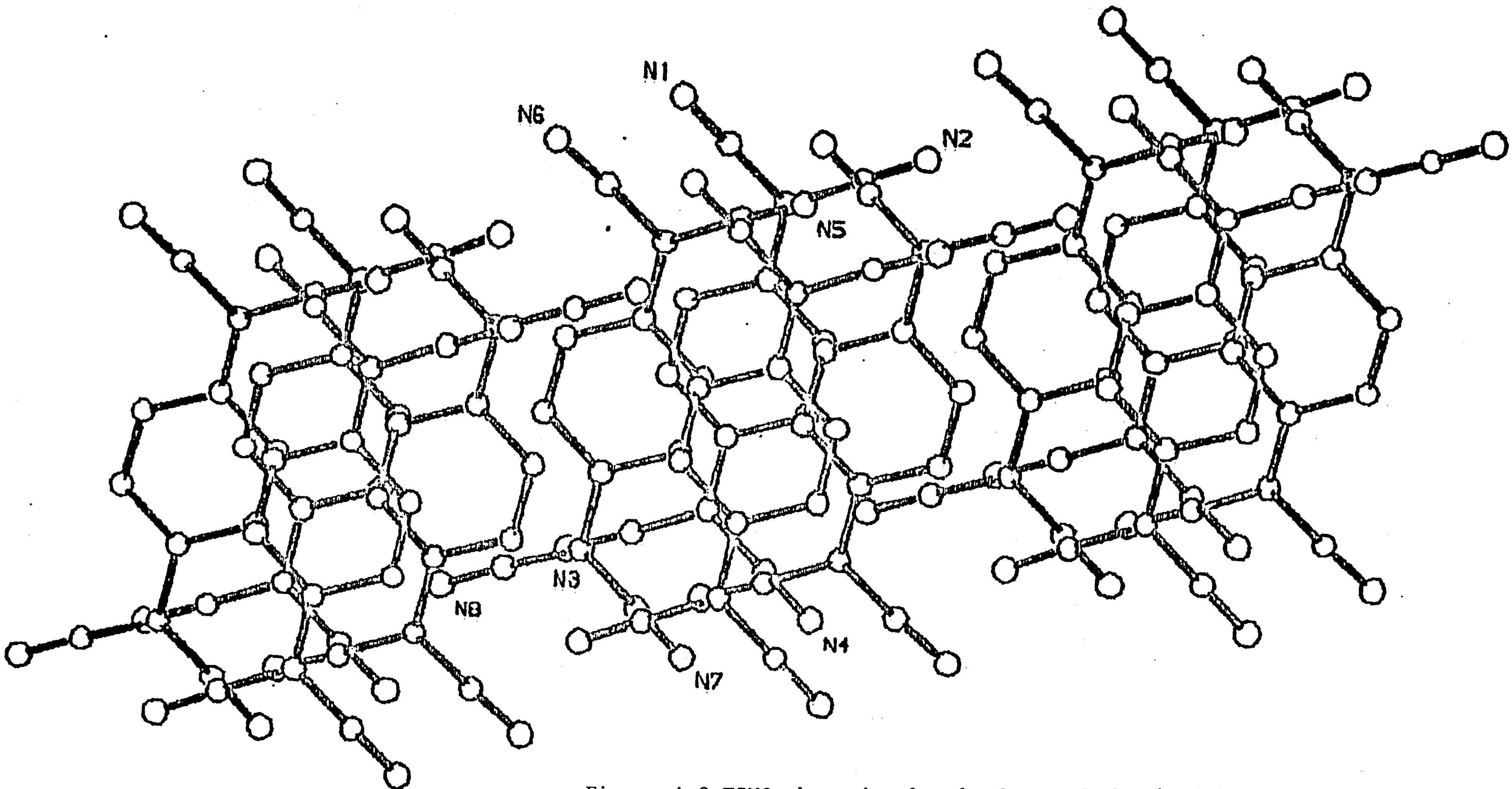

Figure 4.2 TCNQ sheet in the ab-plane of $(DC\emptyset BP)(TCNQ)_4$

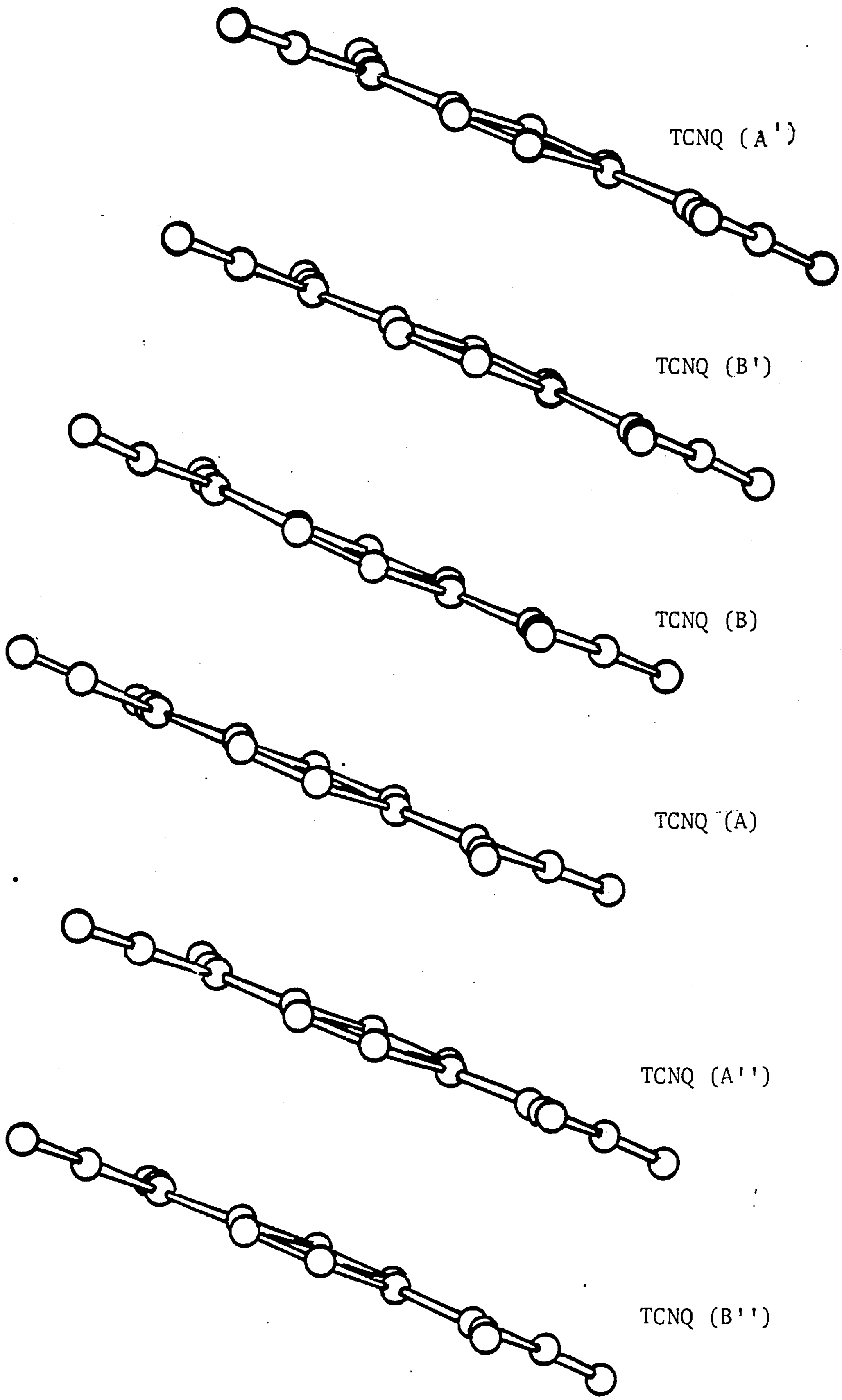

Figure 4.3 Stacking of TCNQ moieties in (DCØBP)$(TCNQ)_4$

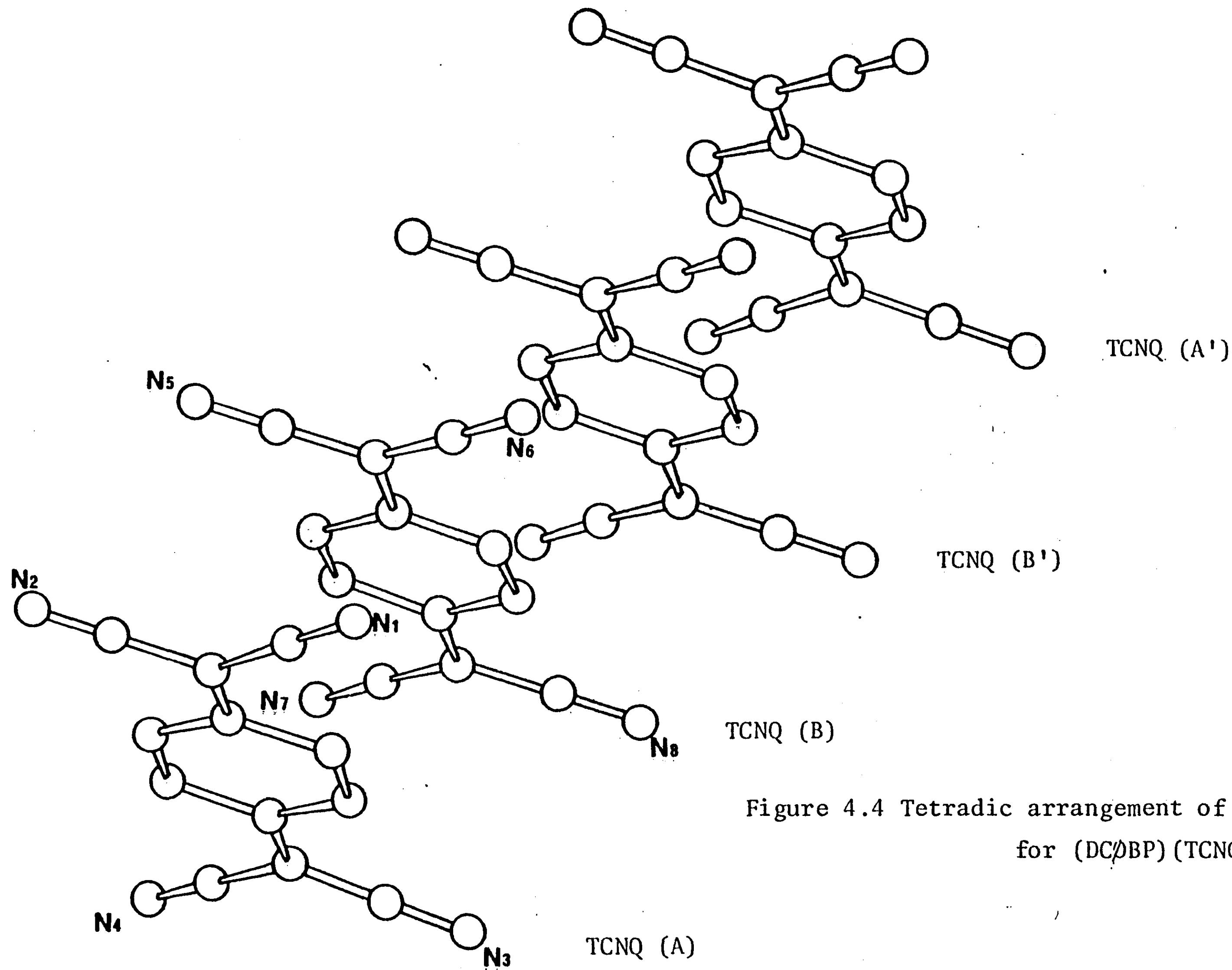

Figure 4.4 Tetradic arrangement of TCNQ molecules for (DCφBP)$(TCNQ)_4$

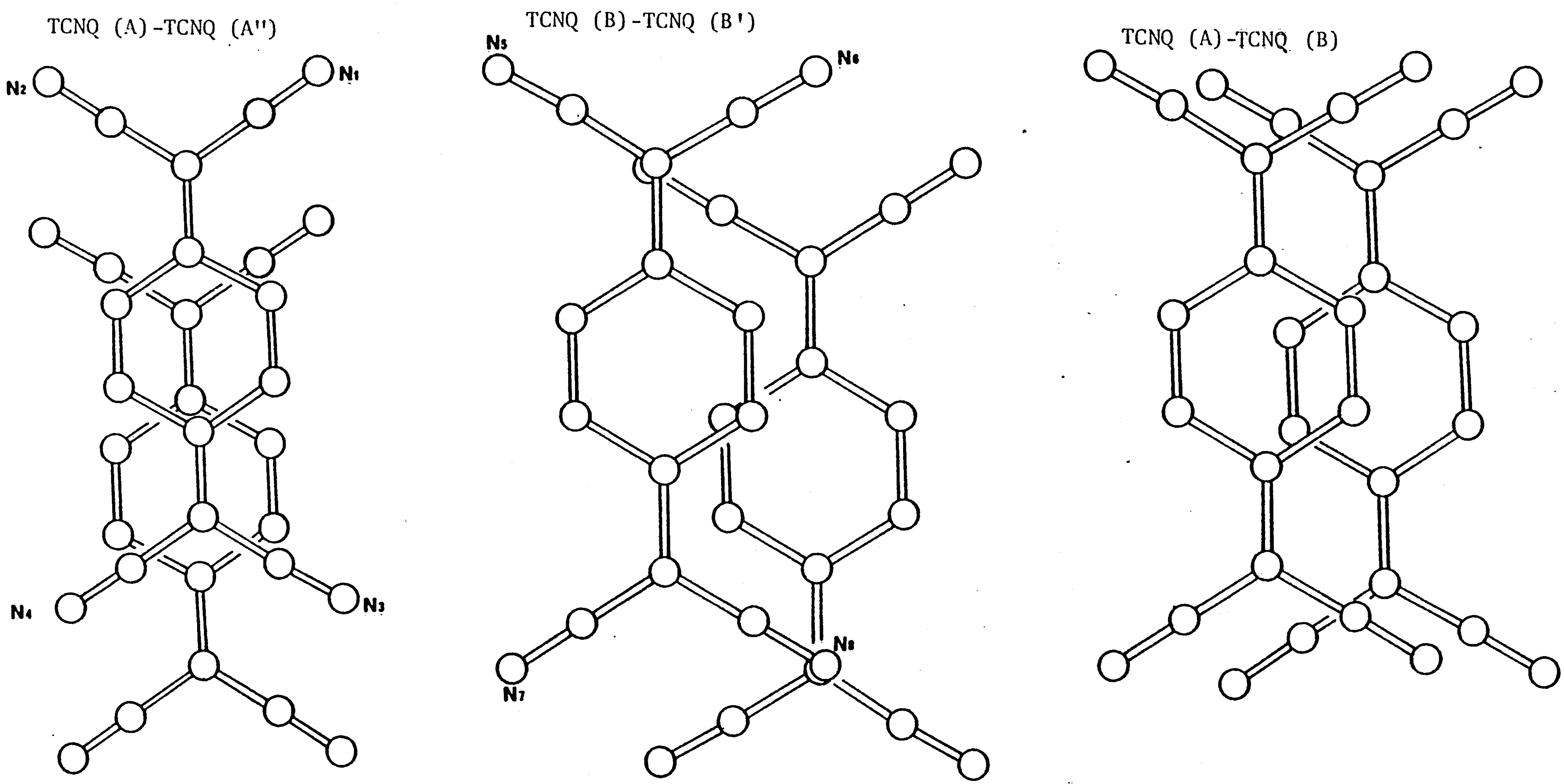

Figure 4.5 Modes of overlap in (DCØBP)$(TCNQ)_4$.

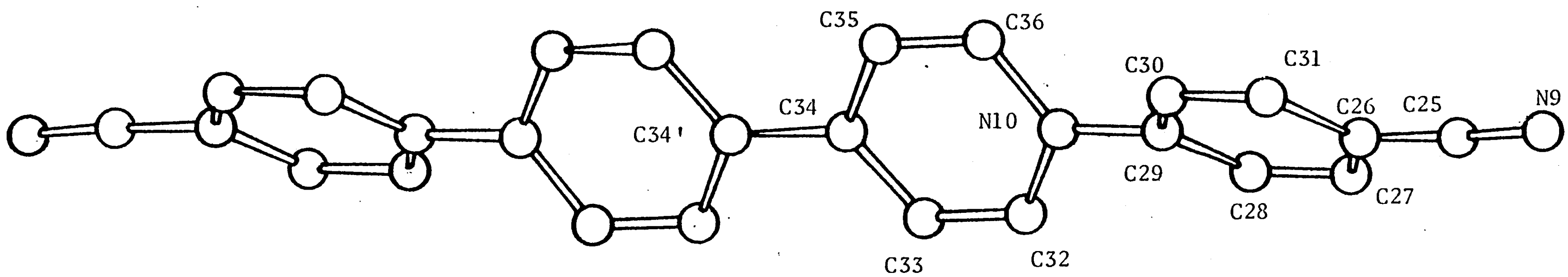

Figure 4.6 The cation in $(DC\emptyset BP)(TCNQ)_4$

Table 4.1 Starting Sets for the Direct Methods Solution of $(DC\emptyset BP)(TCNQ)_4$ in $P\bar{1}$

(i) Starting Sets

h	k	l	Phase Angle (°)	
-5	2	8	0	origin determining reflections
1	3	11	0	
-1	2	3	0	

The following reflections were given phase angles of either 0 or 180° and formed the multisolution starting set:

0 -8 4, 0 -4 2, 6 -2 4, 0 0 12, -5 2 10, 5 -6 5, 0 -4 3, 1 -1 1, 5 -2 4, 4 -4 11, 6 2 2, -5 6 6.

(ii) Figures-of-merit

E -map	Parachor	M(Abs)	NQT	Phase Angle*
1	3.534	0.903	-0.649	+ + + + - - - - + - + - + + -
2	3.146	0.825	-0.570	+ + + + - - + - - - - + + + -
3	2.835	0.782	-0.491	+ + + + - + + - + - + - - - -
4	2.802	1.012	-0.342	+ + + + - + - - + + + - + - -

*The order of the reflections is the same as that given in (i), with + and - corresponding to phase angles of 0 and 180° respectively.

Table 4.2 Bond Distances (Å) and Angles (°) with Estimated Standard Deviations in Parentheses

DCØBP ion

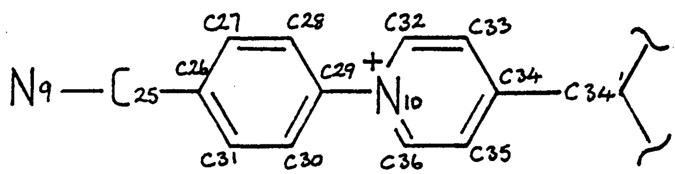

Bond Distances

N9-C25	1.134(5)	C29-N10	1.455(4)
C25-C26	1.447(5)	N10-C32	1.349(4)
C26-C27	1.396(4)	C32-C33	1.364(5)
C27-C28	1.377(5)	C33-C34	1.401(4)
C28-C29	1.383(5)	C34-C35	1.387(5)
C29-C30	1.377(4)	C35-C36	1.365(5)
C30-C31	1.384(5)	C36-N10	1.366(4)
C31-C26	1.374(5)		

Bond Angles

N9-C25-C26	177.5(4)	C30-C29-N10	119.5(3)
C25-C26-C27	118.8(3)	C29-N10-C32	120.7(3)
C25-C26-C31	120.3(3)	C29-N10-C36	119.7(3)
C31-C26-C27	120.8(3)	C32-N10-C36	119.6(3)
C26-C27-C28	119.1(3)	N10-C32-C33	121.3(3)
C27-C28-C29	119.2(3)	C32-C33-C34	120.5(3)
C28-C29-C30	122.3(3)	C33-C34-C35	117.0(3)
C29-C30-C31	118.3(3)	C34-C35-C36	121.2(3)
C30-C31-C26	120.4(3)	C35-C36-N10	120.4(3)
C28-C29-N10	118.3(2)		

Table 4.2 contd.

TCNQ (A)

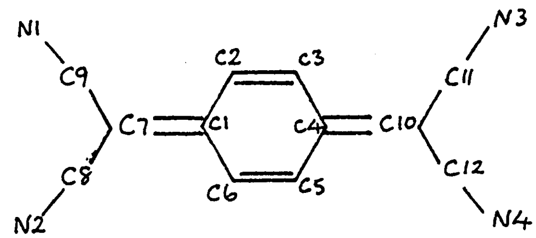

Bond Distances

N1-C9	1.148(4)	C4-C5	1.446(5)
N2-C8	1.145(5)	C5-C6	1.348(5)
C7-C9	1.429(4)	C6-C1	1.429(4)
C7-C8	1.441(5)	C10-C4	1.384(5)
C7-C1	1.393(5)	C10-C11	1.431(6)
C1-C2	1.439(5)	C10-C12	1.435(4)
C2-C3	1.346(5)	N3-C11	1.143(6)
C3-C4	1.433(4)	N4-C12	1.143(4)

Bond Angles

N1-C9-C7	178.2(4)	C3-C4-C5	117.0(3)
N2-C8-C7	179.4(3)	C4-C5-C6	121.1(3)
C9-C7-C8	114.8(3)	C5-C6-C1	121.4(3)
C9-C7-C1	122.5(3)	C3-C4-C10	122.3(3)
C8-C7-C1	122.7(3)	C5-C4-C10	120.7(3)
C7-C1-C2	120.5(3)	C4-C10-C11	122.0(3)
C7-C1-C6	121.8(3)	C4-C10-C12	122.1(3)
C2-C1-C6	117.6(3)	C11-C10-C12	115.9(3)
C1-C2-C3	120.9(3)	N3-C11-C10	178.8(3)
C2-C3-C4	121.8(3)	N4-C12-C10	178.9(5)

Table 4.2 contd.

TCNQ (3)

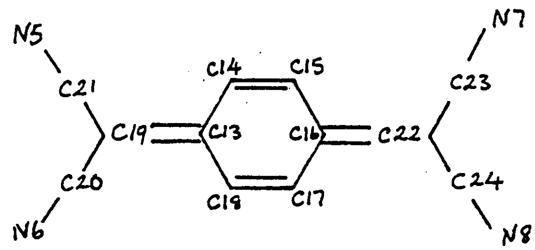

Bond Distances

N5-C21	1.143(4)	C16-C17	1.433(5)
N6-C20	1.151(6)	C17-C18	1.359(5)
C19-C20	1.425(6)	C18-C13	1.425(4)
C19-C21	1.418(4)	C22-C16	1.398(5)
C19-C13	1.399(5)	C22-C23	1.424(5)
C13-C14	1.436(5)	C22-C24	1.421(4)
C14-C15	1.355(5)	N7-C23	1.151(5)
C15-C16	1.420(4)	N8-C24	1.151(4)

Bond Angles

N5-C21-C19	177.6(4)	C16-C17-C18	120.9(3)
N6-C20-C19	179.6(3)	C17-C18-C13	121.1(3)
C20-C19-C21	116.7(3)	C18-C13-C14	117.9(3)
C20-C19-C13	122.2(3)	C15-C16-C22	121.4(3)
C21-C19-C13	121.0(3)	C17-C16-C22	121.0(3)
C19-C13-C14	120.3(3)	C23-C22-C16	121.5(3)
C19-C13-C18	121.8(3)	C24-C22-C16	122.3(3)
C13-C14-C15	120.4(3)	C23-C22-C24	116.2(3)
C14-C15-C16	121.9(3)	N7-C23-C22	179.1(3)
C15-C16-C17	117.7(3)	N8-C24-C22	178.5(4)

Table 4.3 Distances (Å) of Selected Bonds in the Independent TCNQ Molecules

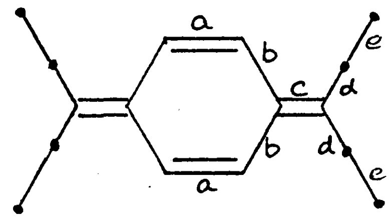

	a	b	c	d	e	Ref.
TCNQ (A)	1.346(5)	1.439(5)	1.393(5)	1.429(4)	1.148(4)	p.w.
	1.348(5)	1.429(5)		1.441(5)	1.145(5)	
TCNQ (B)	1.355(5)	1.436(5)	1.399(5)	1.418(6)	1.143(4)	p.w.
	1.359(5)	1.425(4)		1.425(6)	1.151(6)	
$TCNQ^{\circ}$	1.346	1.448	1.374	1.440	1.138	39
$TCNQ^{-\frac{1}{2}}$	1.355	1.433	1.396	1.424	1.145	84
$TCNQ^{-}$	1.362	1.424	1.413	1.417	1.149	86

Table 4.4 Short intermolecular contacts (Å) for ([illegible])(TCNQ)$_4$

(i) Between TCNQ molecules

H2 ---- N2^{i}	2.504	H14 ---- N6^{i}	2.485
N2 ---- H2^{ii}	2.504	N6 ---- H14^{ii}	2.485
N3 ---- H5^{i}	2.506	N7 ---- H17^{i}	2.435
H5 ---- N3^{ii}	2.506	H17 ---- N7^{ii}	2.435

(ii) Between cation and anion

N1 ---- H32^{iv}	2.255	N4 ---- H30^{v}	2.864
H32 ---- N1^{iii}	2.255	H30 ---- N4^{v}	2.864
N5 ---- H33^{iv}	2.315	N1 ---- H30^{iv}	2.799
H33 ---- N5^{iii}	2.315	H30 ---- N1^{iii}	2.799
N5 ---- H35^{v}	2.718	N7 ---- H28	2.598
H35 ---- N5^{v}	2.718	H28 ---- N7^{ii}	2.598
N4 ---- H31^{vi}	2.532	N3 ---- H27^{i}	2.732
H31 ---- N4^{vi}	2.532	H27 ---- N3^{ii}	2.732

Symmetry codes

none x, y, z; (^{i}) -1+x,y,z; (^{ii}) 1+x,y,z; (^{iii}) 1+x,y,1+z; (^{iv}) -1+x,y, -1+z; (^{v}) -x,-y,-z; (^{vi}) 2-x,1-y,1-z.

4.4 Crystal Structure Analysis of N,N'-Diethyl-4,4'-bipyridiniumethane Tetrakis-7,7,8,8-tetracyanoquinodimethanide, (DEPA)(TCNQ)$_4$

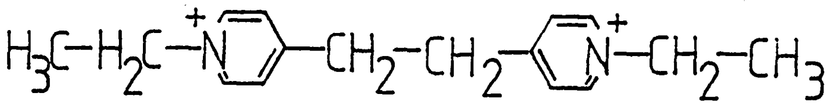

(DEPA)

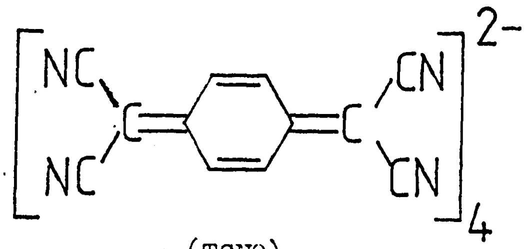

(TCNQ)$_4$

4.4.1 Determination of the Space Group

The systematic absences noted from the preliminary Weissenberg and precession photographs (h0l, l = 2n + 1; 0k0, k = 2n + 1) are consistent with the monoclinic space group, $P2_1/c$. In this centrosymmetric space group, the asymmetric unit must contain two independent TCNQ moieties and half a (DEPA) ion. Thus, the (DEPA) ion must lie on a centre of symmetry.

4.4.2 Data Collection

A crystal of approximate dimensions 0.15 x 0.20 x 0.30mm was mounted with the c-axis coincident with the rotation (ω) axis of a Stöe Stadi 2 two-circle diffractometer. Intensity data were collected using monochromated Mo-Kα radiation and the background-ω-scan-background technique. Of the 3280 unique reflections measured, only 953 had $I \geq 3\sigma(I)$ and these were used in subsequent analysis and refinement. The small number of observed reflections was due to the fact that the tube intensity was continually decreasing as the intensity data was being collected. Corrections were made for Lorentz and polarization effects but not for absorption effects.

4.4.3 Structure Solution and Refinement

Structure analysis and refinement were carried out using the SHELX automatic centrosymmetric multisolution package. The collected intensity was merged and the $|E|$-statistics produced for ranges of $\sin\theta/\lambda$, indicated that the crystal was centrosymmetric:

$\sin\theta/\lambda$	0.07 - 0.14	- 0.21	- 0.28	- 0.35	- 0.42	- 0.49	- 0.56	- 0.63
$\|E\|$	0.853	1.051	1.005	0.995	0.990	1.027	1.000	1.000
$\|E^2-1\|$	0.842	1.410	1.050	1.059	0.992	1.212	1.033	0.807

The starting sets produced by the sign expansion pathway are given in [Table 4.5(i)]. From the convergence procedure the seven $|E|$-maps with the highest figures-of-merit were produced [Table 4.5(ii)]. The majority of the non-hydrogen atom positions for the two independent TCNQ moieties were located from the $|E|$-map with the fifth largest figure-of-merit. The remaining non-hydrogen atom positions for half a (DEPA) ion and the two independent TCNQ moieties were located from successive difference Fourier maps. Inter-layer scale factors were applied in an effort to scale the poor intensity data. The thermal parameters for the non-hydrogen atom positions were allowed to refine anisotropically except those which became non-positive definite. The weighting scheme adopted was $w = 6.9101/[\sigma^2(F_o) + 0.000165\,(F_o)^2]$. Full matrix refinement with most of the non-hydrogen atoms having anisotropic temperature factors gave a final R-value of 0.129 with the weighted R-value (R_w) being 0.1282. The final difference-Fourier map showed no peaks greater than 0.22 eÅ^{-3}. Final positional and thermal parameters are given in Appendix A1.4, mean plane data in Appendix A2.4, observed and calculated structure factors in Appendix A3.4, with bond distances and angles in Table 4.6.

4.4.4 Description of the Structure

The structure comprises segregated stacks of TCNQ molecules and (DEPA) ions (Figure 4.7). The TCNQ molecules stack in columns, made up of tetradic units, parallel to the b-axis, and in sheets, held together by short N - - - HC intermolecular contacts, parallel to the bc-plane

(Table 4.7). The sheets of TCNQ molecules are interleaved by sheets of (DEPA) ions (Figure 4.8).

Although there are tetrads present in the TCNQ columns, the poor overlap, both between diadic units within the tetrad and also between adjacent tetrads, indicate that the arrangement of TCNQ molecules may be best considered in terms of weakly interacting diadic units.

The independent diadic pair, TCNQ (A1) and TCNQ (B1) are (Figure 4.9) related to:

(i) TCNQ (A3) and TCNQ (B3) by a c-glide plane perpendicular to the b-axis at 0.25b;

(ii) TCNQ (A4) and TCNQ (B4) by a two-fold screw axis at 0, y, 0.25;

(iii) TCNQ (A2) and TCNQ (B2) by a centre of symmetry at 0, 0.5, 0.

The mode of overlap between the TCNQ molecules in the diadic pairs [i.e. TCNQ (An), TCNQ (Bn); n = 1, 2, 3, 4] is of the desired type: exocyclic double bond to quinonoid ring, with a d-spacing of 3.202Å (Figure 4.10). The overlap between adjacent diads is poor (Figures 4.11, 4.12) with d-spacings varying from 3.596Å[TCNQ (A1)-TCNQ (A3)] to 3.402Å[TCNQ (B1)-TCNQ (B2)].

The (DEPA) ion is a symmetrical bipyridinium ion and lies on a centre of symmetry at 0.5, 0.5, 0.5, the centre being between C32 and C32′(Figure 4.13). The terminal ethyl groups are twisted out of the plane of the rings by 62.61° (Appendix A2.4).

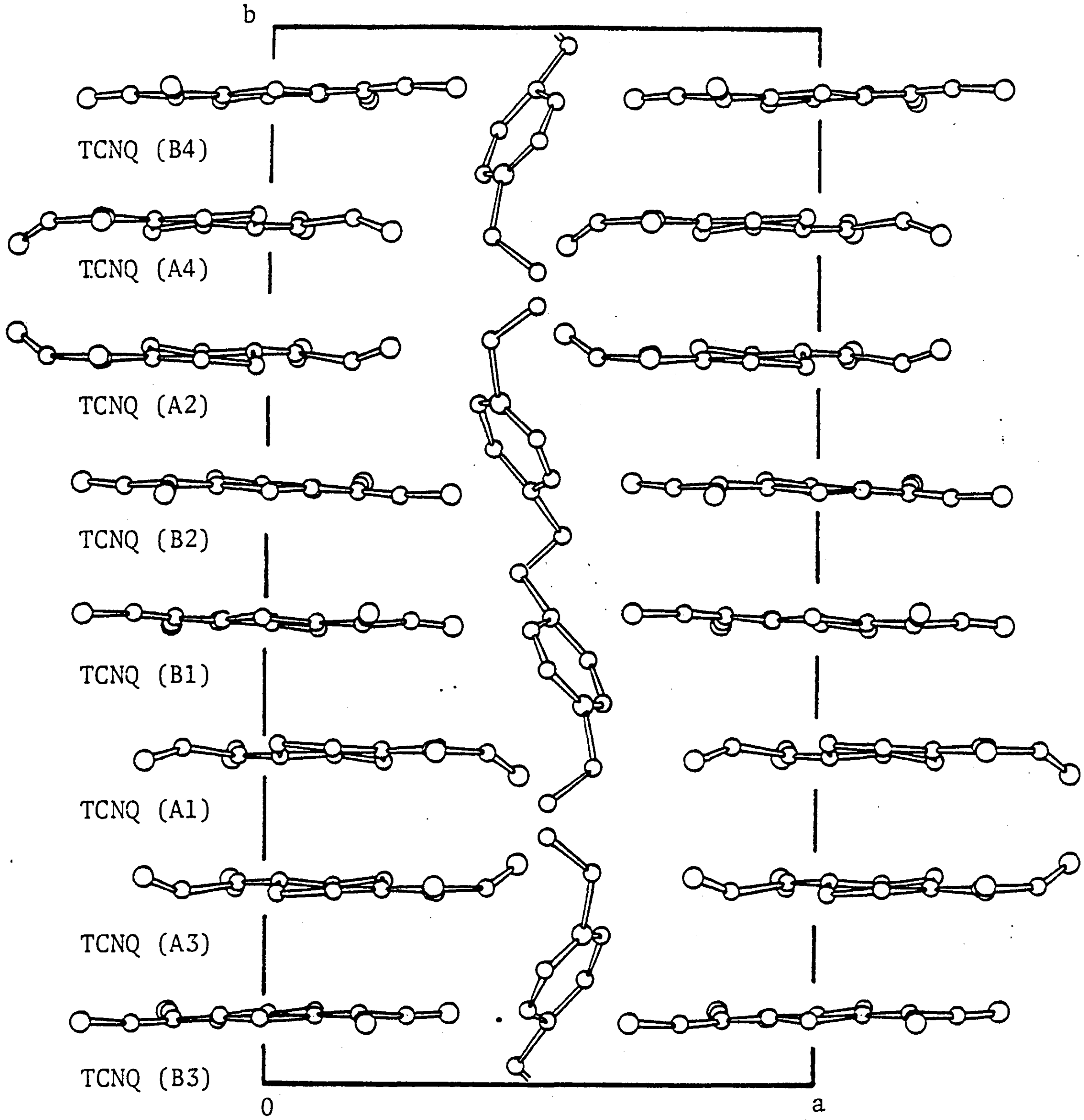

Figure 4.7 Packing diagram for (DEPA)$(TCNQ)_4$;
view down the c-axis.

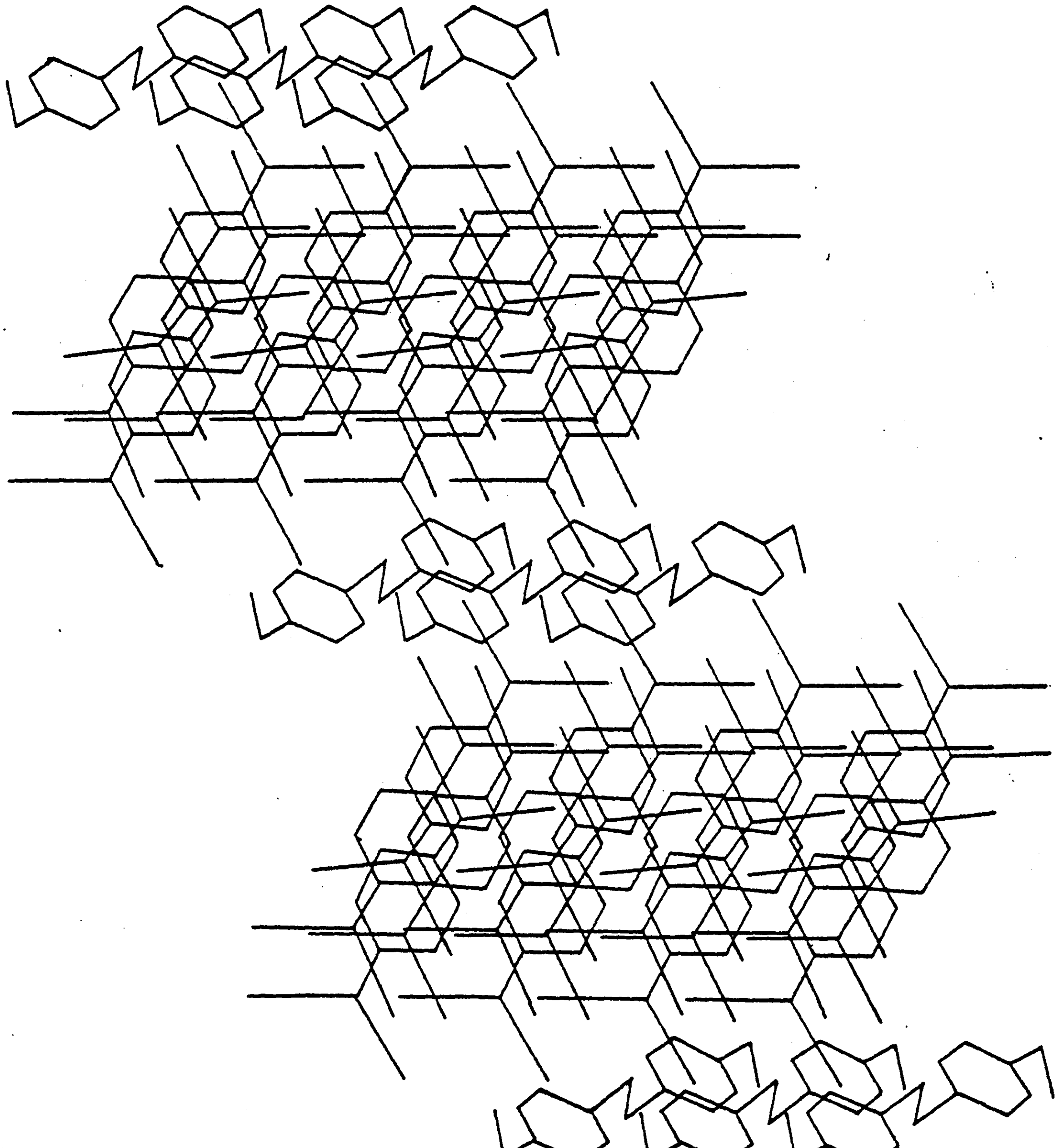

Figure 4.8 Projection down the b-axis showing sheets of TCNQ molecules and sheets of (DEPA) ions.

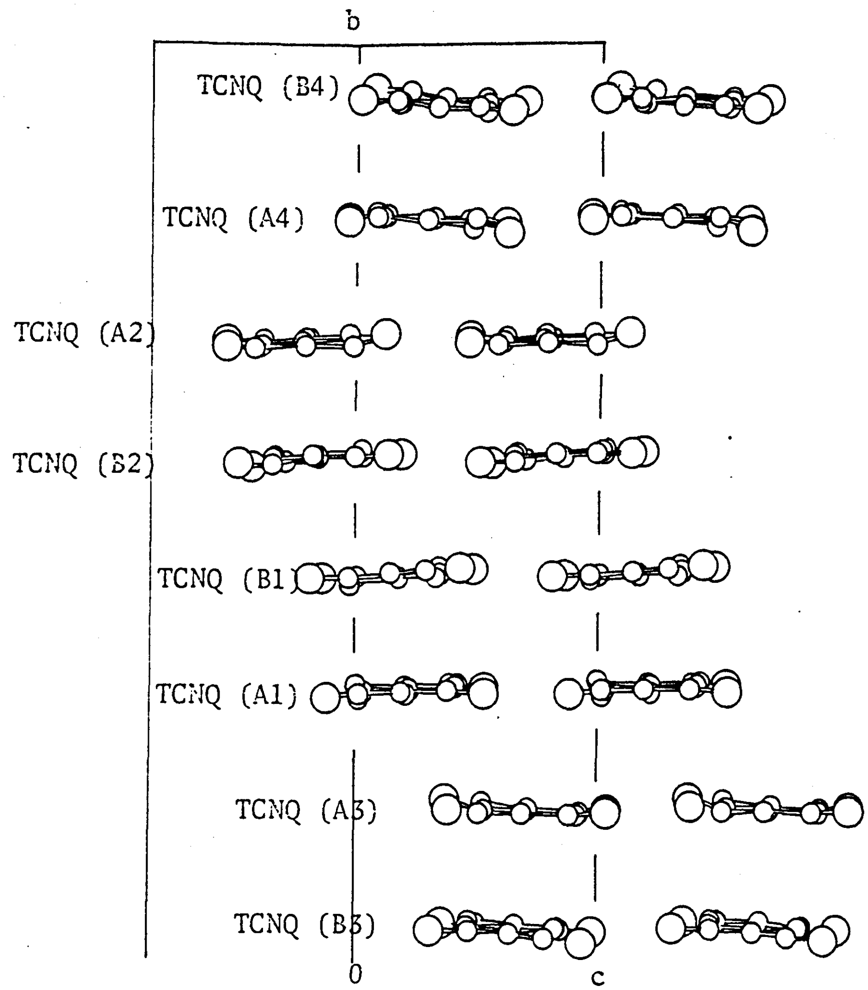

Figure 4.9 View down the C10-C4 bond showing the irregular stacks in $(DEPA)(TCNQ)_4$

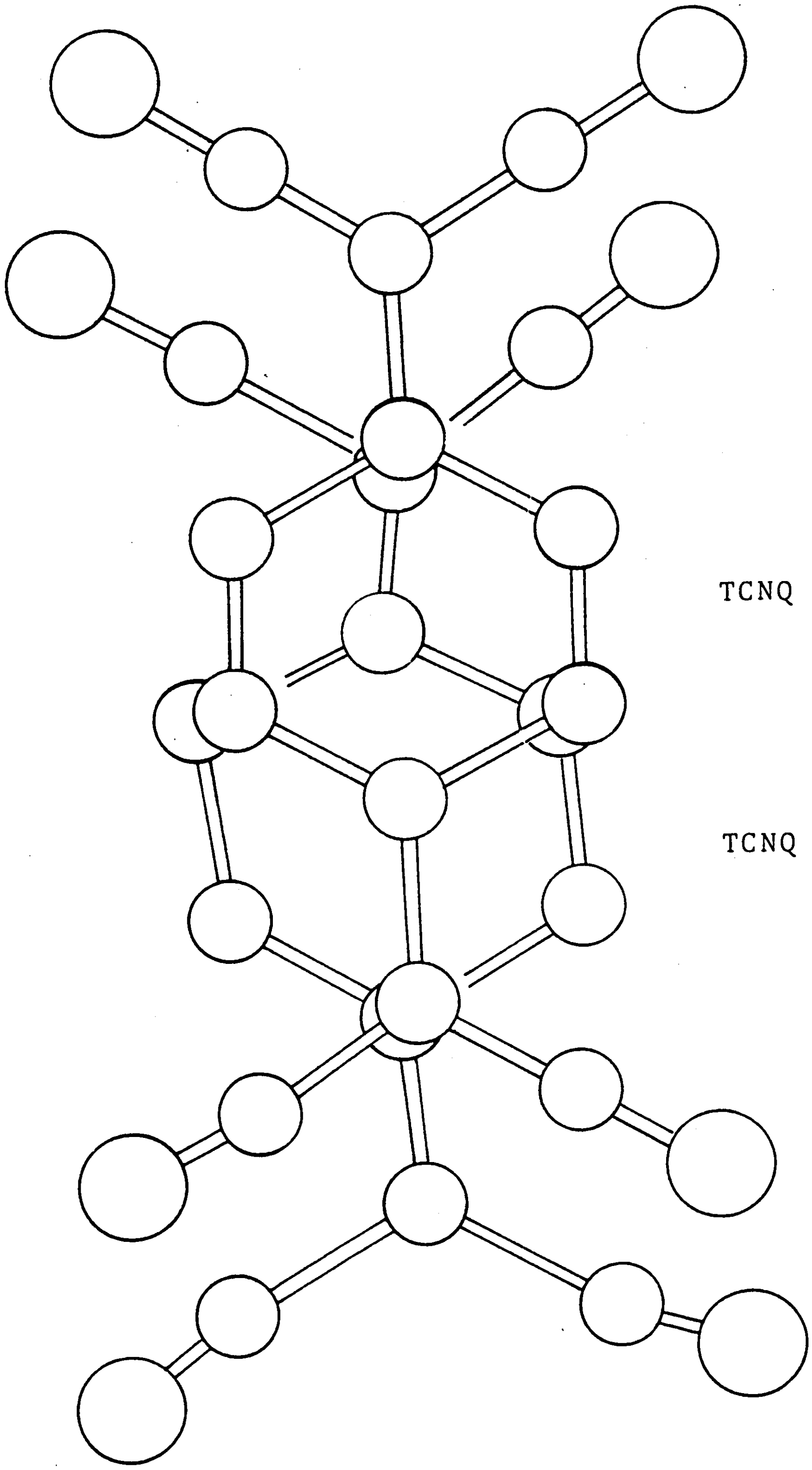

Figure 4.10 Overlap between TCNQ (A1) and TCNQ (B1).

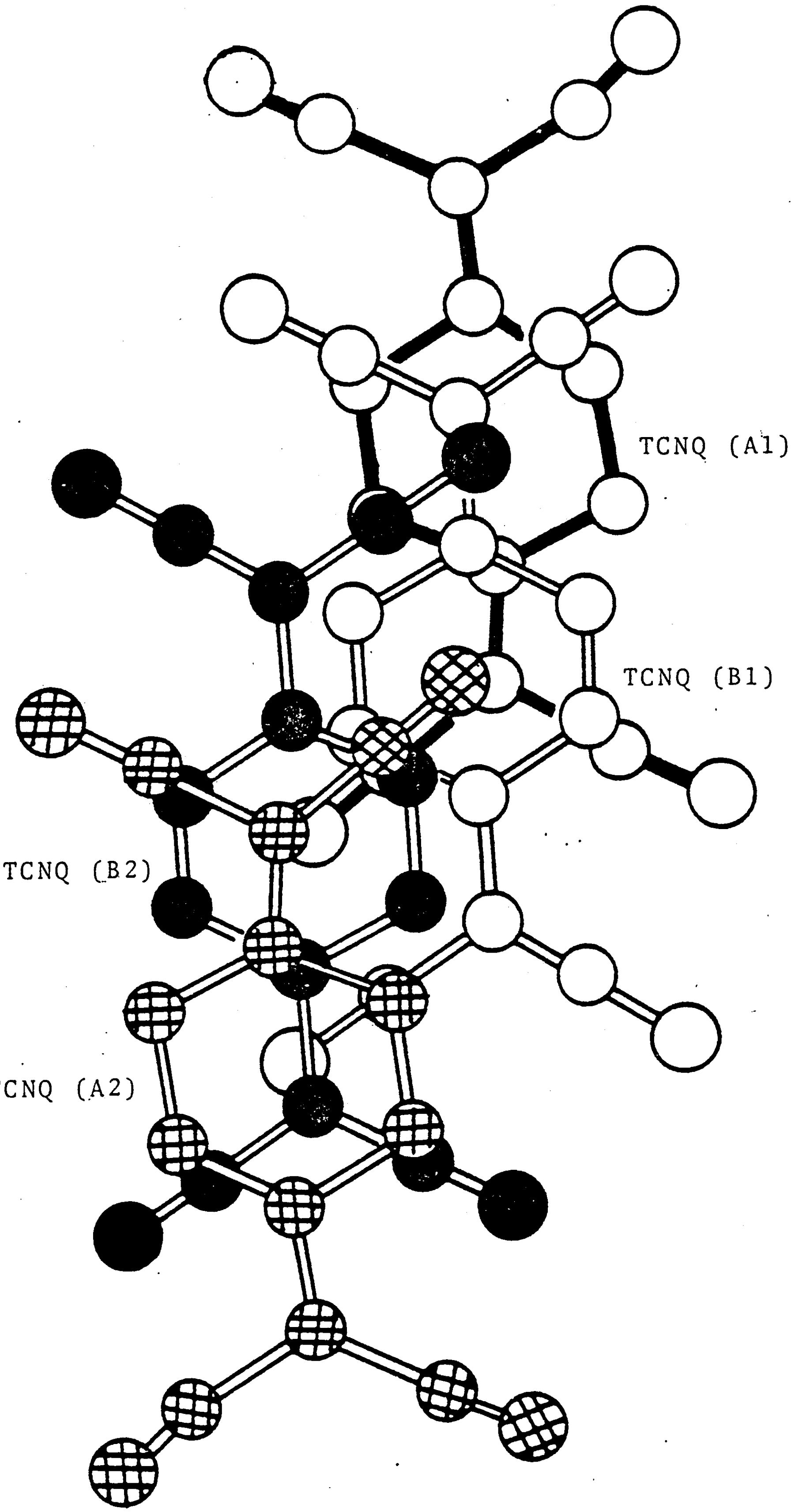

Figure 4.11 Overlap between TCNQ (A1), TCNQ(B1), TCNQ (A2), and TCNQ (B2).

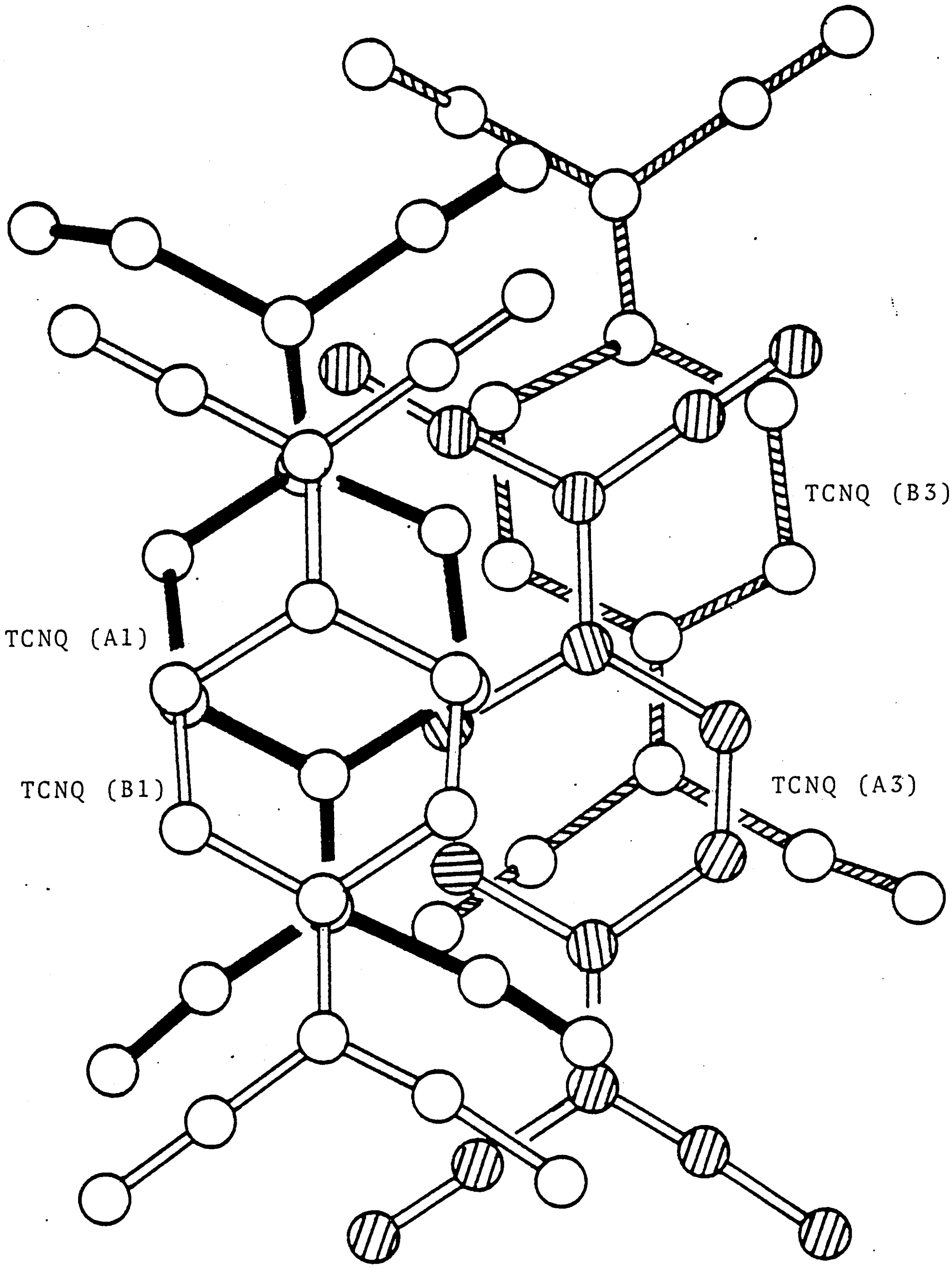

Figure 4.12 Overlap between TCNQ (A1), TCNQ (B1), TCNQ (A3), and TCNQ (B3).

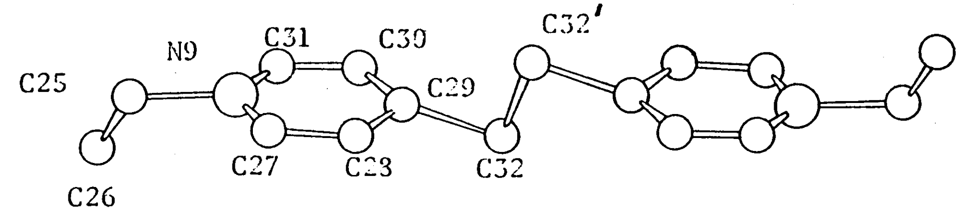

Figure 4.13 The cation in $(DEPA)(TCNQ)_4$

Table 4.5 Starting Sets for the Direct Methods Solution of (DBFA)(TCNQ)$_4$ in $P2_1/c$

(i) Starting Sets

h	k	l	Phase Angle (°)	
2	4	1	0	origin determining reflections
1	12	5	0	
2	5	5	0	

The following reflections were given phase angles of either 0 or 180° and formed the multisolution starting set:

0 16 0, 0 2 6, 0 6 6, 0 8 0, 1 8 0, -6 4 1, 1 16 0, 0 10 6, -6 12 1, 1 4 5, 0 14 6, -8 4 5.

(ii) Figures-of-merit

E-map	Parachor	M(Abs)	NQT	Sign of Phase Angles*
1	3.904	1.046	-0.704	+ + + + - + - + - - - + + - + + -
2	3.572	1.084	-0.604	+ + + + + - - + - - + - + - - - +
3	3.329	0.991	-0.532	+ + + + - + - - - + + - + - + + -
4	3.298	1.045	-0.516	+ + + + - + - + - - - + + - + - -
5	3.075	0.984	-0.451	+ + + + + - - - - + - + + - - - +
6	2.949	0.787	-0.526	+ + + + - + - - - + + + + - + - -
7	2.949	0.891	-0.468	+ + + + - + - + + - + + - - + - -

*The order of the reflections is the same as that given in (i), with + and - corresponding to a phase angle of 0 and 180° respectively.

Estimated Standard Deviations in Parentheses

(DEPA) ion:

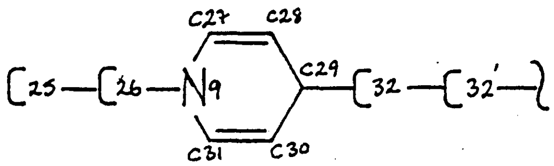

Bond Distances

C25-C26	1.560(56)	C28-C29	1.354(45)
C26-N9	1.707(38)	C29-C30	1.500(50)
N9-C27	1.336(45)	C30-C31	1.318(40)
N9-C31	1.285(39)	C29-C32	1.709(32)
C27-C28	1.418(35)	C32-C32′	1.559(52)

Bond Angles

C25-C26-N9	111.2(2.2)	C29-C30-C31	112.9(3.2)
C26-N9-C27	112.3(2.5)	C30-C31-N9	126.8(2.8)
C26-N9-C31	121.9(2.5)	C28-C29-C32	118.9(2.3)
C31-N9-C27	125.8(2.4)	C30-C29-C32	119.6(2.7)
N9-C27-C28	111.9(2.9)	C28-C29-C30	117.1(2.6)
C27-C28-C29	124.8(2.8)		

TCNQ (A1)

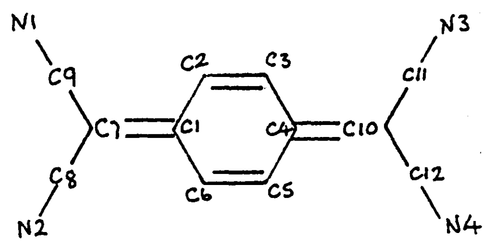

Bond Distances

N1-C9	1.071(23)	C4-C5	1.446(40)
N2-C8	1.212(43)	C5-C6	1.518(25)
C9-C7	1.455(26)	C6-C1	1.478(30)

Table 4.6 contd.

C8-C7	1.576(42)	C4-C10	1.363(26)
C7-C1	1.238(23)	C10-C11	1.591(46)
C1-C2	1.418(39)	C10-C12	1.608(34)
C2-C3	1.460(16)	C11-N3	1.035(49)
C3-C4	1.520(19)	C12-N4	1.019(29)

Bond Angles

N1-C9-C7	174.5(2.4)	C3-C4-C5	117.4(1.2)
N2-C8-C7	174.9(2.2)	C4-C5-C6	129.0(1.7)
C9-C7-C8	110.2(1.5)	C5-C6-C1	107.2(2.0)
C9-C7-C1	132.3(2.8)	C10-C4-C3	115.5(2.2)
C8-C7-C1	117.1(2.2)	C10-C4-C5	127.0(1.9)
C7-C1-C2	112.3(2.2)	C4-C10-C11	125.2(1.8)
C8-C1-C6	118.5(2.6)	C4-C10-C12	114.9(2.4)
C6-C1-C2	127.0(1.6)	C11-C10-C12	119.9(1.6)
C1-C2-C3	122.0(1.4)	C10-C11-N3	159.0(3.1)
C2-C3-C4	114.9(1.3)	C10-C12-N4	166.7(3.2)

TCNQ (B1)

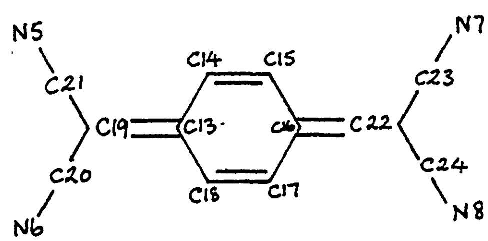

Bond Distances

N5-C21	1.253(30)	C16-C17	1.408(23)
N6-C20	1.224(40)	C17-C18	1.287(16)
C21-C19	1.356(26)	C18-C13	1.436(26)
C20-C19	1.217(38)	C16-C22	1.511(20)
C19-C13	1.383(21)	C22-C23	1.340(41)
C13-C14	1.420(36)	C22-C24	1.390(24)

Table 4.[illegible] contd.

C14-C15	1.353(22)	C23-N7	1.129(42)
C15-C16	1.457(25)	C24-N8	1.078(24)

Bond Angles

N5-C21-C19	176.8(2.4)	C15-C16-C17	121.6(1.2)
N6-C20-C19	178.1(2.6)	C16-C17-C18	119.9(1.2)
C21-C19-C20	113.2(1.6)	C17-C18-C13	121.0(2.2)
C20-C19-C13	126.4(1.7)	C15-C16-C22	115.4(1.9)
C21-C19-C13	120.4(2.2)	C17-C16-C22	122.9(1.4)
C18-C13-C14	118.8(1.5)	C16-C22-C23	122.8(1.6)
C19-C13-C14	122.6(1.7)	C16-C22-C24	121.2(2.0)
C19-C13-C18	118.2(2.2)	C24-C22-C23	115.1(1.4)
C13-C14-C15	121.3(1.8)	C22-C23-N7	177.6(2.5)
C14-C15-C16	116.3(2.1)	C22-C24-N8	169.5(2.1)

(i) Between adjacent TCNQ columns

C22 - - - - $N5^{i}$	3.389	C9 - - - - $N1^{iii}$	3.278
C24 - - - - $N5^{i}$	3.431	C4 - - - - $N1^{iv}$	3.416
C17 - - - - $N8^{ii}$	3.438	N1 - - - - $C4^{v}$	3.416
C18 - - - - $N8^{ii}$	3.389	C6 - - - - $N4^{ii}$	3.350

(ii) Between cation and anion

C31 - - - - $N6^{iii}$	3.429	N5 - - - - $C27^{vi}$	3.431
C26 - - - - $N3^{v}$	2.463	N2 - - - - $C27^{vii}$	3.261
C26 - - - - $N4^{ii}$	3.397	N6 - - - - $C28^{vii}$	3.427
N4 - - - - $C26^{iii}$	3.397	N6 - - - - $C31^{vi}$	3.429
N3 - - - - $C26^{v}$	2.463		

Symmetry code:

none x, y, z; (^{i}) -x, 1-y, -z; (^{ii}) x, y, -1+z; (^{iii}) x, y, 1+z;
(^{iv}) x, $\frac{1}{2}$-y, $\frac{1}{2}$+z; (^{v}) x, $\frac{1}{2}$-y, -$\frac{1}{2}$+z; (^{vi}) -1+x, y, -1+z; (^{vii}) -1+x, y, z.

4.5 Relationship Between Structure and Conductivity for the Bipyridinium Salts $(DC\phi BP)(TCNQ)_4$ and $(DEPA)(TCNQ)_4$

Studies have been carried[95] out on the influence of the cation upon the nature of the TCNQ-stacking in bipyridinium-TCNQ complexes. It is primarily the nature of the TCNQ stacking which appears to determine the conductivity of such complexes; a homosoric stacking being required for high conductivity (Chapter One).[95] The bipyridinium cations have been classified into two major groups:

a) Segmented

This type comprises three planar segments which are symmetrically non-planar, and the overall length of the cation has been considered[95] to be an important factor in determining both the stoichiometry of the complex and also the nature of the TCNQ stacking.

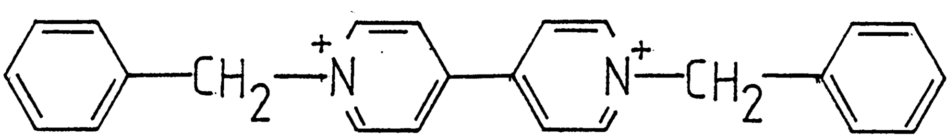

(DBzBP)

b) Symmetrical non-planar or planar

This type comprises bipyridinium salts wherein the pyridinium rings may be linked by an ethylene unit or an alkyl chain of varying length (e.g. ethyl, propyl, ...). Again the overall length of the bipyridinium cation appears to influence the stoichiometry of the complexes and the nature of the TCNQ stacking.

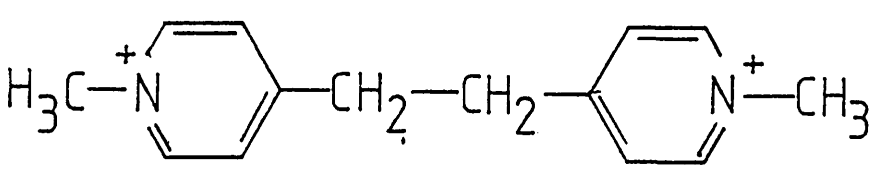

(DMPA)

In the present study, complexes of TCNQ containing a segmented cation, (DCØBP)$(TCNQ)_4$, and a symmetrical planar cation, (DEPA)$(TCNQ)_4$, have been examined and their structural properties are now compared with related bipyridinium salts and correlated with their conductivities.

a) <u>(DCØBP)(TCNQ)</u>$_4$

Conductivity measurements[178] show the complex to be a poor semiconductor (Figure 4.14). In the light of the structural analysis this result is readily understood:

(i) In (DCØBP)$(TCNQ)_4$, the TCNQ columns exhibit tetradic groups wherein the d-spacings are irregular and the modes of overlap are poor (Section 4.3.4, Figure 4.5). These factors cause a reduction in the mobility of the charge carriers.

(ii) The network of short intermolecular electrostatic interactions between TCNQ moieties increases the bi-dimensionality, while those between anion and cation stacks increase the tri-dimensionality of the system. To be a good organic conductor these TCNQ salts are required to be uni-dimensional i.e. homosoric.

(DCØBP) is an example of a segmented cation. It comprises three non-planar segments i.e. the bipyridinium mid-section and the two terminal cyanophenyl groups. The structure of (DCØBP)$(TCNQ)_4$ shows some surprising differences to the arrangements found in related complexes.

The most closely related complexes to (DCØBP)$(TCNQ)_4$ that have been crystallographically examined are (DBzBP)$(TCNQ)_4$,[82] (DBzPA)$(TCNQ)_5$,[93] and (DBzPE)$(TCNQ)_5$.[88]

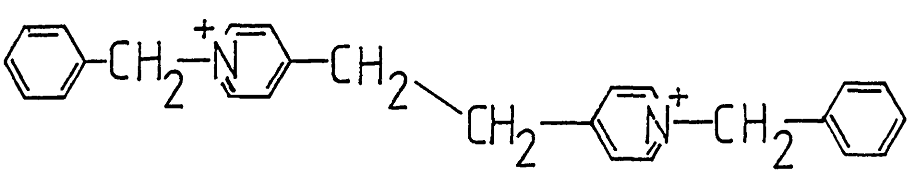

(DBzPA)

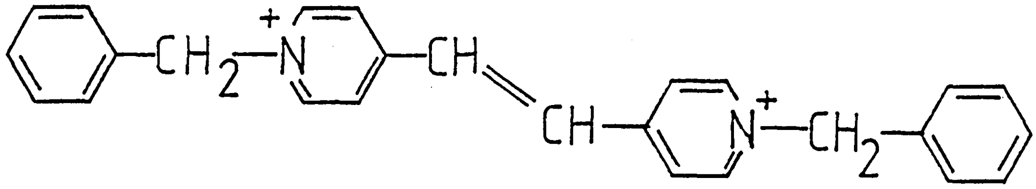

(DBzPE)

For the (DBzPA) and the (DBzPE) cations, TCNQ complexes having a 1:5 stoichiometry rather than a 1:4 are formed (Figure 4.15). This differing stoichiometry has been attributed to the presence of a longer central unit in the segmented (DBzPA) and (DBzPE) bipyridinium cations compared to (DCØBP) for example [82]. In (DBzBP)$(TCNQ)_4$ although the 1:4 stoichiometry is the same as in the (DCØBP) salt, the stacking arrangement of the TCNQ molecules is quite different. Thus, the inter-TCNQ spacings within the columns are more regular than in (DCØBP)$(TCNQ)_4$ (Figure 4.16). In addition, the modes of overlap in the (DBzBP) salt are good within a tetrad and poor between adjacent tetrads (Figure 4.16) whilst the TCNQ overlap in (DCØBP)$(TCNQ)_4$ is poor within a tetrad and good between adjacent tetrads (Figure 4.5). Overall the (DBzBP)$(TCNQ)_4$ [82] system is more homosoric than that found in (DCØBP)$(TCNQ)_4$. Since the overall length of the two cations is similar it appears that the different TCNQ stackings may result from the presence of the terminal cyano groups in (DCØBP)$(TCNQ)_4$. These strongly electron-withdrawing groups appear to facilitate electrostatic anion-cation interactions, as indicated by the great number of short contacts (Table 4.7). This localization of attractions between anion and cation stack produces irregular spacings in the TCNQ stacks and thereby reduces the chances of good overlap. An additional factor may be the relative orientation of the terminal phenyl ring with respect to the central planar unit. The cation lies on a centre of symmetry in both complexes and hence the central pyridinium unit is required to be planar. In $(DCØBP)(TCNQ)_4$ the two cyanophenyl rings are twisted out of the central pyridinium plane by 38.7°, but in $(DBzBP)(TCNQ)_4$, the terminal phenyl rings exhibit a dihedral angle of 66.9° with the central mean plane.[82] In $(DBzPA)(TCNQ)_5$[93] and $(DBzPE)(TCNQ)_5$[88] the dihedral angles between the pyridine and phenyl rings of the cation are also far larger than that found in the (DCØBP) complex, being 74.8° and 76.1° respectively. The smaller dihedral angle in the (DCØBP) complex may be related to the many short anion - - - - cation distances, the smaller angle facilitating the close approach of the cations to the TCNQ stacks.

b) $\underline{(DEPA)(TCNQ)}_4$

The conductivity measurements[179] show the complex to be a poor semiconductor (σ_{300K} = 0.002Scm^{-1}, E_a = 0.27eV). The structural analysis correlates well with these findings:

(i) The TCNQ stacks are very irregular, being made up of tetradic units which may be best considered as weakly interacting 'sheets' of diadic units (Figure 4.9).

(ii) The overlap between molecules in each diad is good but there is very little direct overlap between adjacent pairs of diads.

(iii) The network of short intermolecular electrostatic contacts drastically reduces the uni-dimensionality of the system. $(DEPA)(TCNQ)_4$ can be considered to belong to the group of TCNQ complexes containing a symmetrical-planar bipyridinium ion. The (DEPA) cation in the present structure must be planar as it is centered on a centre of symmetry.

It is interesting to note that from a reaction of $(DEPA)(I)_2$ with neutral TCNQ, one of three complexes may be produced or indeed, all three from the same mother liquor. The stoichiometry of all three differ,

(i) $(DEPA)_2(TCNQ)_9(H_2O)_x$,[97] although the crystal structure has not been determined, the water molecules trapped in the lattice are likely to provide a source of disorder. Such disorder would enable the TCNQ stacks to be stabilized and indeed at low temperatures, the complex is found to be highly conducting.

(ii) $(DEPA)_2(TCNQ)_5$[87]

This is a good semiconductor and the TCNQ molecules are found to be stacked plane-to-plane in columns with d-spacing of 3.22 [TCNQ (A)-TCNQ (B)], 3.23 [TCNQ (B)-TCNQ (C)] and 3.26Å [TCNQ (C)-TCNQ (C′)], (Figure 4.17). The corresponding overlapping modes are good, poor and good (Figure 4.18) i.e. a much more homosoric arrangement compared with $(DEPA)(TCNQ)_4$. The geometry of the (DEPA) ion in the 2:5 complex is not significantly different to that in the 1:4 complex in the present study.

(iii) $(DEPA)(TCNQ)_4$

The poor semiconductor properties are readily understood in terms of the irregular spacings and poor overlaps of the TCNQ molecules.

While such polymorphism is not unknown among complexes of TCNQ e.g. $(NH_4)(TCNQ)$;[68] $(DEPE)(TCNQ)_4$ and $(DEPE)(TCNQ)_4(H_2O)_x$[92], it is difficult to see why the stoichiometries (1:4, 2:5, 2:9) should be found in the DEPA salts and why the TCNQ stacking for the two anhydrous salts should be so different.

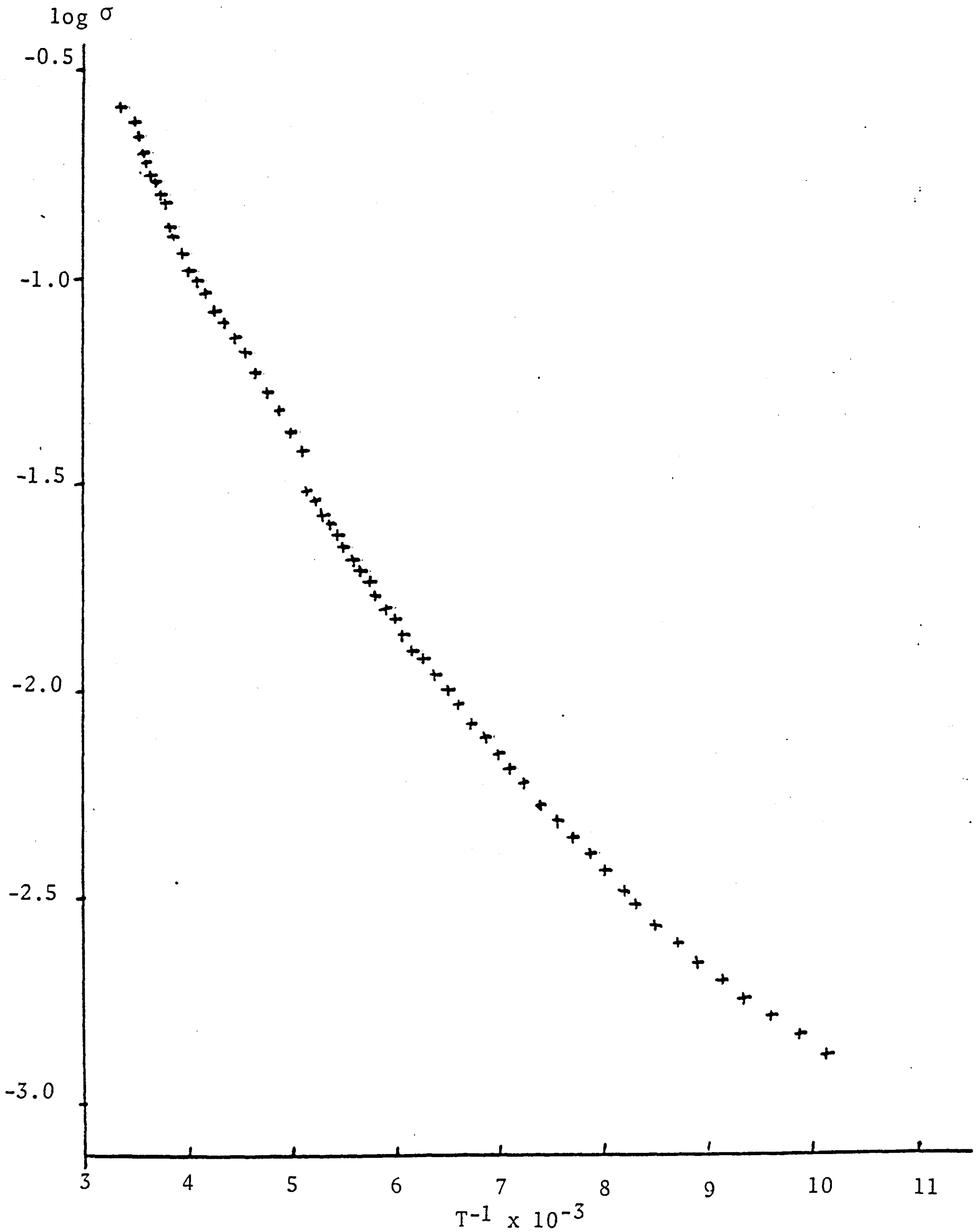

Figure 4.14 Conductivity versus temperature for (DCØBP)$(TCNQ)_4$

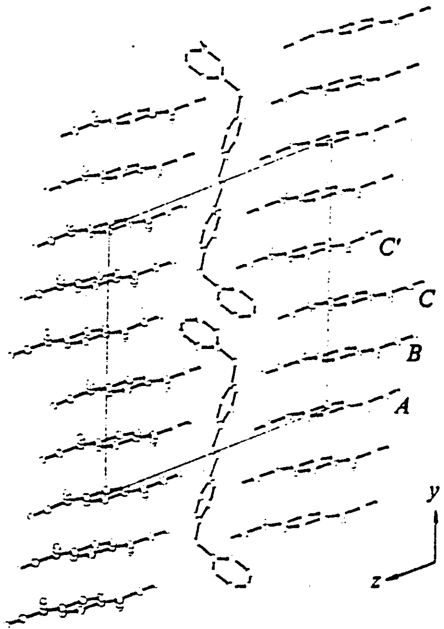

(a)

(i) projection along the a-axis.

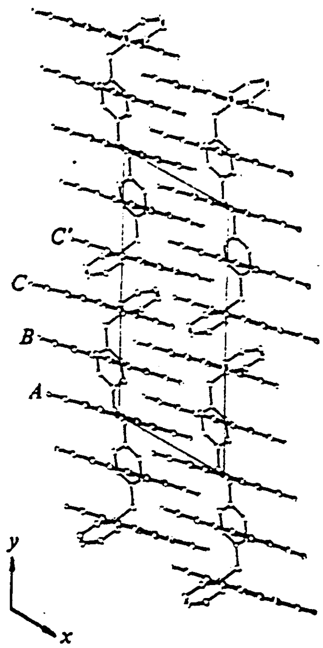

(b)

(ii) projection along the c-axis.

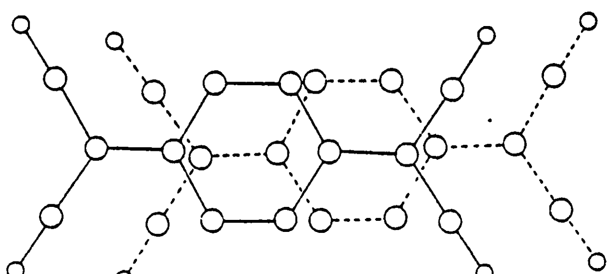

(a)

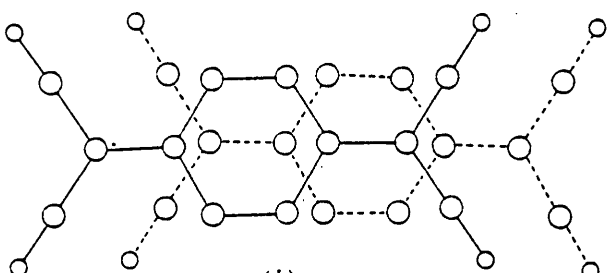

(b)

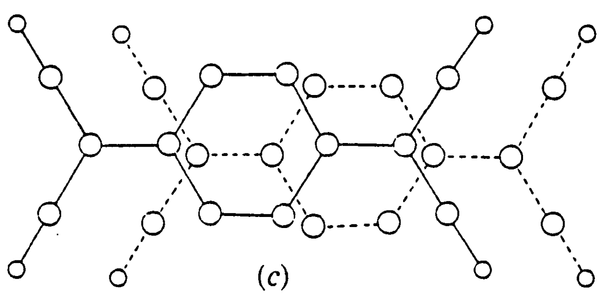

(c)

Figure 4.15 Packing diagrams for (DBzPE)$(TCNQ)_5$ and the modes of overlap.

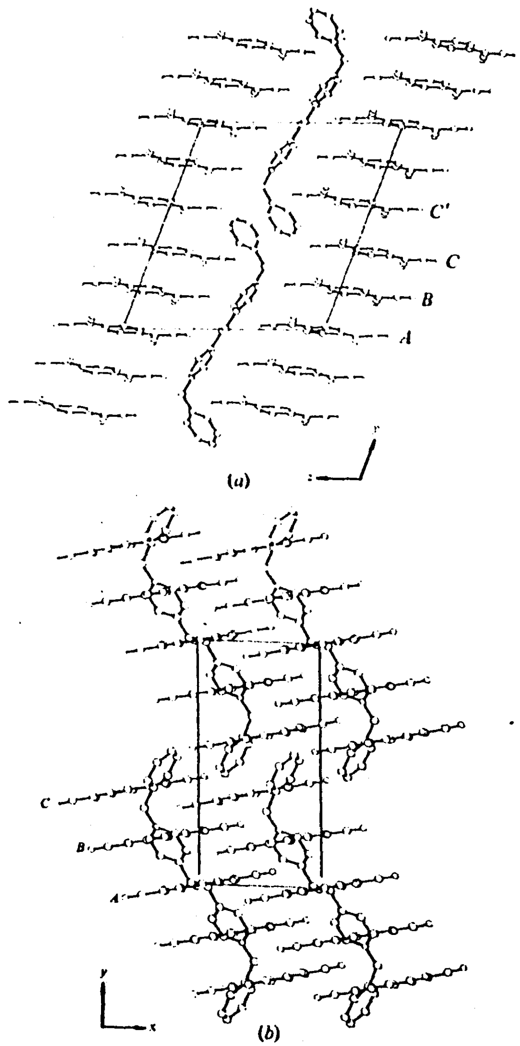

Figure 4.15 Packing diagrams for $(DBzPA)(TCNQ)_5$

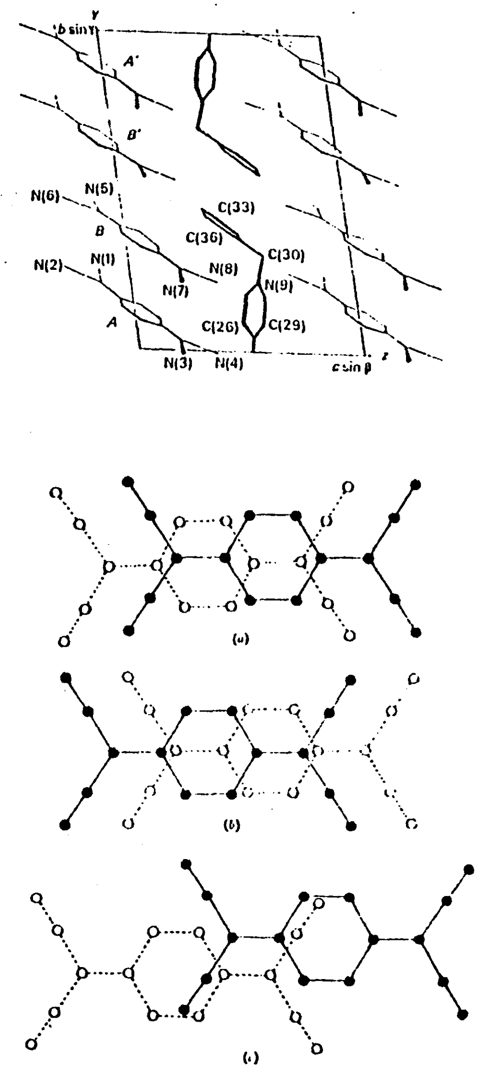

Figure 4.16 Projection along the a-axis for $(DBzBP)(TCNQ)_4$ and the modes of overlap.

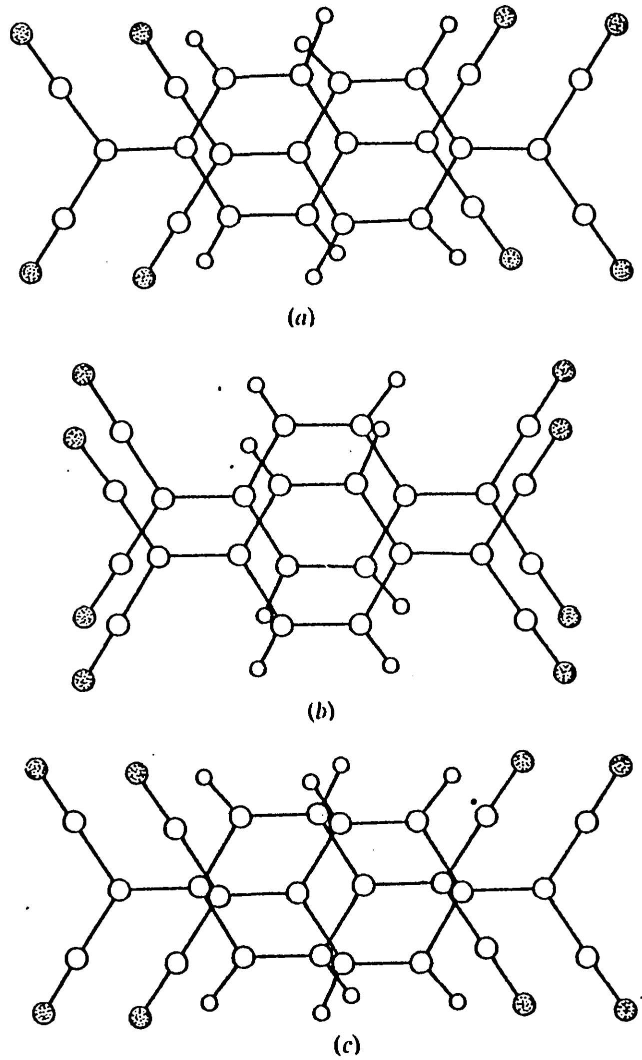

Figure 4.18 Overlaps for $(DEPA)_2(TCNQ)_5$

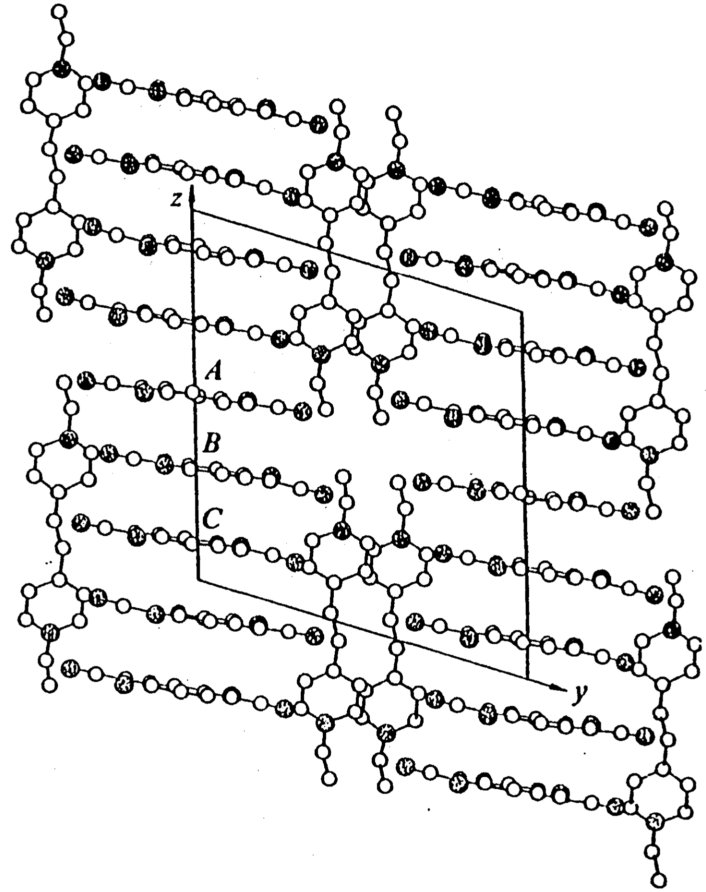

Figure 4.17 Projection along the a-axis for $(DEPA)_2(TCNQ)_5$

CHAPTER FIVE

The crystal structure of the heterosoric TCNQ complex, (4,4′-bipyridylethylene)(7,7,8,8-tetracyanoquinodimethane), (DPE)(TCNQ)

Contents

5.1 Introduction

TCNQ is known to form heterosoric mixed stack complexes which exhibit many features characteristic of 1:1 charge-transfer complexes.[13-35] The 1:1 complex formed between TCNQ and the bipyridyl moiety, 4,4′-bipyridylethylene, is such a complex and the crystal structure of (DPE)(TCNQ), (I), is presented in the following sections.

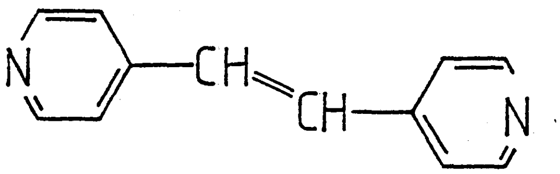

(DPE)

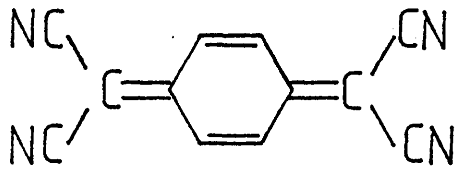

(TCNQ)

5.2 Crystal Data

(DPE)(TCNQ), $C_{24}H_4N_6$, M_r = 386.3, Monoclinic, a = 7.262(4), b = 9.400(5), c = 14.496(4)Å, β = 91.75(5)°, U = 989.2Å^{-3}, Z = 2, μ(Mo-K$_\alpha$) = 0.46cm^{-1}, D_m = 1.30, D_c = 1.28 gcm^{-3}, F(000) = 400.

5.3 Determination of the Space Group

The systematic absences noted from the preliminary Weissenberg and precession photographs (0k0, k = 2n + 1; h0l, l = 2n + 1) are consistent with the monoclinic space group, $P2_1/c$. For a value of Z = 2 and a 1:1 stoichiometry, the asymmetric unit in this centrosymmetric space group must contain half a TCNQ molecule and half a (DPE) molecule, with both molecules lying on centres of symmetry.

5.4 Data Collection

A crystal of approximate dimensions 0.23 x 0.15 x 0.09mm was mounted with the a-axis coincident with the rotation (ω) axis of a Stöe Stadi-

2 two circle diffractometer. Intensity data were collected using monochromated Mo-Kα radiation and the background-ω scan-background technique previously described (Chapter 2, Section 2.5). Of the 1936 unique reflections measured, 828 had $I > 4\sigma(I)$ and these were used in subsequent analysis and refinement. Corrections were made for Lorentz and polarization effects but not for absorption effects.

5.5 Structure Solution and Refinement

Structure analysis and refinement were carried out using the SHELX automatic centrosymmetric multisolution procedure (Chapter 2, Section 2.82). The collected intensity data was merged and the $|E|$-statistics produced for ranges of $\sin\theta/\lambda$ indicated the crystal to be centrosymmetric:

$\sin\theta/\lambda$	0.14 - 0.21	- 0.28	- 0.35	- 0.42	- 0.49	- 0.56	- 0.63	
$\|E\|$	1.036	0.934	1.003	0.980	1.034	1.000	1.000	1.000
$\|E^2-1\|$	1.369	0.931	1.228	0.871	1.179	1.046	0.925	0.869

The starting sets produced by the sign expansion pathway are given in Table 5.1 (i), and the three $|E|$-maps with the highest figures-of-merit were produced, Table 5.1 (ii). All the non-hydrogen atom positions bar one nitrogen atom were readily located from the $|E|$-map with the second largest figure-of-merit. In this solution the TCNQ molecule lies on a centre of symmetry at (1.0, 0.5, 0.5) whilst the (DPE) moiety lies on a centre of symmetry at (0.5, 0.5, 0.5). The remaining nitrogen atom position was located by a difference Fourier synthesis but subsequent least-squares refinement indicated that this trial solution was unsatisfactory for the R-value fell to only 22%, even with all the non-hydrogen atoms being given anisotropic temperature factors.

An alternative solution was then attempted with the TCNQ moiety lying on a centre of symmetry at (1.0, 0.5, 0.0) whilst the (DPE) moiety lay on a centre at (0.5, 0.5, 0.0). This effectively moves the hydrogen atom positions were located from a difference Fourier map and they were included in the structure factor calculations but not refined. The hydrogen atoms associated with the pyridyl ring (H11, H12, H14, H15) were given ideal geometries with the C-H bond distance equal to 1.08Å. A common isotropic temperature factor was applied to all the hydrogen atoms and refined to a final value of $U = 0.062(5)Å^2$.

The weighting scheme $\omega = 1.0000/[\sigma^2(F_o)^2 + 0.01009(F_o)^2]$ was adopted. Full matrix refinement with anisotropic temperature factors applied to all non-hydrogen atoms gave a final R of 0.076 with the weighted R-value, (R_w), being equal to 0.0868. The final difference Fourier map showed no peaks greater than 0.54 $eÅ^{-3}$.

The final positional and thermal parameters are given in Appendix A1.5, mean plane data in A2.5, observed and calculated structure factors in Appendix A3.5, with bond distances and angles in Table 5.2.

5.6 Description of the Structure

The structure comprises mixed stacks of alternating donor (DPE) and acceptor (TCNQ) molecules. These mixed stacks are related in the unit cell by screw axes along the b-axis and c-glide planes, (Figure 5.1). The DPE and TCNQ molecules are essentially parallel to each other, and stack in a face-to-face manner characteristic of 1:1 charge-transfer complexes (Figure 5.1). The donor and acceptor molecules alternate along the a-axis (Figure 5.2), with the separation between adjacent molecules being 3.45Å (Appendix 3.5). This rather large interplanar separation indicates that any charge-transfer present will be limited. This is supported both by an absence of short intermolecular contacts and also by the observation that the bond lengths of the TCNQ molecule are in good agreement with those for the neutral molecule[39] (Table 5.3). The geometry of the TCNQ moiety in the present complex is also similar to that found in other 1:1 heterosoric TCNQ complexes in which the TCNQ

(DPE) and TCNQ molecules is typical of many heterosoric complexes (Figure 5.2) and is for example similar to that observed in (TMBTP)(TCNQ).[32]

The packing arrangement found in the present complex readily compares with that found in a number of other heterosoric complexes. In particular there are striking similarities in unit cell dimensions, space group and lack of short intermolecular contacts (Table 5.4).

The geometry of the (DPE) molecule compares well with that of the substituted bipyridinium cation found in (DBzPE)$(TCNQ)_5$.[88] The latter is a homosoric salt and the greatest differences in the two donor species are found in the C13-C16 and C16-C16′ bond distances, [C13-C16, 1.489(9) (DPE) 1.612(9) DBzPE; C16-C16′, 1.292(9) (DPE), 1.184(11) (DBzPE)]. It is interesting to note that a homosoric complex is obtained from the same reaction mixture from which the present (DPE)(TCNQ) heterosoric complex was obtained.[181] The homosoric complex crystallizes as black needle crystals and has a room temperature conductivity of $\sim$500 Scm^{-1}.[179] In contrast, the room temperature conductivity of the heterosoric (DPE)-(TCNQ) is $\sim 10^{-9} Scm^{-1}$ [179] and this insulating behaviour is to be expected from the structure adopted in the solid state.

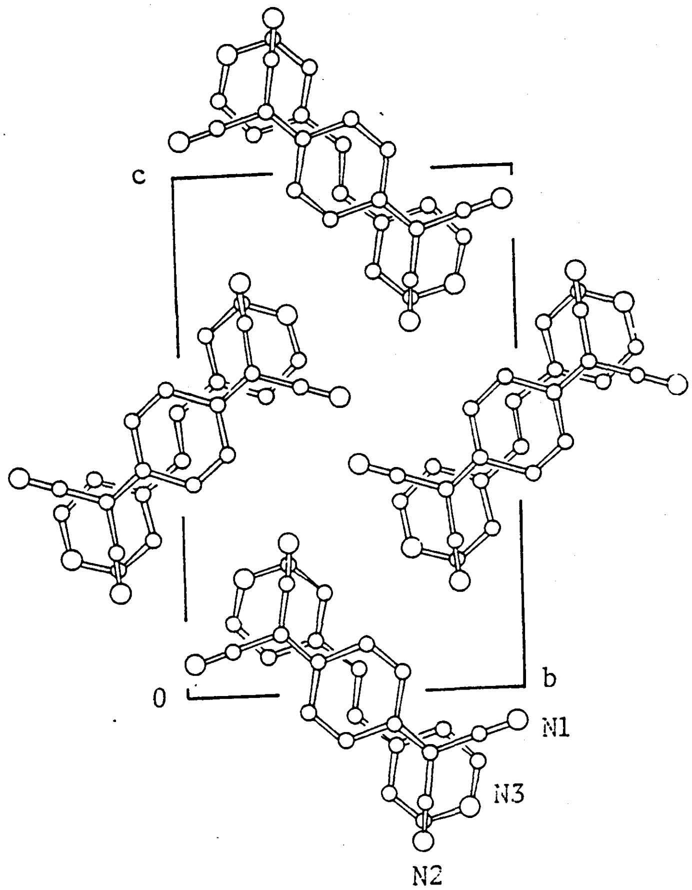

Figure 5.1 Projection of the unit cell contents in the $\bar{b}c$-plane of (DPE)(TCNQ).

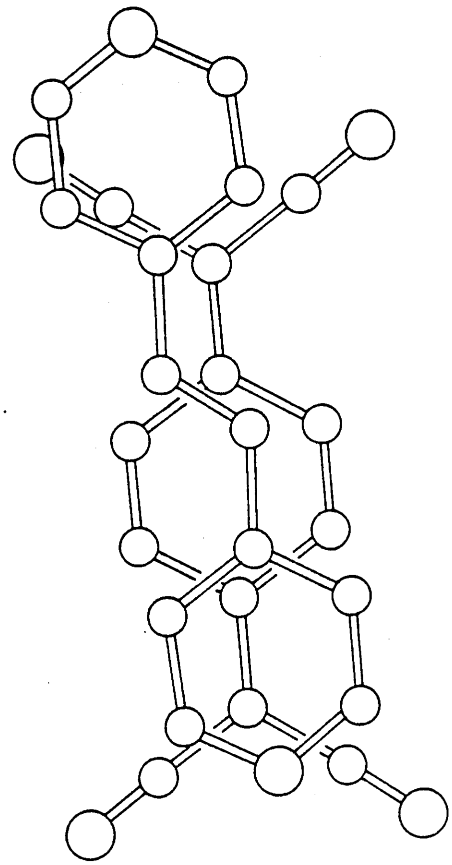

Figure 5.2 Overlap of the TCNQ molecule and the DPE molecule in (DPE)(TCNQ).

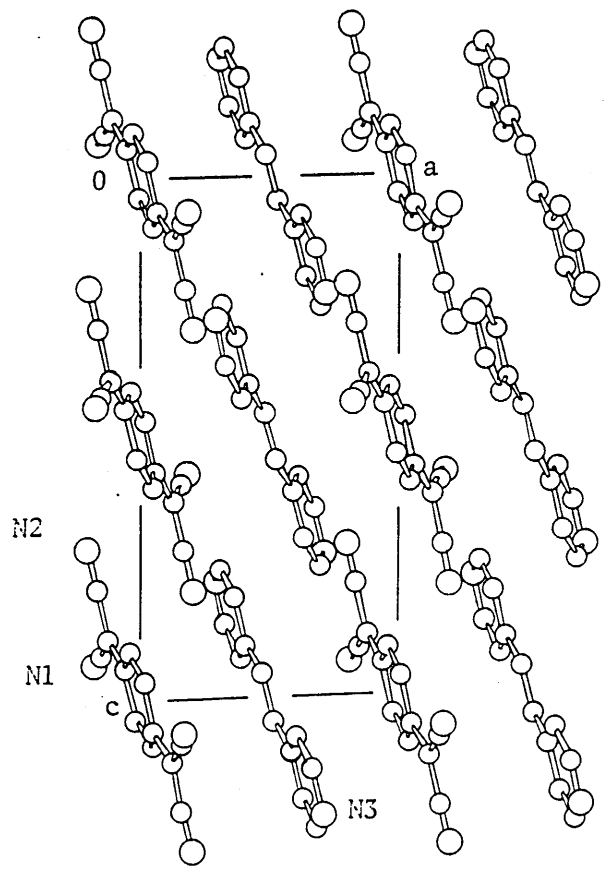

Figure 5.3 Projection down the b-direction in (DPE)(TCNQ)

Table 5.1 Starting Sets for the Solution of (DPE)(TCNQ) in $P2_1/c$

(i) Starting Sets

h	k	l	Phase Angle (°)	
-4	1	2	0	origin determining reflections
-1	3	12	0	
-4	1	3	0	

The following reflections were given phase angles of either 0 or 180°

and formed the multisolution starting set:

0 8 2, -2 0 2, 3 6 8, 1 5 9, -1 3 13, 2 1 0, 4 7 0, -4 2 1, 2 7 1,

-5 4 14, -4 9 4, 1 2 12.

(ii) Figures-of-merit

|E|-map	Parachor	M (abs)	Phases*
1	2.290	0.985	+ + + + − + − + + + + − + + −
2	2.212	1.041	+ + + + + + + + − + + + + + +
3	1.546	0.724	+ + + − + − − + − − + − + − +

*The order of the reflections is the same as that given in (i), with +

and − corresponding to phase angles of 0 and 180° respectively.

Estimated Standard Deviations in Parentheses

Bond Distances (Å)

Symmetry code:

none, (x, y, z); (′), (2.0 - x, 1.0 - y, -z); (″), (1.0 - x, 1.0 - y, -z).

TCNQ

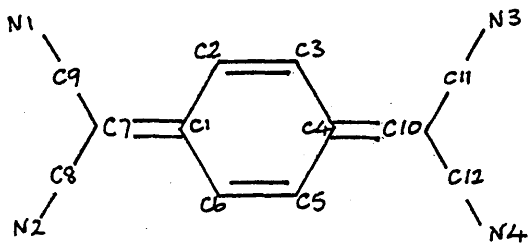

N1-C9	1.131(8)	C1-C2	1.452(7)
N2-C8	1.134(7)	C2-C3	1.327(7)
C7-C9	1.438(7)	C3-C1′	1.451(7)
C7-C8	1.448(7)	C2-H2	0.949(63)
C7-C1	1.361(7)	C3-H3	0.881(67)

DPE

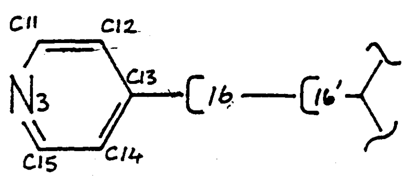

N3-C11	1.322(8)	C13-C14	1.370(9)
N3-C15	1.330(8)	C14-C15	1.364(9)
C11-C12	1.397(9)	C13-C16	1.489(9)
C12-C13	1.405(9)	C16-C16″	1.292(9)
C16-H16	1.099		

Bond Angles (°)

TCNQ

N1-C9-C7	177.1(7)	C1-C2-C3	121.5(4)
N2-C8-C7	176.6(6)	C3-C1-C2	116.8(4)

Table 5.2 contd.

C9-C7-C8	113.5(4)	C2-C3-C1′	121.8(4)
C9-C7-C1	123.1(5)	H2-C2-C1	121.2(3.8)
C8-C7-C1	123.3(4)	H2-C2-C3	117.3(3.8)
C7-C1-C2	121.2(4)	H3-C3-C2	122.1(4.0)
C7-C1-C3′	121.9(4)	H3-C3-C1′	114.4

DPE

N3-C11-C12	123.2(6)	C13-C14-C15	119.6(6)
N3-C15-C14	124.7(6)	C12-C13-C16	124.8(6)
C15-N3-C11	116.7(5)	C14-C13-C16	118.0(6)
C11-C12-C13	118.7(6)	C13-C16-H16	118.5(6)
C12-C13-C14	117.2(6)	H16-C16-C16″	118.3(6)
		C13-C16-C16″	122.9(6)

Table 5.5 Distances (Å) of Selected Bonds in the TCNQ Molecule

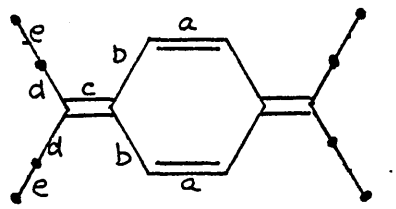

	a	b	c	d	e	Ref.
(DPE)(TCNQ)	1.327(7)	1.452(7)	1.361(7)	1.448(7)	1.134(7)	p.w.
				1.438(7)	1.131(8)	
$TCNQ^{0}$	1.346(3)	1.446(4)	1.374(3)	1.441(4)	1.141(3)	39
				1.440(4)	1.139(3)	
$TCNQ^{-2}$	1.354	1.434	1.396	1.428	1.17	174
$TCNQ^{-}$	1.356	1.425	1.401	1.417	1.15	
(DPDO)(TCNQ)	1.344(5)	1.436(5)	1.361(5)	1.434(5)	1.135(5)	22
				1.431(6)	1.131(5)	
(Pyrene)(TCNQ)	1.33(1)	1.45(1)	1.35(1)	1.43(1)	1.14(1)	24
				1.43(1)	1.14(1)	
(OMTTF)(TCNQ)	1.336	1.443	1.377	1.426	1.147	34
				1.432	1.142	
(PERYLENE)(TCNQ)	1.348(4)	1.449(4)	1.365(4)	1.426(4)	1.150(4)	25
				1.434(4)	1.138(5)	

Table 5.4 Unit Cell Dimensions of Selected Heterosoric TCNQ Complexes

Complex	Space Group	Unit cell dimensions				Ref.
		a/Å	b/Å	c/Å	β/°	
(Perylene)(TCNQ)	$P2_1/c$*	7.32	10.88	14.55	90.4	25
(Pyrene)(TCNQ)	$P2_1/c$*	7.14	10.01	14.73	102.5	24
(DPDO)(TCNQ)	$P2_1/c$	7.037	9.123	15.009	100.45	22
(OMTTF)(DIMEOTCNQ)	$P2_1/c$	7.097	9.426	21.266	93.92	34
(DPE)(TCNQ)	$P2_1/c$	7.262	9.400	14.496	91.75	p.w.

*converted from $P2_1/b$ [c as the unique axis].

Contents

6.1.1 Preparation of $(REtPh_2P)(TCNQ)_2$, where R = Et or R = Me

The phosphonium iodide, $REtPh_2PI$ [R = Me, 0.1678g, 0.4711mmol; R = Et, 0.1767g, 0.4773mmol] was dissolved in the minimum quantity of acetonitrile. TCNQ [R = Me, 0.1938g, 0.9711mmol; R = Et, 0.2009g, 0.9838mmol] was dissolved at reflux in approximately 75-90cm^3 of acetonitrile. The acetonitrile solutions were mixed producing dark olive green solutions. These solutions were allowed to cool slowly and left undisturbed for two days. Long dark-green needle crystals (R = Me) or thick black-purple needle crystals (R = Et) were produced, confirmed by microanalysis to have the stoichiometry $(REtPh_2P)(TCNQ)_2$.

(i) $(MeEtPh_2P)(TCNQ)_2$, $C_{39}H_{26}N_8P$

	% C	% H	% N	% P
Found:	73.62	3.97	17.45	3.92
Required:	73.49	4.11	17.57	4.85

(ii) $(Et_2Ph_2P)(TCNQ)_2$, $C_{40}H_{28}N_8P$

	% C	% H	% N	% P
Found:	73.96	3.97	17.44	3.93
Required:	73.75	4.33	17.19	4.74

Crystals of $(DMBP)(TCNQ)_2$ were prepared in a similar manner by G.J. Ashwell[179]; in all cases the phosphonium and phospholium iodides were provided by D.W.Allen.[180]

6.1.2 Preparation of $(DC\emptyset BP)(TCNQ)_4$[178]

The bipyridinium iodide $(DC\emptyset BP)(I)_2$ [0.2750g, 0.4477mmol] was dissolved in the minimum quantity of water. LiTCNQ [0.2000g, 0.9473mmol] was dissolved at reflux in approximately 150cm^3 of acetonitrile. The solutions were mixed and left to cool slowly. Black needle-like crystals were produced.

6.1.5 Preparation of (DEPA)$(TCNQ)_4$

The bipyridinium iodide (DEPA)$(I)_2$ [0.3021g, 0.5763mmol] was dissolved in the minimum quantity of acetonitrile containing approximately $5cm^3$ of water. TCNQ [0.3995g, 1.9565mmol] was dissolved at reflux in approximately $155cm^3$ of acetonitrile. The acetonitrile solutions were mixed producing a dark olive green solution. This was left to cool slowly and allowed to stand, undisturbed, for one week. Dark red-purple crystals were produced, confirmed by microanalysis to have the stoichiometry (DEPA)$(TCNQ)_4$.

(DEPA)$(TCNQ)_4$, $C_{64}H_{18}N_{38}$

	% C	% H	% N
Found:	72.65	3.48	23.79
Required:	72.57	3.62	23.79

(DPE)(TCNQ) was prepared by G.J.Ashwell and G.Rothwell.[181]

6.2 Conductivity Studies

6.2.1 Conductivity Measurements

Conductivity measurements on $(DMBP)(TCNQ)_2$ were carried out on single crystals, by means of a 'manual' technique. A pictorial description of the apparatus is given in Figure 6.1. A four-probe technique was employed; the crystal was suspended, below a heating block, in the conductivity cell, from four fine copper wires, the contact being made with electrodag silver paint:

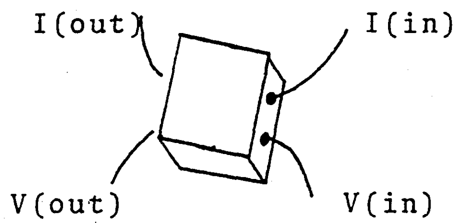

where I_{in} = current passing into the crystal

I_{out} = resultant current passing out of the crystal

V_{in} = voltage applied to the crystal

V_{out} = voltage after passage through the crystal

Readings of resistance were taken using a Keithley 172A multimeter, the temperature was varied by means of an Oxford Instruments Controller, and readings of voltage were taken by means of a copper-constantan thermocouple connected to a Croyden Precision Instruments portable d.c. potentiometer (type P3).

The conductivity studies on $(R_1R_2Ph_2P)(TCNQ)_2$ where R_1, R_2 = Me; R_1, R_2 = Et; R_1 = Me, R_2 = Et , $(DC\emptyset BP)(TCNQ)_4$ and $(DEPA)(TCNQ)_4$ were carried out by G.J.Ashwell and G.H.Cross using a four-probe technique.[178]

6.2.2 Results for $(DMBP)(TCNQ)_2$

For $(DMBP)(TCNQ)_2$ the conductivity measurements were carried out over the temperature range 150-300K. The results are given in Table 6.1 and a plot of log σ (Scm^{-1}) versus 1000/T K^{-1} is given in Figure 6.2. σ is the conductivity given by the reciprocal of the resistance multiplied of the crystal and was found to be $11.99 cm^{-1}$.

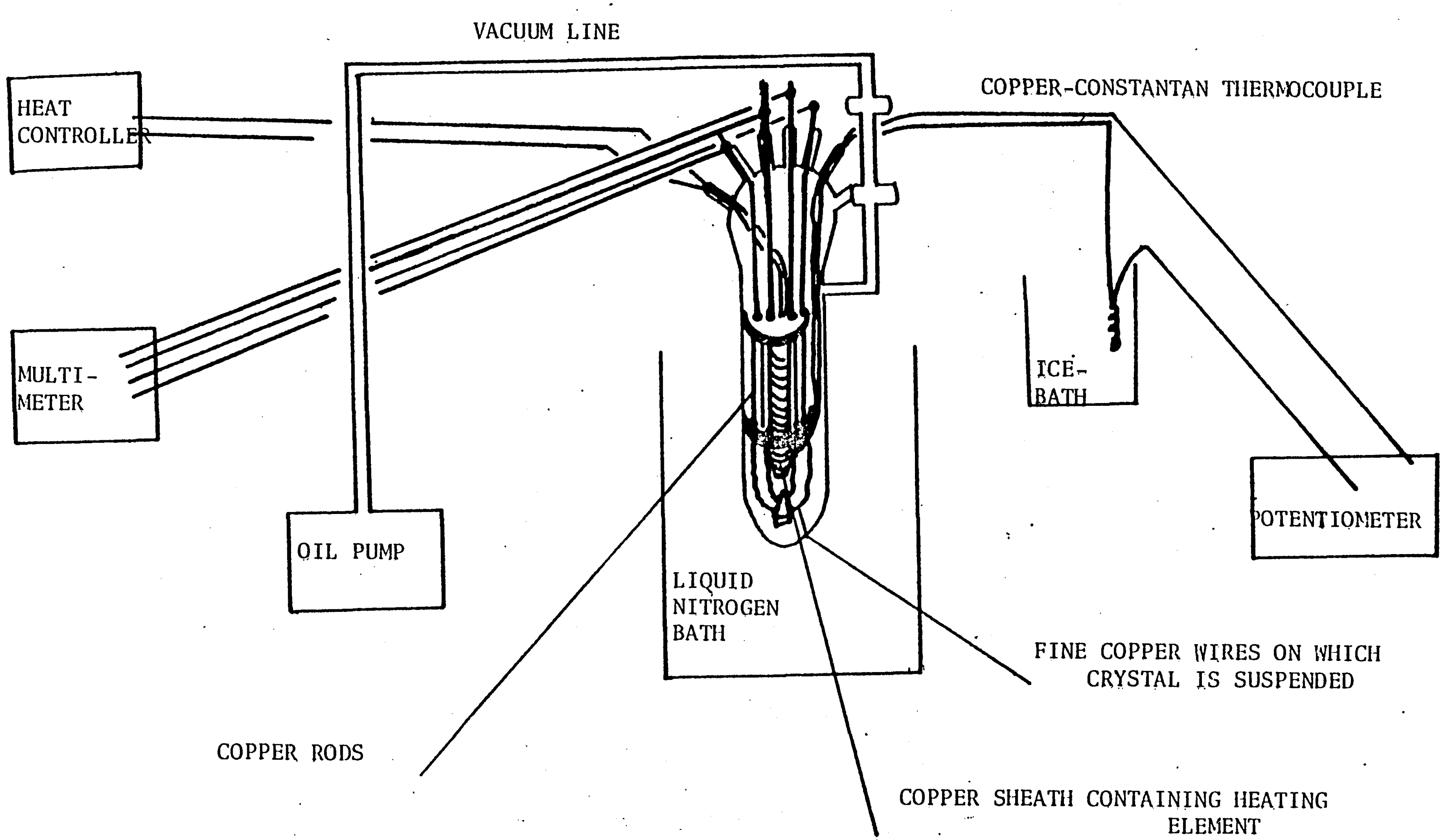

Figure 6.1 Pictorial description of the four-probe conductivity apparatus

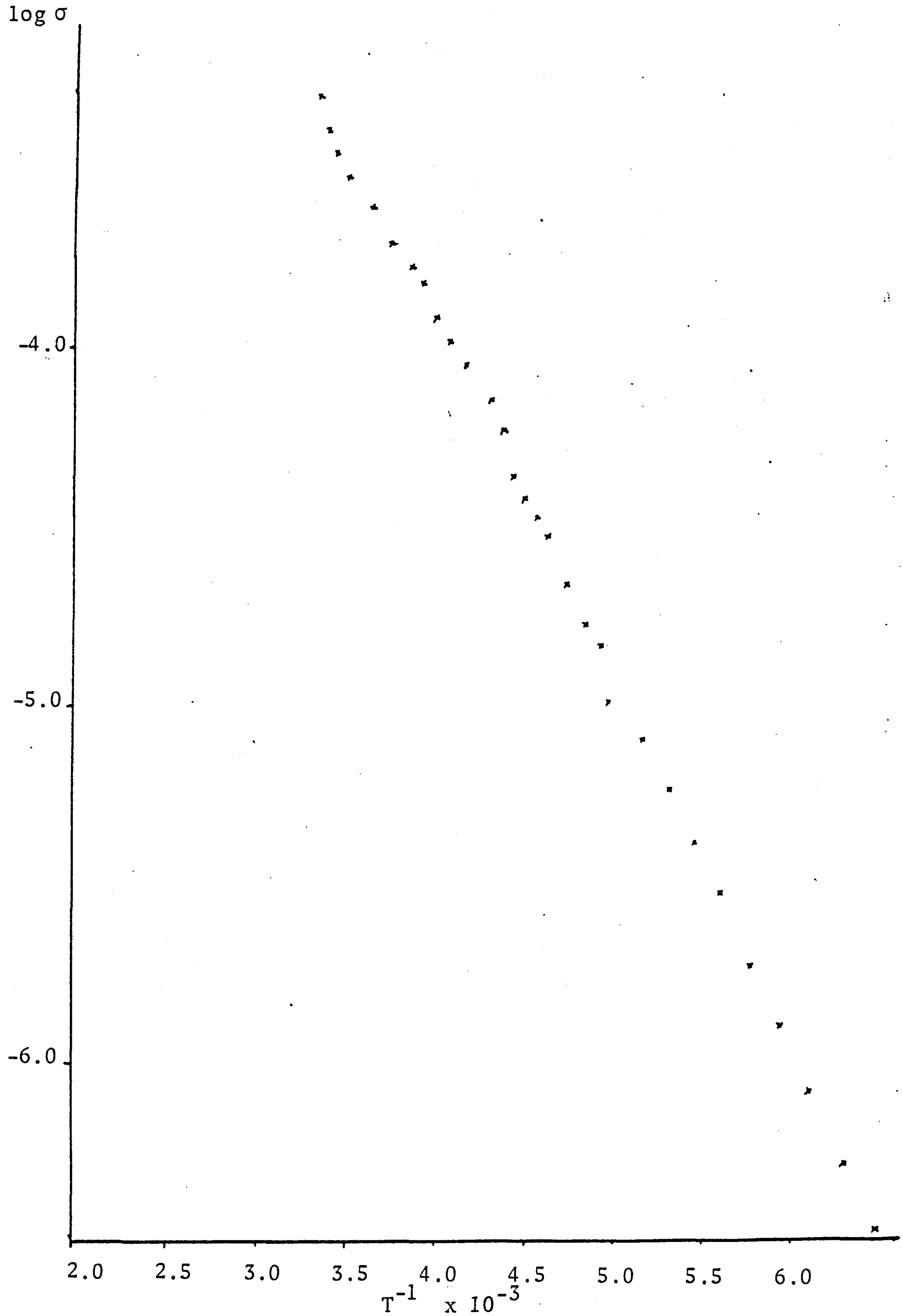

Figure 6.2 Conductivity versus temperature for $(DMBP)(TCNQ)_2$

$\log \sigma = \log(1/R \times L/A)$

where

σ = conductivity (Scm^{-1})

R = resistance (S)

L = thickness of crystal (cm)

A = area of crystal surface (cm^2)

1000/T (K^{-1})	log σ (Scm^{-1})	1000/T (K^{-1})	log σ (Scm^{-1})
3.34	-3.29	4.56	-4.47
3.38	-3.39	4.61	-4.55
3.44	-3.45	4.72	-4.66
3.50	-3.52	4.82	-4.77
3.63	-3.61	4.90	-4.83
3.74	-3.71	4.95	-4.98
3.85	-3.77	5.15	-5.09
3.92	-3.85	5.29	-5.24
3.99	-3.91	5.43	-5.38
4.07	-3.97	5.58	-5.55
4.16	-4.05	5.75	-5.73
4.29	-4.15	5.92	-5.90
4.37	-4.23	6.09	-6.08
4.42	-4.37	6.29	-6.29
4.48	-4.43	6.49	-6.49

The charge-transfer complexes of the strong π-acceptor, 7,7,8,8-tetracyanoquinodimethane, (TCNQ), exhibit unusual physical properties of which the most significant is their anisotropic electrical conductivities. It was in order to more fully understand the relationship between solid state structure and electrical conductivity of such TCNQ complexes that the crystal structures of selected complexes have been studied in the present work.

(i) Dimethyldibenzophospholium Bis-7,7,8,8-tetracyanoquinodimethanide, (DMBP)(TCNQ), (I);

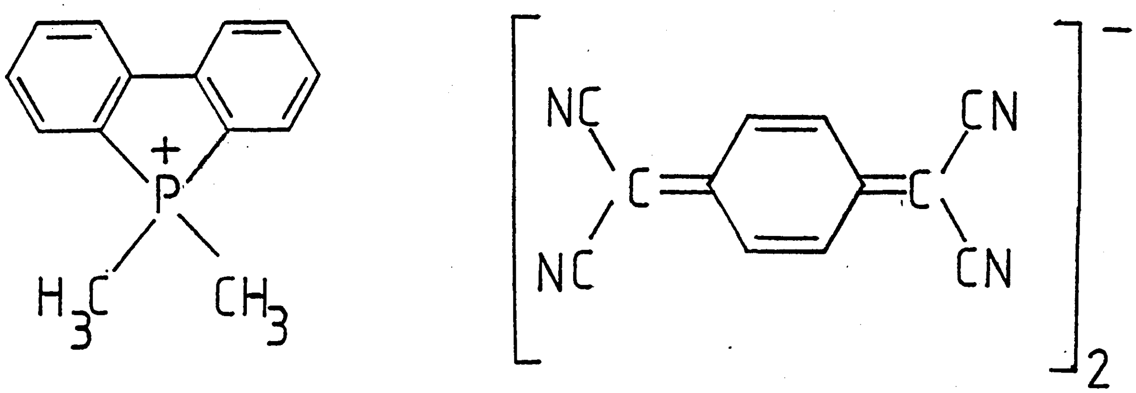

(I)

This semi-conductor belongs to the pseudosoric[95] class of TCNQ complexes. The single crystal analysis shows the TCNQ molecules to be arranged in columns containing diadic units. The latter are held together by a network of short intermolecular contacts thereby forming two-dimensional sheets. The resulting two-dimensionality, the lack of any disorder in the phospholium cation, and the presence of poor overlapping between adjacent TCNQ moieties lead to the low conductivity associated with the complex. The lack of disorder in the phospholium ion is attributed to its planarity and rigidity.

(ii) Dimethyldiphenylphosphonium Bis-7,7,8,8-tetracyanoquinodimethanide, $(Me_2Ph_2P)(TCNQ)_2$, (II);

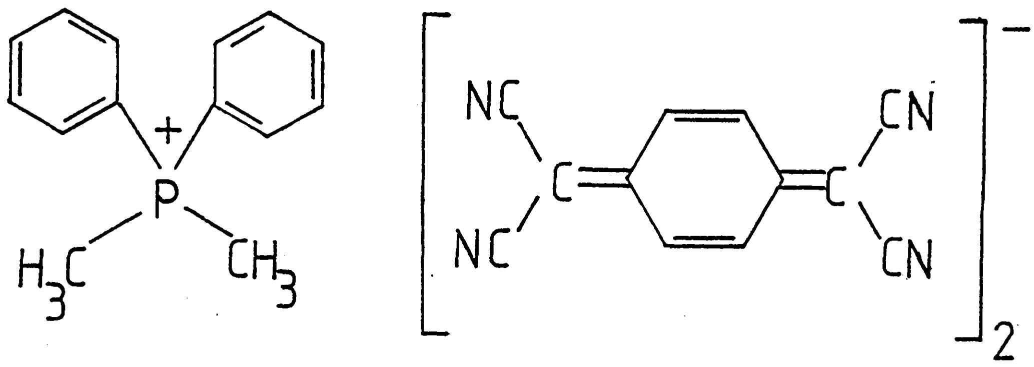

(II)

This is a good semi-conductor belonging to the homosoric[6] class of TCNQ complexes. The preliminary X-ray photographs indicate the presence of disorder in the lattice and this has been attributed to a statistical disorder of the phosphonium cation. At low temperatures the TCNQ stacks appear to be diadic in nature, but as the temperature is raised, so the cation becomes more disordered, thereby facilitating a one-dimensional distortion of the TCNQ stacks which become monadic in nature. The room temperature crystal structure indicates an intermediate monadic/diadic stacking arrangement with average inter-TCNQ distances of 3.25 and 3.30Å.

The related dimethyldiphenyl and methylethyldiphenylphosphonium TCNQ complexes have been examined photographically in order to relate the influence of different substituents in the R_4P^+ phosphonium ions upon the structure adopted and thus upon the observed conductivity. The weak layer-lines present in $(Me_2Ph_2P)(TCNQ)_2$ are not observed in room temperature oscillation photographs of $(Et_2Ph_2P)(TCNQ)_2$ and this is attributed to a more homosoric stacking in the latter complex, in keeping with its higher conductivity. The relative conductivities of such phosphonium TCNQ complexes is very much dependent upon the flexibility and capacity to disorder of the cation. As such it would be a and, if appropriate, single crystal analyses of a series of such complexes over a range of temperatures.

(iii) Dicyanophenyl-4,4′-bipyridylium Tetrakis-7,7,8,8-tetracyanoquinodimethanide, (DCØBP)$(TCNQ)_4$, (III);

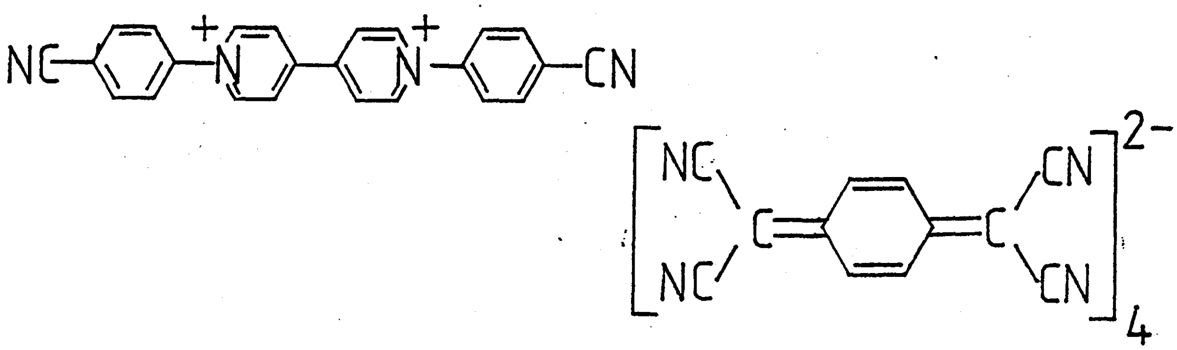

(III)

This is a poor semi-conductor which belongs to the pseudosoric[95] class of TCNQ complexes. The crystal structure shows the TCNQ molecules to be arranged in columns parallel to the b-axis and in sheets parallel to the ab plane. The TCNQ molecules in each column are arranged in tetrads but the poor overlap present in these units indicates that the stacking arrangement is better described as poorly overlapping diads. Extensive electrostatic interactions between the anion and the cation stacks increase the tri-dimensionality of the system and this has been attributed to the presence of the strongly electron-withdrawing cyanophenyl functions. It would be of interest to examine related bipyridinium TCNQ complexes in order to more fully investigate the influence of both length of cation and also of the presence of electron-withdrawing groups upon the solid state structures adopted and the resulting electrical conductivities.

(iv) Diethyl-4,4′-bipyridiniumethane Tetrakis-7,7,8,8-tetracyanoquinodimethanide, (DEPA)$(TCNQ)_4$, (IV);

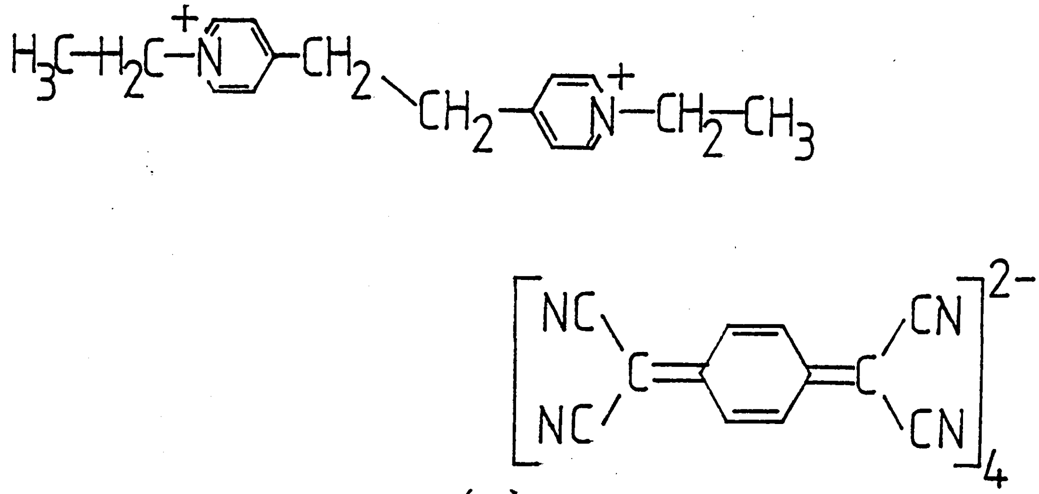

(IV)

This is a poor semi-conductor, which belongs to the pseudosoric[95] class of TCNQ complexes. The X-ray analysis shows the TCNQ molecules to stack in columns made up of tetradic units. However, as with the $(DC\emptyset BP)(TCNQ)_4$ complex, the poor nature of the overlap within these units is such that the arrangement of TCNQ molecules may be best considered in terms of weakly interacting diadic units. The latter are contained within sheets and the numerous electrostatic interactions within the sheets give rise to the observed semi-conductor behaviour. The structural arrangement within $(DEPA)(TCNQ)_4$ and its associated conductivity are compared with the related complexes, $(DEPA)_2(TCNQ)_9$-$(H_2O)_x$ and $(DEPA)_2(TCNQ)_5$.

(v) 4,4′-bipyridylethylene 7,7,8,8-tetracyanoquinodimethane, (DPE)-(TCNQ), (V);

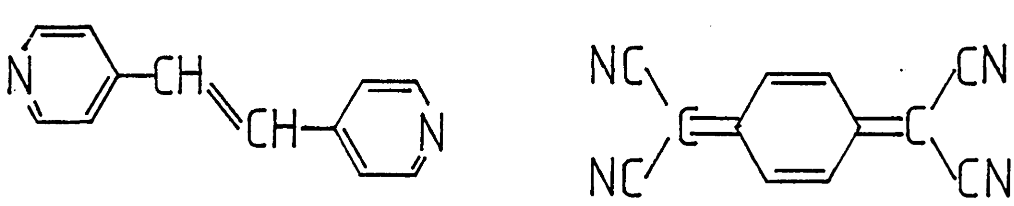

(V)

plexes. It is found to comprise mixed stacks of alternating TCNQ and DPE molecules. Although formally DPE behaves as a donor molecule and TCNQ as an acceptor molecule, the evidence for significant charge-transfer is limited, with the TCNQ molecule having a geometry comparable to that for the uncharged TCNQ^0. Similar structures are found in the (DPDO)(TCNQ),[22] (pyrene)(TCNQ),[24] (perylene)(TCNQ)[25] and (OMTTF)(DIM-EOTCNQ)[34] complexes and charge-transfer also appears to be limited in these cases.

The crystallographic studies presented here indicate the manner in which single crystal X-ray analyses can aid an understanding of the electrical conductivities of TCNQ complexes. The nature of the TCNQ stacking and the electrical properties of such complexes are so interrelated that any attempt to understand their differing conductivities requires a knowledge of the structures in the solid state. To this end, X-ray diffraction and in particular, single-crystal structures, are and will continue to be an essential part of any systematic study.

A.1 APPENDIX ONE

(a) Final positional parameters ($\times 10^4$) of all non-hydrogen atoms are given, with estimated standard deviations in parentheses.

(b) Final thermal parameters ($\times 10^4$) of the form:

(i) Anisotropic parameters

$$\exp\left[-2\pi^2(U_{11}h^2a^{*2} + U_{22}k^2b^{*2} + U_{33}\ell^2c^{*2} + 2U_{12}hka^*b^* + 2U_{13}h\ell a^*c^* + 2U_{33}k\ell b^*c^*)\right]$$

(ii) Isotropic parameters

$$\exp\left[-8\pi^2U\sin^2\theta/\lambda\right]$$

for all non-hydrogen atoms are given, with estimated standard deviations in parentheses.

(c) Final positional parameters ($\times 10^4$) of hydrogen atoms.

A1.1a Fractional Co-ordinates for $(DMBP)(TCNQ)_2$

DMBP ion	X	Y	Z
P	3806(6)	2500	3027(5)
C13	5582(19)	2055(3)	3974(14)
C14	7429(19)	2251(3)	4950(16)
C15	9087(22)	1979(4)	5821(19)
C16	8708(21)	1529(4)	5685(16)
C17	6855(22)	1341(4)	4737(19)
C18	5224(23)	1619(4)	3906(17)
C19	1930(29)	2500	3852(23)
C20	2606(29)	2500	509(19)
TCNQ			
N1	5782(23)	6874(4)	12146(19)
N2	-348(24)	6516(5)	9314(19)
N3	8820(24)	4637(4)	7661(19)
N4	2635(20)	4242(4)	5007(18)
C1	3715(20)	5917(4)	9465(15)
C2	5744(19)	5831(4)	9808(16)
C3	6217(19)	5470(4)	9076(16)
C4	4763(19)	5167(3)	7935(15)
C5	2734(20)	5257(4)	7556(16)
C6	2247(20)	5615(4)	8335(16)
C7	3231(21)	6298(4)	10169(16)
C8	1221(30)	6396(5)	9648(22)
C9	4641(24)	6616(4)	11258(20)
C10	5251(21)	4792(4)	7156(18)
C11	7234(21)	4717(4)	7406(16)
C12	3811(24)	4484(4)	5990(18)

A1.1b Thermal Parameters for (DMBP)(TCNQ)$_2$

	U_{11}	U_{22}	U_{33}	U_{23}	U_{13}	U_{12}
N1	898(128)	554(73)	884(91)	-151(74)	446(85)	-267(77)
N2	584(108)	845(101)	943(101)	-261(80)	225(87)	106(81)
N3	487(92)	726(84)	852(93)	- 26(74)	183(67)	- 57(73)
N4	414(79)	793(85)	660(70)	-193(75)	79(58)	- 38(69)
C1	487(90)	369(67)	347(65)	- 87(54)	- 1(58)	-120(59)
C2	387(84)	394(65)	468(68)	13(60)	89(56)	- 58(57)
C3	328(72)	323(60)	486(70)	9(56)	175(55)	- 27(50)
C4	303(75)	254(52)	370(59)	31(49)	112(50)	- 93(50)
C5	333(85)	626(83)	276(63)	56(61)	56(55)	- 78(63)
C6	432(89)	444(67)	458(67)	- 35(58)	254(62)	61(57)
C7	507(93)	471(73)	310(58)	- 49(56)	34(58)	-204(67)
C8	750(139)	385(76)	691(100)	- 69(73)	80(81)	33(80)
C9	577(144)	359(66)	742(103)	75(68)	340(84)	- 2(66)
C10	405(88)	521(78)	488(71)	- 46(63)	268(60)	60(62)
C11	294(86)	552(76)	376(67)	- 77(58)	134(56)	-117(61)
C12	548(98)	442(77)	406(65)	2(62)	188(63)	193(67)
P	276(21)	299(17)	270(19)	0	103(15)	0
C13	443(78)	305(49)	266(51)	61(41)	116(49)	140(49)
C14	481(76)	398(54)	360(57)	- 37(53)	228(52)	57(55)
C15	487(94)	545(79)	743(88)	120(67)	398(73)	75(65)
C16	696(104)	534(82)	419(71)	247(59)	208(68)	381(71)
C17	617(96)	434(61)	782(91)	-312(62)	408(76)	-149(59)
C18	708(107)	412(65)	637(82)	38(59)	277(77)	177(68)
C19	467(126)	842(139)	660(108)	0	165(90)	0
C20	713(135)	439(96)	295(82)	0	220(84)	0

A1.1c Fractional Co-ordinates of Hydrogen Atoms for $(DMBP)(TCNQ)_2$

	X	Y	Z
H15	10560	2112	6527
H16	9942	1310	6413
H17	6690	985	4618
H18	3743	1489	3233
H19a	2653	2500	5428
H19b	993	2785	3397
H20a	3702	2500	9940
H20b	1647	2212	9946
H2	6888	6059	10658
H3	7736	5413	9369
H5	1586	5035	6648
H6	736	5667	8081

A1.2a Fractional Co-ordinates for $(Me_2Ph_2P)(TCNQ)_2$

	X	Y	Z
TCNQ A			
N1	4742	1665(38)	9122
N2	3921(13)	1218(44)	10763(12)
N3	2511(8)	1289(43)	4689(14)
N4	1661(10)	1293(42)	6368(14)
C1	3491(8)	1309(37)	8416(10)
C2	3111(9)	1112(38)	8518(11)
C3	2762(7)	1197(36)	7834(10)
C4	2776(7)	1434(35)	6985(10)
C5	3211(10)	1260(40)	6844(12)
C6	3683(13)	1417(45)	7596(16)
C7	3850(6)	1178(34)	9145(10)
C8	3804(12)	1116(44)	10043(13)
C9	4427(11)	1497(42)	9188(18)
C10	2396(7)	1407(26)	6171(10)
C11	2453(10)	1193(40)	5313(10)
C12	2029(8)	1114(39)	6224(12)
TCNQ B			
N5	4144(9)	3525(37)	3027(11)
N6	3406(10)	3870(41)	4820(11)
N7	1995(11)	4093(40)	-1412(14)
N8	1195(11)	3849(41)	309(13)
C13	3030(9)	3697(37)	2495(11)
C14	3133(11)	3664(39)	1514(11)
C15	2716(9)	3676(42)	856(14)
C16	2224(7)	3698(39)	845(12)
C17	2282(6)	3738(35)	854(10)
C18	2604(9)	3768(40)	2506(13)

	X	Y	Z
C19	3439(10)	3738(40)	3078(11)
C20	3382(15)	3731(46)	4003(19)
C21	3842(8)	3582(36)	3043(13)
C22	1775(11)	3784(42)	133(13)
C23	1858(11)	3823(43)	- 764(13)
C24	1503(8)	3797(37)	274(11)
(Me_2Ph_2P) ion			
P	401(5)	3809(15)	7182(6)
C31	155(6)	1659(26)	6402(9)
C32	400(6)	682(26)	5923(9)
C33	221(6)	- 956(26)	5368(9)
C34	- 203(6)	-1616(26)	5292(9)
C35	- 448(6)	- 639(26)	5771(9)
C36	- 269(6)	999(26)	6326(9)
C41	764(6)	6014(27)	7717(9)
C42	689(6)	6711(27)	8497(9)
C43	957(6)	8215(27)	9008(9)
C44	1301(6)	9022(27)	8740(9)
C45	1377(6)	8324(27)	7960(9)
C46	1108(6)	6820(27)	7449(9)
C51	531(22)	5836(49)	7597(32)
C61	686(20)	1536(49)	7842(27)
C71	545(15)	3165(44)	6141(21)
C81	- 32(17)	4126(46)	7244(25)
C91	1043(23)	4141(50)	7303(34)
C101	- 162(25)	5524(49)	6868(33)

A1.2b Thermal Parameters for $(Me_2Ph_2P)(TCNQ)_2$

(i) Anisotropic thermal parameters (x 10^3)

	U_{11}	U_{22}	U_{33}	U_{23}	U_{13}	U_{12}
N1	65(5)	81(5)	91(5)	13(5)	39(5)	- 4(5)
N2	190(5)	116(5)	21(5)	14(5)	- 25(5)	- 13(5)
N3	120(5)	106(5)	60(5)	4(5)	69(4)	- 4(5)
N4	95(5)	85(5)	64(5)	8(5)	34(5)	9(5)
C1	64(5)	43(5)	9(4)	- 14(5)	11(4)	- 2(5)
C2	73(5)	42(5)	23(4)	22(5)	9(5)	11(5)
C3	48(5)	30(5)	13(4)	- 5(5)	23(4)	0(5)
C5	96(5)	43(5)	22(4)	2(5)	3(5)	2(5)
C6	125(5)	75(5)	51(5)	- 10(5)	11(5)	- 11(5)
C8	116(5)	89(5)	25(4)	10(5)	22(5)	- 11(5)
C9	61(5)	58(5)	73(5)	- 15(5)	5(5)	- 13(5)
C10	61(5)	41(5)	23(4)	- 3(5)	31(4)	- 2(5)
C11	102(5)	63(5)	6(4)	- 5(5)	17(4)	15(5)
C12	49(5)	48(5)	35(5)	- 8(5)	7(5)	- 3(5)
N5	100(5)	68(5)	27(4)	0(5)	19(5)	15(5)
N6	127(5)	97(5)	23(5)	- 24(5)	- 8(5)	9(5)
N7	150(5)	112(5)	55(4)	- 6(5)	77(4)	- 19(5)
N8	105(5)	86(5)	46(4)	0(5)	15(5)	- 11(5)
C13	78(5)	43(5)	19(4)	- 15(5)	19(5)	14(5)
C14	117(5)	40(5)	14(5)	0(5)	2(4)	6(5)
C15	77(5)	63(5)	49(5)	- 8(5)	49(4)	10(5)
C18	75(5)	46(5)	43(4)	3(5)	37(4)	1(5)
C19	106(5)	57(5)	8(4)	3(5)	- 4(4)	5(5)
C20	133(5)	78(5)	68(4)	11(5)	9(4)	6(5)
C21	53(5)	46(5)	30(4)	7(5)	34(5)	9(5)
C22	85(5)	62(5)	26(4)	2(5)	1(5)	- 1(5)

	U_{11}	U_{22}	U_{33}	U_{23}	U_{13}	U_{12}
C23	99(5)	80(5)	29(4)	16(5)	27(5)	2(5)
P	122(4)	72(4)	40(2)	28(4)	38(2)	- 5(5)
C31	51(5)	37(5)	39(5)	9(5)	- 14(5)	9(5)
C33	78(5)	32(5)	26(5)	- 8(5)	- 4(5)	18(5)
C36	40(5)	27(5)	16(5)	- 3(5)	- 10(5)	8(5)
C43	47(5)	23(5)	25(5)	9(5)	8(5)	-23(5)
C44	98(5)	33(5)	30(5)	- 23(5)	- 12(5)	0(5)
C46	46(5)	39(5)	25(5)	5(5)	28(5)	- 11(5)
C51	62(5)	55(5)	69(5)	2(5)	9(5)	0(5)
C61	81(5)	58(5)	50(5)	7(5)	1(5)	- 13(5)
C71	63(5)	52(5)	33(5)	11(5)	36(5)	16(5)
C81	60(5)	42(5)	43(5)	- 7(5)	26(5)	- 3(5)
C91	86(5)	77(5)	80(5)	5(5)	30(5)	8(5)
C101	85(5)	80(5)	72(5)	- 7(5)	- 1(5)	- 7(5)

(ii) Isotropic thermal parameters

	U		U		U		U
C7	21(3)	C4	28(3)	C16	40(4)	C17	22(3)
C24	31(4)	C32	3(4)	C34	19(4)	C35	7(4)
C41	14(4)	C42	6(4)	C45	53(5)		

A1.3a Fractional Co-ordinates for (DCØBP)(TCNQ)$_4$

	X	Y	Z
DCØBP ion			
N9	13635(5)	6031(3)	3927(2)
C25	12748(5)	5345(3)	4055(2)
C26	11565(4)	4501(2)	4236(2)
C27	10029(4)	3962(2)	3549(2)
C28	8865(4)	3180(2)	3728(2)
C29	9229(4)	2961(2)	4587(2)
C30	10733(4)	3491(2)	5271(2)
C31	11907(4)	4268(2)	5084(2)
N10	7985(3)	2129(2)	4760(2)
C32	8639(4)	1467(2)	5231(2)
C33	7501(4)	640(2)	5340(2)
C34	5614(4)	456(2)	4959(2)
C35	4975(4)	1162(2)	4496(2)
C36	6142(4)	1993(3)	4411(2)
TCNQ(A)			
N1	3017(4)	1804(2)	-3692(2)
N2	8851(5)	2455(3)	-2449(2)
N3	797(5)	4569(3)	1348(2)
N4	6637(5)	5029(3)	2664(2)
C1	5215(4)	3043(2)	-1379(2)
C2	3376(4)	3146(2)	-1305(2)
C3	3015(4)	3575(2)	- 489(2)
C4	4420(4)	3922(2)	343(2)
C5	6265(4)	3816(2)	265(2)
C6	6631(4)	3398(2)	- 555(2)
C7	5581(4)	2612(3)	-2230(2)
C8	7407(5)	2528(3)	-2347(2)

	X	Y	Z
C9	4163(5)	2177(3)	-3045(2)
C10	4063(4)	4362(3)	1187(2)
C11	2253(5)	4481(2)	1285(2)
C12	5484(5)	4732(3)	2014(2)
TCNQ(B)			
N5	137(4)	- 632(2)	-3449(2)
N6	6029(5)	1(3)	-2187(2)
N7	-2199(4)	2095(3)	1479(2)
N8	3603(4)	2711(3)	2859(2)
C13	2367(4)	643(2)	-1184(2)
C14	522(4)	738(2)	-1126(2)
C15	140(4)	1159(2)	- 306(2)
C16	1528(4)	1531(2)	519(2)
C17	3372(4)	1443(2)	460(2)
C18	3769(4)	1018(2)	- 359(2)
C19	2747(4)	176(2)	-2025(2)
C20	4561(6)	79(3)	-2118(2)
C21	1318(5)	- 260(3)	-2823(2)
C22	1116(4)	1958(2)	1362(2)
C23	- 713(5)	2039(3)	1433(2)
C24	2492(5)	2362(3)	2190(2)

A1.3b Thermal Parameters for (DCØBP)(TCNQ)$_4$

	U_{11}	U_{22}	U_{33}	U_{23}	U_{13}	U_{12}
N9	610(23)	822(24)	985(26)	225(20)	323(20)	20(20)
C25	447(23)	665(25)	616(24)	115(20)	163(19)	139(21)
C26	331(19)	484(20)	545(21)	114(17)	158(17)	118(16)
C27	459(21)	578(21)	448(20)	120(17)	98(17)	128(18)
C28	436(20)	554(21)	449(20)	93(16)	71(16)	76(18)
C29	398(20)	501(20)	393(19)	107(15)	116(16)	154(16)
C30	395(20)	569(21)	427(19)	82(16)	13(16)	131(18)
C31	333(19)	579(22)	567(22)	113(18)	53(17)	114(17)
N10	346(16)	521(16)	392(15)	110(13)	21(12)	127(13)
C32	381(20)	626(22)	466(20)	171(17)	35(16)	162(18)
C33	346(20)	576(21)	573(22)	247(18)	6(16)	95(17)
C34	352(19)	498(19)	336(16)	80(15)	31(14)	117(14)
C35	342(19)	554(21)	524(20)	184(17)	26(15)	88(18)
C36	349(20)	608(22)	463(19)	139(16)	- 6(16)	163(17)
N1	422(19)	877(23)	545(20)	89(17)	- 4(16)	73(17)
N2	371(21)	1375(33)	896(26)	10(22)	108(18)	272(21)
N3	455(21)	1127(29)	842(25)	238(20)	223(19)	117(20)
N4	699(24)	1216(29)	492(20)	92(20)	-17(19)	328(21)
C1	318(20)	583(21)	430(20)	148(16)	17(16)	93(16)
C2	298(19)	582(22)	450(20)	117(17)	23(15)	68(16)
C3	263(18)	580(22)	511(22)	161(17)	26(16)	52(16)
C4	345(20)	541(21)	466(21)	184(17)	55(16)	96(16)
C5	318(19)	612(22)	462(21)	138(17)	-10(16)	91(16)
C6	297(19)	639(22)	523(22)	123(18)	0(17)	102(17)
C7	307(19)	659(23)	497(21)	140(18)	12(17)	126(17)
C8	427(25)	786(27)	510(22)	48(19)	10(19)	155(20)
C9	396(21)	646(23)	463(21)	147(18)	126(19)	159(18)

	U_{11}	U_{22}	U_{33}	U_{23}	U_{13}	U_{12}
C10	365(20)	585(22)	445(21)	157(17)	64(17)	73(16)
C11	498(25)	666(25)	509(22)	142(18)	140(19)	65(20)
C12	574(25)	767(27)	452(23)	207(20)	106(21)	220(21)
N5	637(23)	834(23)	534(20)	28(17)	22(17)	278(18)
N6	491(23)	1135(29)	919(27)	86(21)	164(19)	218(20)
N7	430(21)	962(25)	650(21)	68(17)	55(16)	132(18)
N8	603(22)	1000(26)	575(20)	99(18)	-73(18)	247(19)
C13	428(21)	448(19)	516(21)	142(16)	53(17)	97(16)
C14	348(20)	542(21)	507(21)	76(17)	8(17)	107(16)
C15	335(20)	605(22)	504(22)	110(18)	22(17)	89(17)
C16	369(20)	479(20)	452(20)	93(16)	29(16)	77(16)
C17	385(21)	537(21)	473(21)	125(17)	-28(16)	130(16)
C18	351(20)	609(22)	503(21)	127(17)	18(17)	129(17)
C19	388(21)	538(21)	515(21)	149(17)	44(17)	147(17)
C20	539(26)	667(25)	547(24)	118(19)	81(20)	124(21)
C21	490(23)	621(23)	476(22)	101(18)	68(19)	195(19)
C22	381(21)	570(21)	478(21)	107(17)	-18(17)	137(17)
C23	434(24)	644(24)	437(21)	103(17)	- 3(18)	119(19)
C24	468(23)	652(23)	497(22)	137(18)	91(20)	217(19)

A1.3c Fractional Co-ordinates of Hydrogen Atoms for (DCØBP)(TCNQ)$_4$

	X	Y	Z
H27	9757	4158	2888
H28	7687	2739	3202
H30	10991	3299	5934
H31	13096	4694	5609
H32	10090	1591	5527
H33	8057	124	5724
H35	3531	1051	4191
H36	5606	2547	4068
H2	2268	2882	-1915
H3	1628	3661	-456
H5	7374	4080	872
H6	8023	3333	-588
H14	-561	480	-1745
H15	-1263	1207	-275
H17	4459	1712	1074
H18	5173	968	-386

A1.4a Fractional Co-ordinates for (DEPA)(TCNQ)$_4$

	X	Y	Z
N9	5796(19)	3576(9)	3812(25)
C25	5243(30)	2673(16)	4748(31)
C26	6142(23)	3029(13)	5165(31)
C27	6208(24)	3615(12)	2617(29)
C28	5833(21)	4039(10)	1348(25)
C29	5211(23)	4398(12)	1448(29)
C30	4796(26)	4302(15)	2846(31)
C31	5179(19)	3895(9)	3935(22)
C32	4598(19)	4790(11)	-483(24)
N1	- 614(16)	3089(8)	-2232(16)
N2	-2224(19)	3134(10)	1247(21)
N3	4655(21)	3034(11)	7395(27)
N4	3151(16)	3149(9)	11167(18)
C1	317(18)	3107(9)	2742(23)
C2	1208(16)	3122(8)	2577(20)
C3	2161(16)	3067(8)	4244(20)
C4	2152(18)	3148(9)	6172(19)
C5	1206(18)	3177(9)	6187(20)
C6	190(16)	3184(7)	4503(17)
C7	- 411(19)	3147(9)	1167(22)
C8	-1446(20)	3161(9)	1169(20)
C9	- 526(16)	3136(8)	- 795(19)
C10	3050(19)	3157(9)	7724(17)
C11	4073(23)	3164(11)	7629(23)
C12	3025(21)	3183(11)	9769(30)
N5	-1734(17)	4359(10)	-5064(23)
N6	-3338(17)	4488(9)	-1814(19)

	X	Y	Z
N7	3432(16)	4321(8)	4989(19)
N8	1855(13)	4422(7)	8263(19)
C13	- 828(15)	4392(7)	- 58(18)
C14	87(17)	4346(8)	- 126(21)
C15	937(15)	4297(7)	1498(18)
C16	866(15)	4338(9)	3302(17)
C17	- 46(15)	4383(9)	3347(17)
C18	- 845(17)	4365(9)	1773(19)
C19	-1714(16)	4401(8)	-1693(16)
C20	-2522(19)	4452(9)	-1751(21)
C21	-1739(16)	4368(8)	-3456(23)
C22	1833(15)	4338(7)	5093(19)
C23	2702(22)	4339(9)	5042(18)
C24	1874(14)	4425(7)	6893(18)

A1.4b Thermal Parameters for $(DEPA)(TCNQ)_4$

(i) Anisotropic Thermal Parameters

	U_{11}	U_{22}	U_{33}	U_{23}	U_{13}	U_{12}
N9	831(38)	1392(38)	1620(37)	447(38)	750(37)	450(38)
C25	3773(39)	2181(39)	1759(38)	436(38)	1070(38)	1051(39)
C26	2521(38)	1451(38)	3003(38)	505(38)	2488(37)	-225(38)
C28	1392(38)	746(38)	1139(37)	142(37)	852(37)	-239(38)
C29	1361(38)	1109(38)	1803(38)	348(38)	712(38)	319(38)
C31	497(38)	948(38)	723(36)	113(37)	56(37)	33(38)
C32	353(38)	1877(38)	882(37)	-506(38)	-7(37)	27(38)
N1	1026(40)	1561(40)	326(34)	-90(38)	346(36)	303(40)
N2	1332(41)	1410(40)	668(37)	1(39)	648(38)	3(40)

	U_{11}	U_{22}	U_{33}	U_{23}	U_{13}	U_{12}
N3	1438(41)	1582(41)	1474(40)	0(40)	829(40)	124(21)
N4	891(41)	1647(40)	310(35)	400(38)	-141(38)	95(40)
C1	490(41)	562(39)	685(38)	252(39)	80(39)	-36(40)
C2	317(40)	414(39)	554(37)	-93(38)	89(38)	28(39)
C3	420(40)	271(39)	697(37)	64(38)	193(38)	-285(39)
C4	557(40)	1125(40)	331(36)	136(38)	164(38)	-289(40)
C5	614(40)	798(40)	498(37)	-26(38)	286(38)	-439(40)
C6	726(40)	310(39)	267(35)	67(36)	-53(37)	2(39)
C8	858(41)	578(39)	396(36)	-66(38)	47(39)	-177(40)
C9	608(40)	606(39)	500(36)	-215(38)	433(36)	54(39)
C10	1139(41)	907(40)	214(35)	307(37)	166(38)	607(40)
C11	1137(41)	1523(40)	483(38)	-80(39)	53(39)	1125(40)
C12	653(41)	1091(40)	1566(40)	234(40)	413(40)	70(41)
N5	937(37)	1721(37)	1084(35)	-392(36)	650(35)	17(36)
N6	559(37)	1564(37)	510(34)	77(35)	57(35)	173(36)
N7	664(36)	1254(36)	529(33)	-66(35)	234(34)	-185(36)
N8	452(36)	805(35)	705(33)	75(34)	423(33)	-79(35)
C13	372(36)	443(35)	394(32)	-43(33)	205(33)	-263(35)
C14	249(36)	739(36)	669(35)	-90(35)	221(35)	153(36)
C15	530(37)	604(36)	308(32)	-122(33)	153(34)	-42(36)
C16	304(36)	1271(36)	243(31)	-0(34)	145(32)	-421(36)
C17	250(36)	1217(36)	320(31)	-66(34)	202(32)	-211(36)
C18	1092(37)	1003(36)	426(32)	48(34)	533(33)	377(36)
C19	296(36)	842(36)	177(31)	55(33)	-53(33)	273(35)
C20	188(36)	899(36)	579(34)	5(35)	201(35)	35(36)
C21	335(36)	767(36)	802(35)	-163(35)	108(35)	-377(36)
C22	147(36)	543(35)	453(34)	4(34)	143(34)	-30(35)
C23	1366(37)	1034(36)	229(31)	-164(34)	361(34)	-727(36)
C24	173(36)	689(36)	368(32)	179(33)	237(32)	201(35)

(ii) Isotropic Thermal Parameters

	U		U		U
C30	1864(38);	C27	1364(37);	C7	637(34);

A1.5 Final Positional and Thermal Parameters for (DPE)(TCNQ)

(a) Fractional Co-ordinates

	X	Y	Z
N1	11777(11)	257(6)	658(5)
N2	12029(10)	3141(6)	2911(3)
C1	10620(7)	3892(5)	605(3)
C2	10136(8)	3617(5)	-357(3)
C3	9566(8)	4651(5)	-902(3)
C7	11230(7)	2832(5)	1175(3)
C8	11647(9)	3037(6)	2149(4)
C9	11508(10)	1395(6)	868(4)
C11	6717(10)	1431(6)	1383(5)
C12	6084(10)	2443(7)	743(5)
C13	5870(8)	3856(6)	1036(4)
C14	6318(9)	4152(7)	1941(5)
C15	6911(10)	3084(7)	2512(4)
C16	5231(10)	5050(7)	433(5)
N3	7124(8)	1736(5)	2256(3)

(b) Anisotropic Thermal Parameters

	U_{11}	U_{22}	U_{33}	U_{23}	U_{13}	U_{12}
TCNQ						
N1	1104(55)	507(30)	829(38)	-53(27)	-107(34)	146(29)
N2	972(48)	694(31)	431(25)	76(23)	-36(23)	-169(27)
C1	286(32)	454(25)	433(23)	-56(19)	41(18)	-88(18)
C2	563(40)	347(23)	433(25)	-113(19)	26(21)	-19(19)
C3	553(40)	472(26)	304(24)	-84(20)	9(21)	-97(21)
C7	427(38)	377(24)	433(25)	30(17)	-19(20)	-70(18)
C8	540(42)	474(28)	530(31)	67(23)	30(24)	-108(22)
C9	707(48)	487(30)	554(30)	82(24)	-41(26)	-31(26)

	U_{11}	U_{22}	U_{33}	U_{23}	U_{13}	U_{12}
DPE						
N3	764(46)	494(26)	583(28)	159(22)	-88(25)	33(22)
C11	612(49)	521(30)	692(36)	100(27)	-59(28)	-19(26)
C12	556(51)	762(41)	583(33)	115(29)	-76(28)	-23(29)
C13	291(39)	588(34)	856(44)	259(30)	97(28)	29(23)
C14	611(47)	498(31)	732(38)	86(26)	27(30)	19(25)
C15	689(56)	634(36)	566(31)	84(28)	-30(28)	-15(28)
C16	525(48)	686(38)	768(37)	155(34)	41(32)	25(28)

A1.5c Fractional Co-ordinates of Hydrogen Atoms for (DPE)(TCNQ)

	X	Y	Z
H2	10234(91)	2691(67)	-612(43)
H3	9384(94)	4514(64)	-1517(46)
H11	6872	345	1156
H12	5774	2142	36
H14	6205	5225	2200
H15	7236	3353	3223
H16	5004	6073	777

A.2 Appendix Two

Equations of least-squares planes referred to orthogonal axes with distances (Å) of relevant atoms from the planes in square brackets and estimated standard deviations in parentheses.

A2.1 Mean Plane Data for $(DMBP)(TCNQ)_2$

Plane A : Cation; Five-Membered ring C13, C14, C14', C13'.

$$0.5461X + 0.0000Y - 0.8377Z + 0.7990 = 0.0000$$

[C13, 0.0000(117); C14, -0.0000(127); C13', 0.0000(117);
C14', -0.0000(127); P, 0.0066(40)]

Plane B : Cation; Six-Membered ring C13, C14, C15, C16, C17, C18

$$0.5336X - 0.0325Y - 0.8541Z + 1.0819 = 0.0000$$

[C13, 0.0248(116); C14, -0.0129(126); C15, 0.0012(148);
C16, -0.0011(131); C17, 0.0115(148); C18, -0.0236(141)]

Plane C : TCNQ; C1, C2, C3, C4, C5, C6

$$0.2426X - 0.5320Y - 0.8113Z - 3.9620 = 0.0000$$

[C1, -0.0002(114); C2, 0.0078(118); C3, -0.0042(118);
C4, -0.0071(105); C5, 0.0150(119); C6, -0.0113(119);
N1, 0.3170(143); N2, 0.1531(134); C8, 0.1921(160);
C9, 0.1135(140); C7, 0.0603(119); C10, -0.0080(128);
C11, 0.0704(119); C12, 0.0000(130); N3, 0.0648(135);
N4, 0.0421(128)]

Angles Between the Planes (^{o})

A/B	2.04
B/B'	3.72
A/B'	2.04
B/C	37.08
A/C	35.70

A2.2 Mean Plane Data for $(Me_2Ph_2P)(TCNQ)_2$

Plane A : TCNQ A, C1 → C6

0.0291X + 0.9987Y - 0.0410Z - 5.0509 = 0.0000

[C1, -0.04(2); C2, 0.05(3); C3, 0.01(2); C4, -0.08(2);
C5, 0.09(3); C6, -0.03(3); C9, -0.01(3); C8, 0.03(2);
C7, -0.13(3); N2, -0.21(3); N1, -0.11(3); C10, -0.04(3);
C11, 0.17(3); C12, 0.12(3); N3, 0.16(3); N4, -0.04(3)]

Plane B : TCNQ B, C13 → C18

0.0163X + 0.9998Y - 0.0141Z - 2.2348 = 0.0000

[C13, -0.01(2); C14, 0.01(3); C15, -0.01(2); C16, -0.01(3);
C17, 0.01(3); C18, 0.00(3); C21, 0.02(3); C20, -0.01(3);
C19, -0.06(2); N5, 0.06(3); N6, -0.08(2); C22, 0.05(3);
C23, 0.10(3); C24, 0.04(2); N7, 0.06(3); N8, 0.31(3)]

Plane C : TCNQ A', C1' → C6'

0.0291X + 0.9987Y - 0.0410Z + 1.5020 = 0.0000

Angles Between the Planes ($^\circ$)

A/B 1.71

A2.3 Mean Plane Data for (DCØBP)(TCNQ)$_4$

Plane A : (DCØBP) ion, N10 - C36

0.3802X - 0.3540Y - 0.8545Z + 4.6604 = 0.0000

[N10, 0.0166(28); C36, -0.0153(31); C35, 0.0016(29);
C34, 0.0107(29); C33, -0.0098(29); C32, -0.0038(29)]

Plane B : (DCØBP) ion, C26 - C31

0.7250X - 0.5972Y - 0.3430Z - 0.0599 = 0.0000

[C26, 0.0018(30); C27, -0.0018(30); C28, -0.0000(30);
C29, 0.0020(30); C30, -0.0020(30); C31, 0.0001(30);
C25, -0.0571(38); N9, -0.1549(38)]

Plane C : TCNQ(A), C1 - C6

0.0665X + 0.9804Y - 0.1855Z - 5.0906 = 0.0000

[C1, 0.0003(28); C2, -0.0061(28); C3, 0.0084(28);
C4, -0.0047(28); C5, -0.0009(28); C6, 0.0030(28);
N1, -0.2324(28); N2, 0.1073(40); C9, -0.1064(40);
C8, 0.0639(40); C7, 0.0059(40); C10, 0.0060(40);
C11, 0.0064(40); C12, 0.0265(40); N3, 0.0069(40);
N4, 0.0525(40)]

Plane D : TCNQ(B), C13 - C18

0.0553X + 0.9790Y - 0.1964Z - 1.7103 = 0.0000

[C13, -0.0040(28); C14, 0.0042(28); C15, -0.0018(28);
C16, -0.007(28); C17, 0.0008(28); C18, 0.0016(28);
N5, -0.2699(28); N6, -0.0279(40); C20, -0.0332(40);
C21, -0.1474(40); C19, -0.0440(28); C22, -0.0153(28);
C23, -0.0331(40); C24, 0.0249(40); N7, -0.0526(40);
N8, 0.0866(40)]

Angles Between the Planes (°)

A/B 38.72

C/D 0.89

A2.4 Mean Plane Data for $(DEPA)(TCNQ)_4$

Plane A : pyridinium function N9, C27 - C31, C32

-0.5037X - 0.6130Y - 0.6087Z + 11.1805 = 0

[N9, 0.094(23); C27, 0.014(30); C28, -0.056(25);
C29, -0.176(29); C30, -0.055(34); C31, 0.027(23);
C32, 0.153(25); C25, 1.720(37); C26, 0.360(31)]

Plane B : ethyl substituent, N9, C26, C25

0.5174X - 0.4574Y - 0.7233Z + 2.2886 = 0

[N9, 0.000(23); C26, 0.000(29); C25, 0.000(35); C27, 1.094
(28); C28, 1.161(24); C29, 0.176(28); C30, -0.989(32);
C31, -0.948(22); C32, 0.546(24)]

Plane C : TCNQ(A), C1 - C6

0.0694X + 0.9960Y - 0.0559Z - 7.9586 = 0

[C1, -0.060(23); C2, 0.084(21); C3, -0.063(21); C4, 0.025(23);
C5, -0.001(23); C6, 0.016(18); N1, 0.108(21); N2, -0.164(26);
N3, -0.083(29); N4, -0.182(23); C7, 0.066(23);
C8, -0.007(23); C9, 0.149(21); C10, 0.045(23);
C11, 0.177(29); C12, -0.019(29)]

Plane D : TCNQ(A)', C1' - C6'

0.0694X - 0.9960Y - 0.0559Z + 5.2911 = 0

Plane E : TCNQ(B), C13 - C18

-0.0711X - 0.9974Y - 0.0095Z + 11.2527 = 0

[C13, -0.037(18); C14, -0.018(21); C15, 0.046(18);
C16, -0.020(23); C17, 10.038(18); C18, 0.067(23);
N5, 0.057(26); N6, -0.046(23); N7, -0.224(21);
N8, -0.256(18); C19, 0.006(21); C20, -0.040(23);
C21, 0.063(21); C22, -0.093(18); C23, -0.190(23);
C24, -0.290(18)]

Plane F : TCNQ(B)', C13' - C18'

-0.0711X - 0.9974Y - 0.0095Z + 14, 6544 = 0

Angles Between the Planes (^{o})

A/B 62.61, A/C 52.30 A/D 54.43, A/E;A/F 49.23,

B/C 67.72 B/D 57.87, B/E;B/F 64.75, C/D 10.23

C/E;C/F 3.75 D/E:D/F 8.49

A2.5 Mean Plane Data for (DPE)TCNQ)

Plane A : TCNQ, C1, C2, C3

0.9535X + 0.1768Y - 0.2441Z - 7.7612 = 0

[C1, 0.000(5); C2, 0.000(6); C3, 0.000(6); C7, 0.021(5); C8, -0.042(7); C9, 0.096(7); N1, 0.176(8); N2, -0.062(7)]

Plane B : TCNQ', C1', C2', C3'

0.9535X + 0.1768Y - 0.2441Z - 0.8365 = 0

Plane C : DPE, N3, C11 - C15, C16

0.9515X + 0.1930Y - 0.2397Z - 4.3591 = 0

[N3, 0.000(6); C11, 0.003(7); C12, -0.001(7); C13, -0.007 (6); C14, 0.004(7); C15, -0.002(7); C16, 0.003(7)]

Plane D : DPE pyridinium function N3, C11 - C15

0.9510X + 0.1941Y - 0.2406Z - 4.3572Z = 0

[N3, -0.002(6); C11, 0.003(7); C12, 0.000(7); C13, -0.004 (6); C14, 0.006(7); C15, -0.003(7); C16, 0.009(7)]

Angles Between the Planes ($^{\circ}$)

A/B 0.0 , C/D 0.08, A/C:B/C 0.97, A/D:B/D 1.02

A.3 APPENDIX THREE

Tables of Observed and Calculated Structure Factors

A3.1 OBSERVED AND CALCULATED STRUCTURE FACTORS FOR (DMBP)$(TCNQ)_2$

OBSERVED AND CALCULATED STRUCTURE FACTORS FOR THE PHOSPHOLIUM TCNQ DATA

H	K	L	FO	FC	H	K	L	FO	FC	H	K	L	FO	FC	H	K	L	FO	FC	H	K	L	FO	FC
[illegible]	[illegible]	[illegible]	[illegible]	[illegible]	[illegible]	[illegible]	[illegible]	[illegible]	[illegible]	[illegible]	[illegible]	[illegible]	[illegible]	[illegible]	[illegible]	[illegible]	[illegible]	[illegible]	[illegible]	[illegible]	[illegible]	[illegible]	[illegible]	[illegible]

A3.2 OBSERVED AND CALCULATED STRUCTURE FACTORS FOR $(Me_2Ph_2P)(TCNQ)_2$

OBSERVED AND CALCULATED STRUCTURE FACTORS FOR TCNQ PHOSPHONIUM 2:1 COMPLEX

H	K	L	FO	FC	H	K	L	FO	FC	H	K	L	FO	FC	H	K	L	FO	FC	H	K	L	FO	FC
[illegible]	[illegible]	[illegible]	[illegible]	[illegible]	[illegible]	[illegible]	[illegible]	[illegible]	[illegible]	[illegible]	[illegible]	[illegible]	[illegible]	[illegible]	[illegible]	[illegible]	[illegible]	[illegible]	[illegible]	[illegible]	[illegible]	[illegible]	[illegible]	[illegible]

A3.3 OBSERVED AND CALCULATED STRUCTURE FACTORS FOR (DCØBP)(TCNQ)$_4$

[illegible]

A3.3 cont.

OBSERVED AND CALCULATED STRUCTURE FACTORS FOR [illegible] COMPLEX

H	K	L	FO	FC	H	K	L	FO	FC	H	K	L	FO	FC	H	K	L	FO	FC
[illegible]	[illegible]	[illegible]	[illegible]	[illegible]	[illegible]	[illegible]	[illegible]	[illegible]	[illegible]	[illegible]	[illegible]	[illegible]	[illegible]	[illegible]	[illegible]	[illegible]	[illegible]	[illegible]	[illegible]

A3.4 OBSERVED AND CALCULATED STRUCTURE FACTORS FOR (DEPA)(TCNQ)$_4$

OBSERVED AND CALCULATED STRUCTURE FACTORS FOR DEPA TCNQ COMPLEX

H	K	L	FO	FC
[illegible]	[illegible]	[illegible]	[illegible]	[illegible]

A3.5 OBSERVED AND CALCULATED STRUCTURE FACTORS FOR (DPE)(TCNQ)

OBSERVED AND CALCULATED STRUCTURE FACTORS FOR (DPE)(TCNQ) [illegible]

[illegible]

1. D.S.ACKER, R.J.HARDER, W.R.HERTLER, W.MAHLER, L.R.MELBY, R.E.BENSON, and W.E.MOCHEL, J.Amer.Chem.Soc., 1960, 82, 6408.

2. D.S.ACKER and W.R.HERTLER, J.Amer.Chem.Soc., 1962, 84, 3370.

3. L.R.MELBY, R.J.HARDER, W.R.HERTLER, W.MAHLER, R.E.BENSON, and W.E.MOCHEL, J.Amer.Chem.Soc., 1962, 84, 3374.

4. W.J.SIEMONS, P.E.BIERSTEDT and R.G.KEPLER, J.Chem.Phys., 1963, 39, 3523.

5. L.R.MELBY, Can.J.Chem., 1965, 43, 1448.

6. D.J.DAHM, P.HORN, G.R.JOHNSTON, M.G.MILES, and J.D.WILSON, J.Cryst. Mol.Struct., 1975, 5, 27.

7. Inorganic Chemistry, Vol.I, C.S.G.PHILLIPS and R.J.P.WILLIAMS, Oxford Clarendon Press, 1965, p.195-227, p.587.

8. Inorganic Chemistry, Vol.I, C.S.G.PHILLIPS and R.J.P.WILLIAMS, Oxford Clarendon Press, 1965, p.22.

9. A.HOEKSTRA, T.SPOELDER, and A.VOS, Acta Cryst., 1972, B28, 14.

10. I.SHIROTANI and H.KOBAYASHI, Bull.Chem.Soc.Jpn., 1973, 46, 2595.

11. V.F.KAMINSKII, R.P.SHIBAEVA, L.O.ATOVMYAN, E.B.YAGUBSKII, and M.L.KHIDEKEL, Soviet Physics: Doklady (Akademiya Nauk. SSSR Doklady)., 1974, 215, 176.

12. A.W.HANSON, Acta Cryst., 1978, B34, 2339.

13. R.M.WILLIAMS and S.C.WALLWORK, Acta Cryst., 1968, B24, 168.

14. M.OHMASA, M.KINOSHITA, and H.AKAMATU, Bull.Chem.Soc.Jpn., 1969, 42, 2402.

15. R.H.COLTON and D.E.HENN, J.Chem.Soc.(B)., 1970, 1532.

16. M.OHMASA, M.KINOSHITA, and H.AKAMATU, Bull.Chem.Soc.Jpn., 1971, 44, 3296.

18. I.IKEMOTO, K.CHIKAISHI, K.YAKUSHI, and H.KURODA, Acta Cryst., 1972, B28, 3502.

19. B.MAYOH and C.K.PROUT, J.Chem.Soc., Farad.Trans.II, 1972, 1072.

20. L.B.COLEMAN et al., Phys.Lett., 1972, 42A, 15.

21. I.GOLDBERG and U.SHMUELI, Acta Cryst., 1973, B29, 421.

22. I.GOLDBERG and U.SHMUELI, Acta Cryst., 1973, B29, 432.

23. I.GOLDBERG and U.SHMUELI, Acta Cryst., 1973, B29, 440.

24. C.K.PROUT, I.J.TICKLE, and J.D.WRIGHT, J.Chem.Soc., Perkin II, 1973, 528.

25. I.J.TICKLE and C.K.PROUT, J.Chem.Soc., Perkin II, 1973, 720.

26. I.J.TICKLE and C.K.PROUT, J.Chem.Soc., Perkin II, 1973, 727.

27. K.YAKUSHI, I.IKEMOTO, and H.KURODA, Acta Cryst., 1974, B30, 835.

28. K.YAKUSHI, I.IKEMOTO and H.KURODA, Acta Cryst., 1974, B30, 1738.

29. R.P.SHIBAEVA and O.V.YAROCHKINA, Soviet Physics: Doklady (Akademiya Nauk. SSSR Doklady)., 1975, 20, 304.

30. B.SHAANAN, U.SHMUELI, and D.RABINOVICH, Acta Cryst., 1976, B32, 2574.

31. S.FLANDROIS, P.DELHAES, J.AMIELL, C.BRUN, E.TORREILLES, J.M.FABRE, and L.GIRAL, Phys.Letts., 1978, A66, 244.

32. B.F.DAROCHA, D.D.TITUS and D.J.SANDMAN, Acta Cryst., 1979, B35, 2445.

33. M.KONNO, Y.SAITO, K.YAMADA, and H.KAWAZURA, Acta Cryst., 1980, B36, 1680.

34. D.CHASSEAU and C.HAUW, Acta Cryst., 1980, B36, 3131.

35. D.CHASSEAU and F.LEROY, Acta Cryst., 1981, B37, 454.

NATO-ASI Series B25, 1977, New York: Plenum.

37. J.S.MILLER and A.J.EPSTEIN, Synthesis and Properties of Low-Dimensional Materials, Ann.N.Y.Acad.Sci., 1978, 313.

38. W.A.HATFIELD, Molecular Metals, NATO Conf.Series VI, Materials Science, Vol.I, 1979, New York: Plenum.

39. R.E.LONG, R.A.SPARKS, and K.N.TRUEBLOOD, Acta Cryst., 1965, 18, 932.

40. C.J.FRITCHIE, Acta Cryst., 1966, 20, 892.

41. C.J.FRITCHIE and P.ARTHUR, Acta Cryst., 1966, 21, 139.

42. A.W.HANSON, Acta Cryst., 1968, B24, 768.

43. P.GOLDSTEIN, K.SEFF, and K.N.TRUEBLOOD, Acta Cryst., 1968, B24, 778.

44. J.G.VEGTER, T.HIBA, and J.KOMMANDER, Chem.Phys.Lett., 1969, 3, 427.

45. A.REMBAUM, A.M.HERMANN, F.E.STEWART, and F.GUTMANN, J.Chem.Phys., 1969, 73, 513.

46. H.KOBAYASHI, Y.OHASHI, F.MARUMO, and Y.SAITO, Acta Cryst., 1970, B26, 459.

47. H.KOBAYASHI, F.MARUMO, and Y.SAITO, Acta Cryst., 1971, B27, 373.

48. A.T.McPHAIL, G.M.SEMENIUK, and D.B.CHESNUT, J.Chem.Soc.(A), 1971, 2174.

49. T.SUNDARESAN and S.C.WALLWORK, Acta Cryst., 1972, B28, 491.

50. T.SUNDARESAN and S.C.WALLWORK, Acta Cryst., 1972, B28, 1163.

51. N.SAKAI, I.SHIROTANI, and S.MINOMURA, Bull.Chem.Soc.Jpn., 1972, 45, 3314.

53. M.KONNO and Y.SAITO, Acta Cryst., 1973, B29, 2815.

54. D.CHASSEAU, J.GAULTIER, C.HAUW, and J.JAUD, C.R.Hebd.Seances Acad.Sci., Ser.C: 1973, 276, 751.

55. L.B.COLEMAN, J.A.COHEN, A.F.GARITO, and A.J.HEEGER, Phys.Rev.B., 1973, 7, 2122.

56. H.KOBAYASHI, Bull.Chem.Soc.Jpn., 1974, 47, 1346.

57. J.JAUD, D.CHASSEAU, J.GAULTIER, and C.HAUW, C.R.Hebd.Seances Acad.Sci., Ser.C: 1974, 278, 769.

58. M.J.RICE, Phys.Bull., 1975, 493.

59. B.MOROSIN, Phys.Letts., 1975, 53A, 455.

60. R.P.SHIBAEVA and V.I.PONOMAREV, Soviet Physics - Crystallography (Kristallografiya)., 1975, 20, 183.

61. D.CHASSEAU, J.GAULTIER, and C.HAUW, Acta Cryst., 1976, B32, 3262.

62. S.Z.GOLDBERG, R.EISENBERG, J.S.MILLER, and A.J.EPSTEIN, J.Amer. Chem.Soc., 1976, 98, 5173.

63. H.PORADOWSKA and A.GRZECHOWSKA, Ann.Chem.(Warsaw)., 1976, 50, 869.

64. B.VAN BODEGOM, J.L.DE BOER, and A.VOS, Acta Cryst., 1977, B33, 602.

65. A.BOSCH and B.VAN BODEGOM, Acta Cryst., 1977, B33, 3013.

66. R.P.SHIBAEVA, L.P.ROZENBERG, and R.M.LOBKOVSKAYA, Soviet Physics - Crystallography (Kristallografiya)., 1977, 22, 159.

67. R.J.VAN DER WAL and B.VAN BODEGOM, Acta Cryst., 1978, B34, 1700.

68. H.KOBAYASHI, Acta Cryst., 1978, B34, 2818.

69. P.DUPUIS, S.FLANDROIS, P.DELHAES, and C.CONLON, J.Chem.Soc., Chem. Comm., 1978, 337.

Acta Cryst., 1979, B35, 1652.

71. R.J.VAN DER WAL and B.VAN BODEGOM, Acta Cryst., 1979, B35, 2003.

72. R.J.FLEMING, M.A.SHAIKH, B.W.SKELTON, and A.H.WHITE, Aust.J.Chem., 1979, 32, 2187.

73. A.FILHOL and J.GAULTIER, Acta Cryst., 1980, B36, 592.

74. H.ENDRES, H.J.KELLER, W.MORONI, and D.NÖTHE, Acta Cryst., 1980, B36, 1435.

75. A.FILHOL, C.M.E.ZEYEN, P.CHENAVAS, J.GAULTIER and P.DELHAES, Acta Cryst., 1980, B36, 2719.

76. A.BRAU, J.P.FARGES, H.GRASSI and P.DUPUIS, Phys.Status Solidi A, 1980, 59, K129.

77. H.MORSSINK and B.VAN BODEGOM, Acta Cryst., 1981, B37, 107.

78. P.KAMMINGA and B.VAN BODEGOM, Acta Cryst., 1981, B37, 114.

79. B.VAN BODEGOM and J.L.DE BOER, Acta Cryst., 1981, B37, 119.

80. B.VAN BODEGOM, Acta Cryst., 1981, B37, 857.

81. B.VAN BODEGOM and A.BOSCH, Acta Cryst., 1981, B37, 863.

82. T.SUNDARESAN and S.C.WALLWORK, Acta Cryst., 1972, B28, 2474.

83. G.J.ASHWELL, S.C.WALLWORK, S.R.BAKER and P.I.C.BERTHIER, Acta Cryst., 1975, B31, 1174.

84. G.J.ASHWELL, D.D.ELEY, S.C.WALLWORK, and M.R.WILLIS, Proc.Roy. Soc., 1975, A343, 461.

85. G.J.ASHWELL, D.D.ELEY, R.J.FLEMING, S.C.WALLWORK, and M.R.WILLIS, Acta Cryst., 1976, B32, 2948.

86. G.J.ASHWELL, D.D.ELEY and M.R.WILLIS, Nature, 1976, 259, 201.

87. G.J.ASHWELL, D.D.ELEY, S.C.WALLWORK, M.R.WILLIS, G.D.WELCH and J.WOODWARD, Acta Cryst., 1977, B33, 2252.

M.R.WILLIS, Acta Cryst., 1977, B33, 2258.

89. G.J.ASHWELL, D.D.ELEY, N.J.DREW, S.C.WALLWORK, and M.R.WILLIS, Acta Cryst., 1977, B33, 2598.

90. G.J.ASHWELL, V.E.BARTLETT, J.K.DAVIES, D.D.ELEY, S.C.WALLWORK, M.R.WILLIS, A.HARPER, and A.C.TORRANCE, Acta Cryst., 1977, B33, 2602.

91. R.B.SOMOANO, V.HADEK, S.P.S.YEN, A.REMBAUM, C.H.HSU, D.J.DECK, T.DATTA, and A.M.HERMANN, Phys.Status Solidi B, 1977, 81, 281.

92. G.J.ASHWELL, D.D.ELEY, M.R.WILLIS, and J.WOODWARD, Phys.Status Solidi B, 1977, 79, 629.

93. G.J.ASHWELL, D.D.ELEY, N.J.DREW, S.C.WALLWORK, and M.R.WILLIS, Acta Cryst., 1978, B34, 3608.

94. G.J.ASHWELL, Phys.Status Solidi B, 1978, 85, K7.

95. G.J.ASHWELL, Phys.Status Solidi B, 1978, 86, 705.

96. G.J.ASHWELL and S.C.WALLWORK, Acta Cryst., 1979, B35, 1648.

97. G.J.ASHWELL, Proceedings of the Int.Conf. on Low-Dimensional Conductors, Boulder, 1981.

98. A.J.SCHULTZ and G.D.STUCKY, J.Phys.Chem.Solids, 1971, 38, 269.

99. J.FERRARIS, D.O.COWAN, V.WALATKA, and J.H.PERLSTEIN, J.Amer. Chem.Soc., 1973, 95, 948.

100. T.E.PHILLIPS, T.J.KISTENMACHER, J.P.FERRARIS, and D.O.COWAN, J.Chem.Soc., Chem.Comm., 1973, 471.

101. L.B.COLEMAN, M.J.COHEN, D.J.SANDMAN, F.G.YAMAGISHI, A.F.GARITO, and A.J.HEEGER, Solid State Commun., 1973, 12, 1125.

102. T.J.KISTENMACHER, T.E.PHILLIPS, and D.O.COWAN, Acta Cryst., 1974, B30, 763.

103. E.M.ENGLER and V.V.PATEL, J.Amer.Chem.Soc., 1974, 96, 7376.

104. L.I.BURAVOV, O.N.EREMENKO, R.B.LYUBOVSKII, L.P.ROZENBERG, M.L. KHIDEKEL, R.P.SHIBAEVA, I.F.SHCHEGOLEV, and E.B.YAGUBSKII, Soviet Physics - JETP (Zhurnal Eksperimentalnoi i Teoreticheskoi Fiziki)., 1974, 20, 208.

105. R.H.BLESSING and P.COPPENS, Solid.State.Comm., 1974, 15, 215.

106. E.M.ENGLER and V.V.PATEL, J.Chem.Soc., Chem.Comm., 1975, 671.

107. A.N.BLOCH, D.O.COWAN, K.BECHGAARD, R.H.BANKS, and T.O.POEHLER, Phys.Rev., 1975, 34, 1561.

108. R.P.SHIBAEVA and L.P.ROZENBERG, Soviet Physics - Crystallography (Kristallografiya)., 1975, 20, 581.

109. T.J.KISTENMACHER, T.E.PHILLIPS, D.O.COWAN, J.P.FERRARIS, A.N. BLOCH, and T.O.POEHLER, Acta Cryst., 1976, B32, 539.

110. T.E.PHILLIPS, T.J.KISTENMACHER, A.N.BLOCH, and D.O.COWAN, J.Chem. Soc., Chem.Comm., 1976, 334.

111. G.A.THOMAS et al., Phys.Rev., 1976, B13, 5105.

112. R.L.GREENE, J.J.MAYERLE, R.SCHUMAKER, G.CASTRO, P.M.CHAIKIN, S.ETEMAD, and S.J.LA PLACA, Solid State, Commun., 1976, 20, 943.

113. C.BERG, K.BECHGAARD, J.R.ANDERSEN, and C.S.ANDERSEN, Tet.Lett., 1976, 1719.

114. K.BECHGAARD, T.J.KISTENMACHER, A.N.BLOCH, and D.O.COWAN, Acta Cryst., 1977, B33, 417.

115. T.E.PHILLIPS, T.J.KISTENMACHER, A.N.BLOCH, J.P.FERRARIS, and D.O.COWAN, Acta Cryst., 1977, B33, 422.

116. P.DELHAES, S.FLANDROIS, J.AMIELL, G.KERYER, E.TORREILLES, J.M. FABRE, L.GIRAL, C.JACOBSEN, and K.BECHGAARD, Journ. de Phys., 1977, 35, L233.

State Commun., 1977, 22, 139.

118. J.R.COOPER, D.JEROME, S.ETEMAD, and E.M.ENGLER, Solid State Commun., 1977, 22, 257.

119. A.N.BLOCH, T.F.CURRUTHERS, T.O.POEHLER, and D.O.COWAN, as in ref. 36, p.47.

120. D.CHASSEAU, G.COMBERTON, J.GAULTIER, and C.HAUW, Acta Cryst., 1978, B34, 689.

121. J.R.ANDERSEN, K.BECHGAARD, C.S.JACOBSEN, G.RINDORF, H.SOLING, and N.THORUP, Acta Cryst., 1978, B34, 1901.

122. D.CHASSEAU, J.GAULTIER, C.HAUW, J.M.FABRE, L.GIRAL and E. TORREILLES, Acta Cryst., 1978, B34, 2811.

123. S.MEGTERT, J.P.POUGET, R.COMES, A.F.GARITO, K.BECHGAARD, J.M. FABRE, and L.GIRAL, Le. Journal de Physique, Letts., 1978, 39, L118.

124. R.M.FRIEND, D.JEROME, J.M.FABRE, L.GIRAL, and K.BECHGAARD, J. Phys., 1978, C11, 263.

125. G.KERYER, J.AMIELL, S.FLANDROIS, P.DELHAES, E.TORREILLES, J.M. FABRE, and L.GIRAL, Proc. Conf. Quasi I-D Conductors, 1. Dubrovnik, 1978.

126. S.ETEMAD, E.M.ENGLER, T.D.SCHULTZ, T.PENNY, and B.A.SCOTT, Phys. Rev., 1978, B17, 513.

127. C.S.JACOBSEN, K.MORTENSEN, J.R.ANDERSEN, and K.BECHGAARD, Phys. Rev. B., 1978, 18, 905.

128. G.KERYER, J.AMIELL, S.FLANDROIS, P.DELHAES, E.TORREILLES, J.M. FABRE, and L.GIRAL, Solid State Commun., 1978, 26, 541.

129. G.KERYER, P.DELHAES, J.AMIELL, S.FLANDROIS, and B.TISSIER, Phys. Status Solidi B, 1980, 100, 251.

130. [illegible] Acta Cryst., 1981, B37, 1225.

131. H.SOLING, G.RINDORF, and NIELS THORUP, Acta Cryst., 1981, B37, 1716.

132. D.CHASSEAU, J.GAULTIER, C.HAUW, and P.DELHAES, Acta Cryst., 1981,

133. K.KROGMANN, Angew.Chem., Int.Ed., 1967, 8, 35.

134. R.P.SHIBAEVA, L.O.ATOVMYAN, and L.P.ROZENBERG, J.Chem.Soc., Chem. Comm., 1969, 649.

135. R.P.SHIBAEVA, L.O.ATOVMYAN, and M.N.ORFANOVA, J.Chem.Soc., Chem. Comm., 1969, 1494.

136. R.P.SHIBAEVA, A.E.SHVETS, and L.O.ATOVMYAN, Soviet Physics: Doklady (Akademiya Nauk, SSSR Doklady)., 1972, 16, 514.

137. S.Z.GOLDBERG, R.EISENBERG, J.S.MILLER, and A.J.EPSTEIN, J.Amer. Chem.Soc., 1976, 98, 5173.

138. G.J.ASHWELL, D.D.ELEY, S.C.WALLWORK, M.R.WILLIS, G.F.PEACHEY, and D.B.WILKOS, Acta Cryst., 1977, B33, 843.

139. VU DONG, H.ENDRES, H.J.KELLER, W.MORONI, and D.NÖTHE, Acta Cryst., 1977, B33, 2428.

140. J.J.MAYERLE, Inorg.Chem., 1977, 16, 916.

141. H.J.KELLER, I.LEICHERT, M.MEGNAMISI-BELOMBE, D.NÖTHE, and J.WEISS, Z.Anorg.Allg.Chem., 1977, 429, 231.

142. H.ENDRES, H.J.KELLER, W.MORONI, D.NÖTHE, and VU DONG, Acta Cryst., 1978, B34, 1703.

143. H.ENDRES, H.J.KELLER, W.MORONI, D.NÖTHE, and VU DONG, Acta Cryst., 1978, B34, 1823.

144. G.A.CANDELA, L.J.SWARTZENDRUBER, J.S.MILLER, and M.J.RICE, J. Amer.Chem.Soc., 1979, 101, 2755.

L.J.SWARTZENDRUBER, and J.S.MILLER, J.Amer.Chem.Soc., 1979, 101, 2756.

146. J.S.MILLER, A.H.REIS, E.GEBERT, J.J.RITSKO, W.R.SALANECK, L.KOVNAT, T.W.CAPE, R.P.VAN DUYNE, J.Amer.Chem.Soc., 1979, 101, 7111.

147. N.MATSUMOTO, Y.NONAKA, S.KIDA, S.KAWANO, and I.UEDA, Inorg.Chim. Acta, 1979, 37, 27.

148. S.R.WILSON, P.J.CORVAN, R.P.SEIDERS, D.J.HODGSON, M.BROOKHART, W.E.HATFIELD, J.S.MILLER, A.H.REIS, Jr., P.K.ROGAN, E.GEBERT, and A.J.EPSTEIN, Nato.Conf.Ser.6, 1979, 407.

149. P.CASSOUX and A.GLEIZES, Inorg.Chem., 1980, 19, 665.

150. C.WILLI, A.H.REIS, E.GEBERT, and J.S.MILLER, Inorg.Chem., 1981, 20, 313.

151. B.MOROSIN, H.J.PLASTAS, L.B.COLEMAN, and J.M.STEWART, Acta Cryst., 1978, B34, 540.

152. G.H.STOUT and L.H.JENSEN, X-Ray Structure Determination, A Practical Guide, McMillan, 1965.

153. G.M.SHELDRICK, SHELX 76, Program for Crystal Structure Determination, 1976, Univ. of Cambridge.

154. P.MAIN, S.E.HULL, L.LESSINGER, G.GERMAIN, J.P.DECLERCQ, and M.M.WOOLFSON, MULTAN 78, A System of Computer Programs for the Automatic Solution of Crystal Structures from X-ray Diffraction Data, 1978, Univs. of York and Louvain, Belgium.

155. A.BRAVAIS, Journ. de l'Ecole Polytech., 1850, 19, 1.

156. International Tables for X-ray Crystallography, Volume I, 1952, Kynoch Press: Birmingham.

157. W.L.BRAGG, Proc.Cambridge Phil.Soc., 1913, 17, 43.

159. A.L.PATTERSON, Z.Krist., 1935, A90, 517.

160. H.LIPSON and W.COCHRAN, The Determination of Crystal Structures, 1957, G.Bell: London, pp. 12-15, 150-198.

161. M.J.BUEGER, Vector Space, 1959, Wiley: New York, pp 5-29, 41-64.

162. J.KARLE and H.HAUPTMANN, Acta Cryst., 1956, 9, 635.

163. International Tables for X-ray Crystallography, Volume II, 1959, Kynoch Press: Birmingham.

164. I.L.KARLE, K.S.DRAGONETTE, and S.A.BRENNER, Acta Cryst., 1965, 19, 713.

165. J.KARLE and H.HAUPTMAN, Acta Cryst., 1950, 3, 181.

166. H.HAUPTMAN and J.KARLE, Solution of the Phase Problem, I, The Centrosymmetric Crystal, A.C.A. Monograph No.3, Polycrystal Book Service: Pittsburgh.

167. D.SAYRE, Acta Cryst., 1952, 5, 60.

168. W.COCHRAN and M.M.WOOLFSON, Acta Cryst., 1955, 8, I.

169. M.M.WOOLFSON, Acta Cryst., 1954, 7, 61.

170. J.KARLE and I.L.KARLE, Acta Cryst., 1966, 21, 849.

171. G.GERMAIN, P.MAIN, and M.M.WOOLFSON, Acta Cryst., 1970, B26, 274.

172. M.M.WOOLFSON, Crystallographic Computing Techniques, 1975, p.85, Munksgaard: Copenhagen.

173. G.GERMAIN, P.MAIN, and M.M.WOOLFSON, Acta Cryst., 1971, A27, 368.

174. F.H.HERBSTEIN, Perspectives in Structural Chemistry, Vol.IV, pp.166-395, 1971, edited by J.D.Dunitz and J.A.Ibers, John Wiley: New York.

Cornell Univ. Press: Ithaca, New York.

176. D.W.ALLEN, I.W.NOWELL, A.C.OADES, and P.E.WALKER, J.Chem.Soc., Perkin Trans. I, 1978, 98.

177. J.J.DE BOER and D.BRIGHT, Acta Cryst., 1974, B30, 797.

178. G.J.ASHWELL and G.H.CROSS, personal communication.

179. G.J.ASHWELL, personal communication.

180. D.W.ALLEN, personal communication.

181. G.J.ASHWELL and G.ROTHWELL, personal communication.

The author has,

(a) Completed a computing course at the Polytechnic dealing with Fortran programming;

(b) participated in Departmental research colloquia, and presented a colloquium on her own work;

(c) attended appropriate research colloquia at the University of Sheffield;

(d) completed the following reading study programme:

(i) 'X-Ray Structure Determination, a Practical Guide', G.H.Stout and L.H.Jenson, MacMillan, 1968.

(ii) 'Structure Determination by X-Ray Crystallography', M.F.C. Ladd and R.A.Palmer, Plenum, 1977.

(iii) 'Crystallography and its Applications', L.D.Dent. Glasser, Van Nostrand, 1977.

(iv) 'Direct Methods of Crystallography', M.M.Woolfson, Clarendon Press, 1961.